2 THE PHYSICS DRIVING THE UPGRADE OF CEBAF TO 12 GeV

This chapter describes in more detail the powerful physics case behind the push for doubling CEBAF's energy to 12 GeV. The material is organized in terms of the campaigns outlined in Section 1.A.

2.A Campaign 1: Testing the Origin of Quark Confinement

The goal of the Hall D project is the definitive and detailed measurement of the spectrum of exotic hybrid mesons. These first-ever manifestations of the gluonic degrees of freedom in the spectroscopy of hadrons will lead to an understanding of the most novel and spectacular prediction of QCD – confinement. The most fruitful place to search for these mesons is in the light-quark sector, and the optimal probe is the photon, which is expected to be far more effective in uncovering these states than beams of π or K mesons have been.

The power of the photon probe lies in its virtual $q\bar{q}$ structure: the quark spins are aligned as opposed to π or K mesons in which the quark spins are antiparallel. Unfortunately, almost all data on the spectroscopy of mesons below 3 GeV/c^2 come from π and K-induced reactions, central production in p-induced reactions, and $\bar{p}p$ annihilations. Tantalizing indications for gluonic excitations have emerged from these studies, but the evidence is far from solid, and the details needed for a full understanding are missing. The data in hand on the photoproduction of light mesons are sparse indeed, essentially nonexistent. Spectroscopy experiments rely on detecting complicated decays of produced mesons and on the full reconstruction of the reactions in which they are created. Large statistical samples are also required.

Up to now, photon beams of sufficient energy, flux, and other requisite beam characteristics could not be produced. The determination of quantum numbers of mesons is also greatly aided by using photon beams which are linearly polarized. The superb electron beam characteristics (small transverse emittance and energy spread) of the CEBAF accelerator make possible the employment of the coherent bremsstrahlung technique for producing photon beams with a high degree of linear polarization. Hybrid mesons, including those with exotic quantum numbers, are expected to lie in the range from 1.5 to 2.5 GeV/c^2. To reach these masses requires photons in the energy range from 8 to 9 GeV. This is based on the requirement that mesons are produced sufficiently above threshold that line shapes are not distorted. This band of photon energies also allows for a solenoid-only-based

detector which, particularly for high-flux photon beams, is optimal in achieving 4π hermeticity.

With an electron beam energy of 12 GeV, photon fluxes of up to 10^8 photons/s with 50% linear polarization in the desired energy range are achievable. Even with initial fluxes of only 10^7 photons/s, the statistical sample collected after the first year of running will exceed those collected with incident hadron beams by at least an order of magnitude. With this sample size collected using a hermetic and well-understood detector, the application of the partial wave analysis (PWA) technique will be able to uncover the exotic states, even if they are produced with cross sections only a few percent of those for conventional mesons. Indeed, theoretical considerations [Af98, Is99b] lead us to believe that the exotic hybrids will be produced with cross sections which are nearly comparable to those of conventional mesons.

In what follows, we will expand on:

1. *The role of glue in QCD.* This will include a discussion of how the gluons form flux tubes, and how their excitations lead to mesons with the gluon degree of freedom excited, in particular exotic hybrids. This general picture is not restricted to a particular model but follows from the first principles of QCD.

2. *The current evidence for gluonic excitations.* The evidence comes from overpopulation of conventional nonets, and from possible glueball and exotic hybrid sightings in $\bar{p}p$ annihilations and π-induced interactions.

3. *Why the light-quark sector is the most fruitful venue for these searches.* We will compare this to searches in the charm or beauty quark sectors, or in e^+e^- annihilations.

4. *Why photons are expected to be particularly effective in producing exotic hybrids.* Its spin structure makes the photon a qualitatively different probe from π and K beams. In addition, there are meager data in hand on the photoproduction of light- quark mesons.

5. *The importance of the PWA technique in uncovering exotic mesons.* The PWA is a powerful analysis tool that has been successfully employed in experiments to uncover states which are not evident from a simple examination of mass spectra – "bump-hunting". The importance of a hermetic detector with excellent resolution and rate capability and sensitivity to a wide variety of decay modes will be explored.

6. *Why linear polarization of the photon beam is important for this search.* Linear polarization aids in determination of the J^{PC} quantum numbers, is essential in determining the production mechanism, and can be used as a filter for exotics once the production mechanism is isolated.

7. *Why the ideal photon energy range is from 8 to 9 GeV.* In order to reach the desired mass range we need to be far enough above threshold to avoid line-shape distortions. We also want to be high enough in energy to kinematically separate the production of baryon resonances from the production of meson resonances. This need for higher photon energies, however, has an upper limit because of additional considerations: the choice of a (simpler) solenoid-only-based detector limits the maximum energy, and the possibility of increased flux and linear polarization (both of which increase as the photon energy is decreased for a fixed available electron energy).

8. *The desired electron energy.* Having established the desired range of photon beam energies, an electron energy of 12 GeV provides sufficient flux and degree of linear polarization.

This then is the overview of the major physics thrust of the Hall D project. In addition to studying hybrid mesons, both with exotic as well as non-exotic quantum numbers, we will have the opportunity to study the $s\bar{s}$ sector as well. Little is known about $s\bar{s}$ mesons. Knowledge about this spectroscopy will allow us to connect from the light-quark (u and d) and the heavy-quark (c and b) sectors. Details are provided in Section 2.A.6 below.

The Hall D collaboration formed to carry out this physics currently consists of about 90 physicists from 27 institutions. The team also includes a contingent of theorists who are working closely with experimenters to focus the physics goals, to develop the analysis formalism and to ensure that the results uncovered by the experiment will be used to achieve the ultimate goal – understanding the confinement mechanism of QCD.

2.A.1 Spectroscopy of Gluonic Excitations

Flux tubes

Quantum chromodynamics (QCD) describes the interactions of quarks and gluons, and along with the electroweak theory they form the successful standard model of particle physics. At short distance scales, where perturbative techniques are applicable, QCD describes high-energy experimental phenomena both qualitatively and quantitatively. QCD is distinct from QED in that the force carriers of the former (gluons) carry color charge whereas for the latter the photons are electrically neutral. The gluonic degrees of freedom are experimentally evident at high momenta and manifested in the observation of gluon jets and the details of their production.

At large distance scales, the situation is far different. Here the successful calculational tech-

niques of the perturbative regime cannot be used. We must rely on first-principles lattice QCD calculations or QCD-inspired models. On the experimental side there is little or no evidence of gluonic degrees of freedom as epitomized in the spectroscopy of hadrons. However, there are many indications that all this is about to change. Developments on the theoretical and experimental fronts give rise to optimism that these gluonic degrees of freedom will be observed, measured, and understood in detail. The prize in understanding these new manifestations of gluonic degrees of freedom (glueballs and hybrid mesons) is grand indeed: an understanding of the confinement mechanism of QCD. The phenomenon of confinement is the most novel and spectacular prediction of QCD – unlike anything seen before.

The development of the flux tube picture of confinement has a long history. It originally emerged in the 1970s when Yoichiro Nambu pointed out that the observation of a linear relationship between the spins of hadrons and the square of their masses could be explained as a consequence of the assumption that the quarks are tied to the ends of a relativistic string with constant mass per length. This assumption also leads to a linearly rising potential between static heavy quarks.

The confinement mechanism is related to the fact that gluons carry the color charge, and becomes evident when we realize that we cannot separate the quarks in a hadron from each other. The field lines of an electric dipole arrange themselves as shown in Fig. 16a. As we separate the two charges, the potential energy falls off like $1/r$ and the force like $1/r^2$. Consider now a quark and antiquark as shown in Fig. 16b. Because of the self-interaction of the gluons the field lines form flux tubes as we increase the separation between the quarks. If we compute the number of field lines intersecting an area perpendicular to the flux tube we notice that this number stays constant as we increase r, suggesting a constant force or linear potential. This leads to confinement since infinite energy is then required to separate the quarks. Recent lattice QCD calculations support the formation of flux tubes as shown in Fig. 17a where the action density (energy density) is plotted for a $q\bar{q}$ pair. The formation of the flux tube is evident. These lattice calculations also show that the potential for the $q\bar{q}$ pair is linear (Fig. 17b) for r greater than about 0.2 fm. Moreover, the energy levels observed for heavy quarkonium are in agreement with a linear potential. Today there is a wide consensus that the Nambu flux tube conjecture was correct and that QCD confines the quarks by flux tube formation.

Conventional mesons

The conventional mesons of the original quark model correspond to the flux tube being in its ground state. The conventional mesons made from the u, d, and s quarks are grouped in

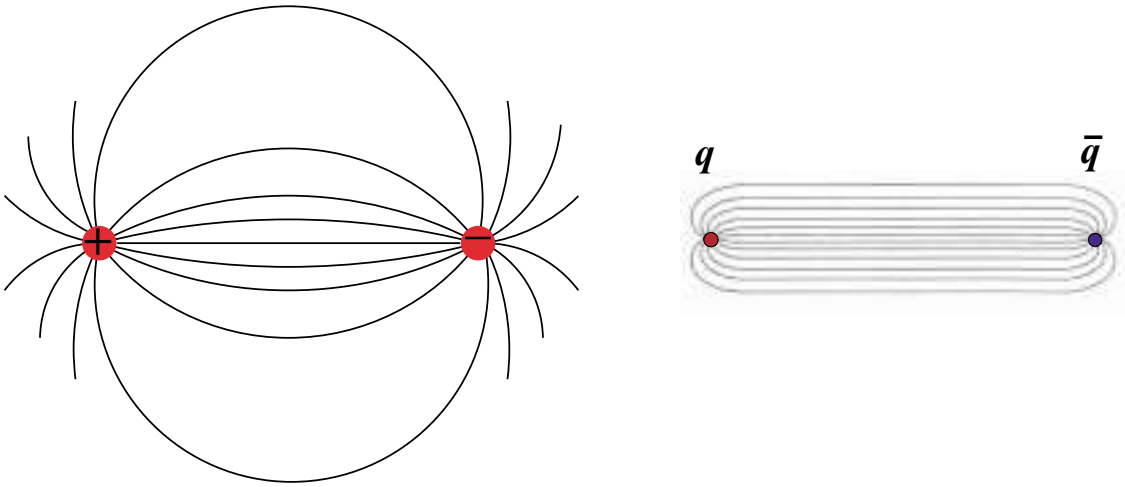

Figure 16: Comparing force field lines for QED and QCD. The field lines for an electric dipole (left); and the color field lines for a quark and antiquark (right).

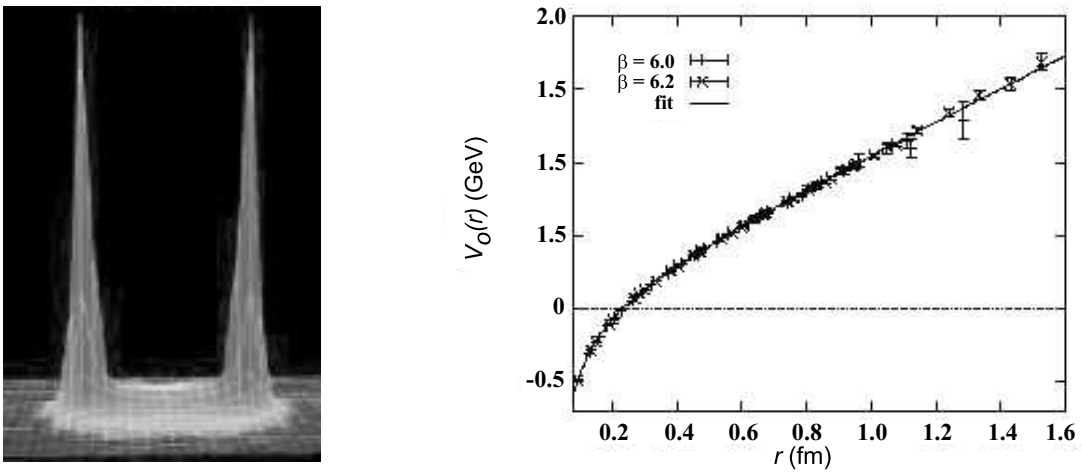

Figure 17: Evidence for flux tubes and linear potentials from lattice QCD. The action density (energy density) in the space surrounding a quark and antiquark (left) [Ba00]; and the inter-quark potential (right) [Ba97].

nonets, each characterized by a given J^{PC} determined by the relative orientation of the spins of the quarks and their orbital angular momentum. The rules for allowed values of J^{PC} follow from the requirements of a fermion-antifermion system: the quark spins can be parallel ($S = 1$) or antiparallel ($S = 0$) with relative orbital angular momentum (L), $\vec{J} = \vec{L} + \vec{S}$, $P = (-1)^{L+1}$ and $C = (-1)^{L+S}$. For these $q\bar{q}$ systems J^{PC} combinations of 0^{--}, 0^{+-}, 1^{-+}, 2^{+-}, ... are not allowed and are referred to as *exotic* quantum numbers. The range of masses of established conventional meson nonets and their radial excitations extend from the π mass up to about 2.5 GeV/c^2.

Mesons and gluonic excitations

Mesons can also be generated when the flux tube or string is *plucked* or excited. The two degenerate first excited states of the string are the two longest-wavelength vibrational modes of this system, and π/r is their excitation energy since both the mass and the tension of this "relativistic string" arise from the energy stored in its color force fields. (This low-lying gluonic spectrum is model-independent for $m \to \infty$.) The vibrational quantum numbers of the string, when added to those of the quarks, can produce mesons with exotic J^{PC} – *exotic hybrids* – hybrids because the mesons manifest both their quark and gluonic content. Because the gluons carry color charge it is also possible to form bound states of glue with no quarks present. Such mesons are called *glueballs*. Figure 18 shows a level diagram giving the range of masses for the conventional $q\bar{q}$ nonets and estimates of the masses of the lightest glueballs and hybrids, and thresholds for possible nearby associated molecular meson-meson bound states.

Focusing on light-quark exotic hybrids

The focus of the Hall D project is in the light-quark hybrid sector. The initial benchmark states will be the exotic hybrids, which cannot mix with $q\bar{q}$ and which therefore have a *smoking gun* signature. Although there is strong circumstantial evidence for glueballs, the possibility of mixing with $q\bar{q}$ complicates their discovery. Lattice QCD predictions about heavy-quark exotic hybrids are at least as reliable as for the light-quark hybrids but the experimental situation is far more problematic. The production cross sections are a few orders of magnitude lower. At the higher energies needed to produce these more massive states many other uninteresting processes can contribute to background. Also, these more massive states have many more decay channels available, decreasing the yield for any one particular mode to be studied. Finally, to unambiguously tag a charm or beauty hybrid one must identify detached vertices, further complicating the experimental setup. Another venue for exotic vector hybrids is production in e^+e^- collisions, but this production is suppressed by an angular momentum barrier (the excited flux tube carries $J = 1$).

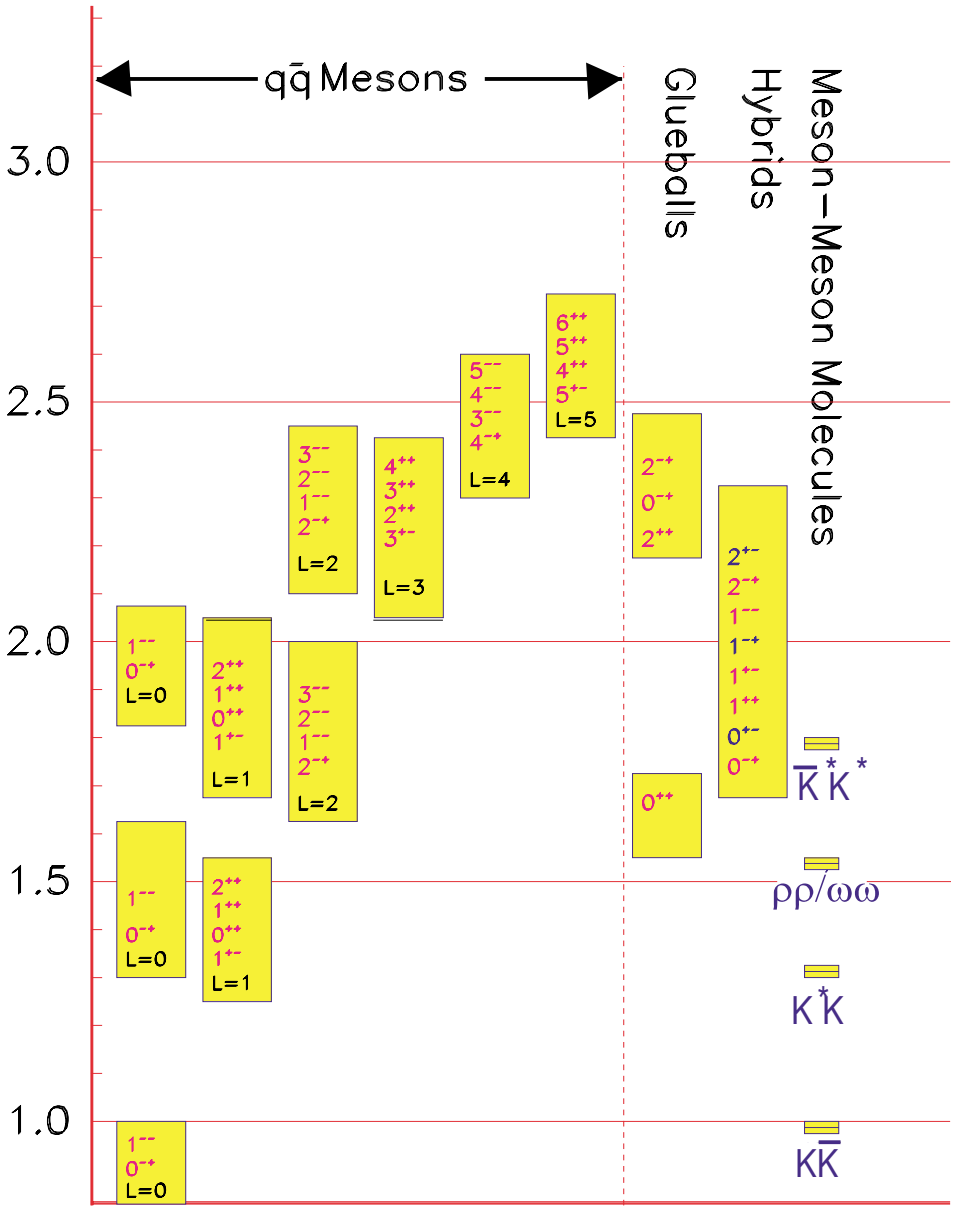

Figure 18: A level diagram showing conventional nonets and expected masses of glueballs, hybrids and molecular thresholds. The vertical axis is in units of GeV/c^2. For the $q\bar{q}$ boxes the L refers to the angular momentum between the quarks and each J^{PC} refers to a nonet of mesons.

From every point of view, photoproduction of light-quark hybrids is expected to be our best handle for providing the information we need to understand confinement.

Observation of gluonic excitations

Lattice QCD and flux tube model calculations are in agreement that the masses of light-quark hybrids range from 1.5 to 2.5 GeV/c^2 with the lightest exotic hybrid ($J^{PC} = 1^{-+}$) having a mass about 2 GeV/c^2 [Be97, Ju97]. After about 15 years of searching we have in hand two candidates for exotic hybrids. The first has a mass of 1.4 GeV/c^2 decaying into $\eta\pi^-$ [Th97, Ab98] – the evidence for this state is not without controversy. The second, perhaps a more firmly established state, is at 1.6 GeV/c^2 and decays into $\rho^0\pi^-$ [Ad98]. Both have the assignment: $J^{PC} = 1^{-+}$. These states were reported by the E852 collaboration which studied $\pi^- p$ interactions using the AGS at Brookhaven National Laboratory. Both states have also been independently confirmed. It is noteworthy that the two candidates have masses below the expectations from lattice QCD and the flux tube model for the lightest exotic hybrid [Ba95]. In addition, the decay modes observed are not those favored by the flux tube model. In this model, the exotic hybrid's favored decay mode is into $S + P$ where S indicates a conventional $q\bar{q}$ meson with $L = 0$ while P indicates a conventional $q\bar{q}$ meson with $L = 1$. This comes about from how the exotic hybrid gives up its spin to the decay daughters, and possibly explains why exotic hybrids have not yet been observed – the decay modes are complicated. A favored mode, for example, would be into $b_1\pi \to \omega 2\pi \to 5\pi$.

Lattice QCD calculations indicate that the lightest glueball is a scalar with a mass in the range from 1.5 to 1.7 GeV/c^2 [Mo97, Ba93, Se95, Ba97]. Indeed there is evidence from the Crystal Barrel experiment, which studied $\bar{p}p$ annihilations at CERN, that the $f_0(1500)$ is a leading candidate for a glueball [Am95, Am96]. There are, however, indications that this state is not a pure glueball but has some mixing with conventional $q\bar{q}$ [Cl00]. There are strong indications that the scalar meson sector contains one or more glueballs since there are several more states observed than can be accommodated in the simple $q\bar{q}$ model. However, the unique identification of a glueball is exacerbated by the possibility of mixing with $q\bar{q}$. Lattice QCD indicates a rich spectrum of glueballs, all with non-exotic quantum numbers, from 1.5 to 2.5 GeV/c^2. The lightest glueball with exotic quantum numbers is predicted to have $J^{PC} = 2^{+-}$ and to have a mass of 4 GeV/c^2 [Mo97].

This then is the tantalizing evidence in hand for gluonic excitations. In the case of the exotic hybrids, the range of masses of putative states observed is significantly lower than expectations, and the observed modes of decay are not those expected to be favored [Is85, Ba95]. Lattice QCD calculations are being refined, and significant progress on reducing the theoretical errors on masses

and more information on decay modes is expected in the next five years as computational techniques improve and computer power keeps increasing. Flux tube model calculations are in hand for both masses and decay modes [Is85, Cl95, Ba95, Ca91]. Given the state of current observations, with their uncertainties and limitations, the flux tube model has not been ruled out. Clearly more data are needed. As will be shown below, photoproduction reactions are expected to be a rich source of hybrids – exotic and non-exotic. Once these states are discovered and mapped out, we will have the data needed to constrain our theoretical understanding of the details of confinement. Without more data, there will be little progress.

2.A.2 Photoproduction of Gluonic Excitations

The photon is expected to be particularly effective in producing a *smoking gun* signature for gluonic excitations: hybrids with exotic J^{PC}. In this regard, we will compare the effectiveness of the π or K as a probe with that of the photon. In the former case, the meson is a $q\bar{q}$ with spins anti-aligned ($S = 0$), and in the latter, the photon is a virtual $q\bar{q}$ with spins aligned ($S = 1$). In both cases, the relative orbital angular momentum is zero ($L = 0$) and the flux tube connecting the quarks is in its ground state. Exotic quantum numbers can also be produced by non-$q\bar{q}$ objects, such as meson-meson molecules, but these states are expected to have very different flavor systematics and production t-dependence than the J^{PC} exotics.

Consider what happens when the beam probe approaches a target proton and scatters. A possible outcome is a transfer of energy that excites the flux tube to its lowest excited state. Lattice QCD and flux tube models both indicate that the lowest excited flux tube has $J = 1$ [Be97, Is85, La97]. The flux tube, or string, can be spinning clockwise or counter-clockwise around the $q\bar{q}$ line leading to two degenerate states – degenerate since the energy should not depend on which way the flux tube is spinning. The states that are linear combinations of these two rotations are eigenstates of parity and charge conjugation leading to two possibilities for the excited flux tube: $J^{PC} = 1^{-+}$ or $J^{PC} = 1^{+-}$. Suppose we start with the $q\bar{q}$ in the $S = 0$ and $L = 0$ (or $J^{PC} = 0^{-+}$ – the π or K) configuration. Combining this with $J^{PC} = 1^{-+}$ or $J^{PC} = 1^{+-}$ of the excited flux tube results in hybrid mesons with $J^{PC} = 1^{++}$ or $J^{PC} = 1^{--}$. These are non-exotic. If, however, we start with $q\bar{q}$ in the $S = 1$ and $L = 0$ (or $J^{PC} = 1^{--}$ – the vector photon) configuration, the resulting hybrid can have $J^{PC} = [0, 1, 2]^{+-}$ for the flux tube with $J^{PC} = 1^{-+}$ and $J^{PC} = [0, 1, 2]^{-+}$ for the flux tube with $J^{PC} = 1^{+-}$. So we see that in the case of the vector probe, the resulting hybrids can have six possible J^{PC} of which half are exotic combinations whereas, for π or K probes, no exotic combinations are generated.

In the next section, we will discuss how the technique of PWA will be used to extract information about the spin and parity of produced states. In a photon beam this process is greatly aided by using photons that are linearly polarized. Linear polarization will be provided using the technique of tagged, coherent bremsstrahlung off a crystal radiator. The details of how this photon beam will be produced are discussed later in this White Paper (see Section 4.E.2).

2.A.3 Partial Wave Analysis and Photon Polarization

Kinematics

The technique used for identifying meson states (their masses, widths and J^{PC}) is partial wave analysis. Consider a specific exclusive process:

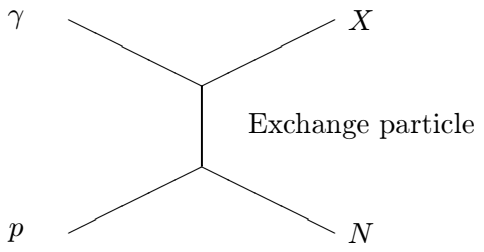

$$\gamma p \to X p$$

$$s = (p_\gamma + p_p)^2$$

$$t = (p_\gamma - p_X)^2$$

The center-of-mass energy squared, s, and the momentum-transfer-squared, t, between the incoming beam and outgoing X are defined in terms of the four-vectors of the particles as above. The behavior of the cross section with s and t depends on the production mechanism, which is usually described in terms of the particle or particles which can be exchanged as shown above. For example, if the exchange particle is a pomeron (diffractive process) the cross section is nearly constant in s. For meson-exchange processes, cross sections typically fall off as $1/s^2$. The dependence on t is typically exponential:

$$\frac{dN}{dt} \propto e^{-\alpha|t|}, \tag{1}$$

with $\alpha \simeq 6$ – 8 GeV^{-2}. For the process above, at high enough photon beam energy, E_γ, we can make the approximation $s \approx 2 \cdot E_\gamma^{m_X}$. For fixed s, and mass of X, m_X, there is a minimum value of $|t|$, or $|t|_{\rm min}$, needed to produce X. This $|t|_{\rm min}$ increases with increasing m_X for fixed E_γ, and decreases with increasing E_γ for fixed m_X. Coupled with the steep dependence implied in equation (1), the dependence of $|t|_{\rm min}$ on m_X will affect event yields. In addition, the line shape of a resonance can be distorted if the variation of $|t|_{\rm min}$ across the width of a resonance is too rapid.

Partial wave analysis goals

The goal of the PWA is to extract information about the line shape of a resonance with mass m_X and to determine the production mechanism and decay modes as well. This necessitates doing the PWA in fine enough bins in mass and $|t|$. Our criteria are to do the PWA in mass bins of 10 MeV/c^2, with roughly ten equally populated bins in $|t|$. With the statistical sample expected after one year of running with 10^7 photons/s, the statistical error in the central peak of an exotic meson for a given bin in $|t|$ will be of order 3%, assuming the exotic is produced with a 5% probability relative to conventional mesons.

It is important to stress here that the detector design focuses on hermeticity and resolution to ensure nearly uniform coverage with well-understood acceptance functions for various decay angles. Kinematic fitting will also be used to identify exclusive processes. The design focuses on the requirements of the PWA. The existence of well-established resonances will be used as benchmarks for the PWA. They also provide benchmarks for the phase variation of candidate exotic states. Furthermore, candidate exotics can appear with multiple decay modes which should give consistent results; *i.e.*, $b_1\pi$ and $f_1\eta$. In addition, the same decay mode, such as $\eta\pi$, should be observed in several channels where $\eta \to \pi^+\pi^-\pi^0$, $\eta \to 3\pi^0$, and $\eta \to 2\gamma$. Each of these modes leads to different acceptances and systematics, providing a powerful check on the PWA results.

This is all nicely illustrated by the PWA performed by the E852 collaboration, which reported the 1^{-+} $\rho^0\pi^-$ exotic state in the reaction $\pi^- p \to \pi^+\pi^-\pi^- p$ at a beam momentum of 18 GeV/c [Ad98]. In Fig. 19, the acceptance-corrected (average acceptance was 25%) distributions of the $\pi^+\pi^-\pi^-$ and $\pi^+\pi^-$ effective masses are shown. The positions of well-established meson states are shown, even though the $a_1(1260)$, for example, does not show up prominently. The PWA assumes a parent decaying into a $\pi\pi$ state and an unpaired π followed by the decay of the $\pi\pi$ state. The resulting decomposition into various waves is shown in Fig. 20. The decomposition now clearly shows the $\pi(1800)$ in the 0^{-+} wave, the $a_1(1260)$ in the 1^{++} wave, the $\pi_2(1670)$ in the 2^{-+} wave, and the $a_2(1320)$ in the 2^{++} wave. Evidence for the exotic 1^{-+} $\rho\pi$ is shown in Fig. 19c and d. Also shown in this figure is the effect of leakage of non-exotic waves. Finally in Fig. 20 a coupled fit to the wave intensities and phase difference between the 1^{-+} and 2^{-+} waves is shown.

We point out here that impressive as these data are, the statistics expected for Hall D will far exceed those of the E852 experiment, and the detector will be far better designed and understood since this project is focused on optimizing the design for this sort of analysis. A test partial wave fit using simulated data and the Hall D Monte Carlo is discussed within the context of the Hall D detector (Section 4E). The ability to do a good partial wave analysis is a critical part of the design

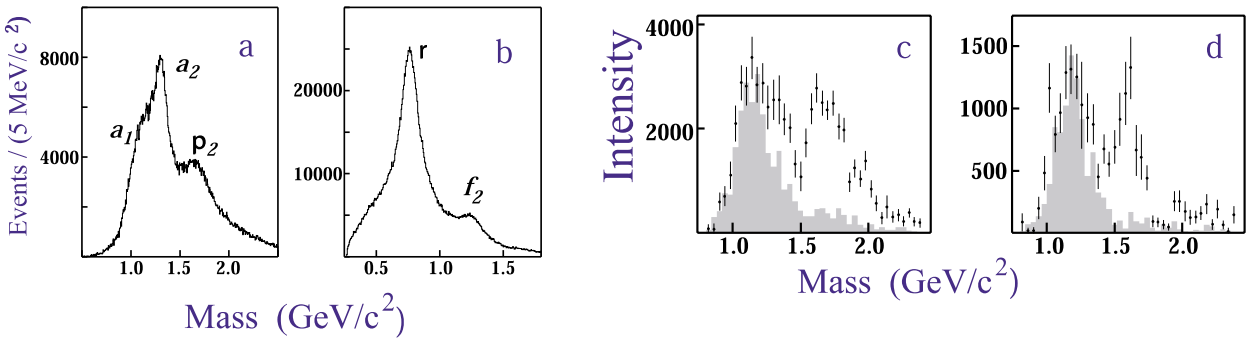

Figure 19: E852 results: acceptance corrected effective mass distributions for the $\pi^+\pi^-\pi^-$ combination (**a**) and the $\pi^+\pi^-$ combination (**b**) (two entries per event). (**c**) and (**d**) show the intensities for the waves corresponding to 1^{-+} into $\rho\pi$, where the two figures correspond to different naturalities of the exchanged particle. The shaded distributions are an estimate of leakage due to non-exotic waves.

of the Hall D detector. A discussion of the PWA technique for specific processes within the context of the Hall D detector is included in the discussion of the apparatus and its design criteria.

Linear and circular polarization

We start with a review of the relationship between linear and circular polarization. A right-handed, circularly polarized photon ($|R\rangle$) has $m = 1$ while for the complementary, left-handed $|L\rangle$ photon $m = -1$. These are related to the linear polarization states, $|x\rangle$ (in production plane) and $|y\rangle$ (perpendicular to production plane) by:

$$|x\rangle = \frac{1}{\sqrt{2}}\left(|R\rangle + |L\rangle\right) \tag{2}$$

$$|y\rangle = \frac{-i}{\sqrt{2}}\left(|R\rangle - |L\rangle\right) \tag{3}$$

We will use these relations in several straightforward cases to show how linear polarization:

1. can provide information on decays in lieu of statistics,

2. is essential in isolating production mechanisms, and

3. can be used as an exotics filter if the production mechanism is known.

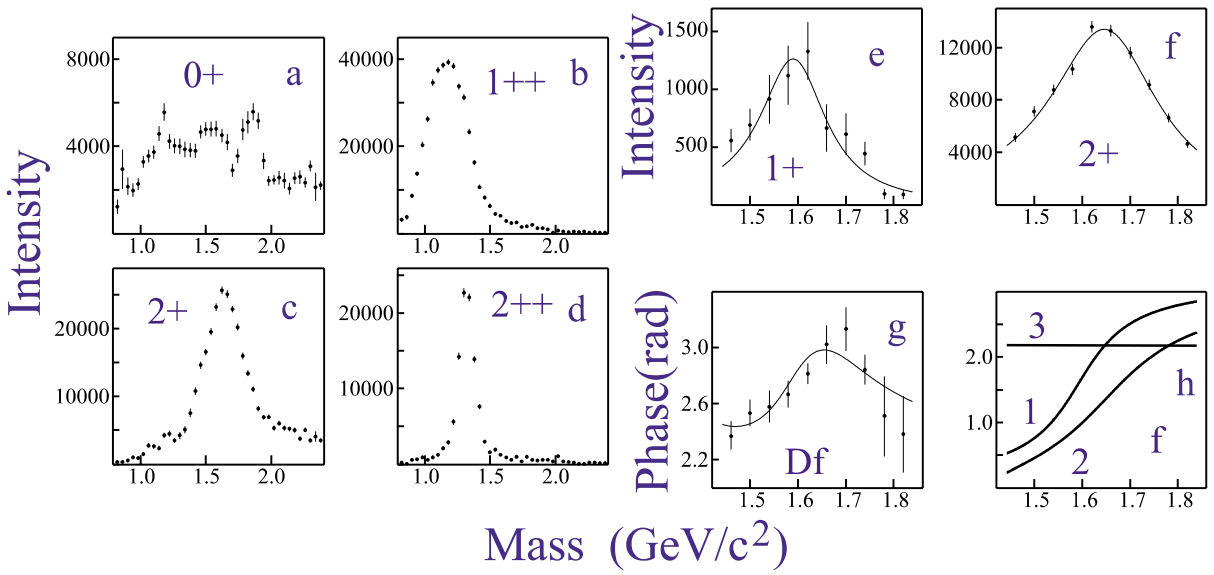

Figure 20: E852 results: the combined intensities for all fit waves. (**a**) is 0^{-+}; (**b**) is 1^{++}; (**c**) is 2^{-+}; and (**d**) is 2^{++}. Figures (**e**) and (**f**) show results for the intensities of a coupled mass-dependent Breit-Wigner fit of the 1^{-+} and 2^{-+} wave. (**g**) shows the phase difference between the two waves, and (**h**) shows the individual phases: 1 is the 1^{-+} wave, 2 is the 2^{-+} wave, and 3 is the background phase.

Linear polarization and statistics

To illustrate how linear polarization provides useful information in the PWA, consider the case of the photoproduction of a vector meson which subsequently decays into two pseudoscalar mesons. Possible examples are $\rho \to \pi\pi$ or $\phi \to K\bar{K}$. Suppose the production mechanism produces the vector meson with the same helicity as the incident photon (or s-channel helicity conservation). In the rest frame of the vector the two-pseudoscalar wavefunction is described by $Y_1^m(\theta, \phi) \propto \sin\theta e^{im\phi}$.

For circularly polarized photons (either $m = 1$ or $m = -1$) the square of this amplitude carries no ϕ information, while for in-plane photons there is a $\cos^2\phi$ dependence and out-of-plane a $\sin^2\phi$ dependence in the decay angular distribution since in these cases we have the sum or difference of Y_1^{+1} and Y_1^{-1} according to equations (2) and (3). Although not essential in determining spin, a gain of statistics is needed to recover a drop in the degree of linear polarization. Indeed our Monte Carlo simulation studies indicate that the increase in statistics necessary for a fixed accuracy in the analysis is proportional to the decrease in polarization.

Linear polarization and the production mechanism

This is best illustrated by considering a specific example. Suppose we produce a vector particle ($J^P = 1^-$) by the exchange of a scalar particle ($J^P = 0^+$, corresponding to natural parity exchange) or a pseudoscalar particle ($J^P = 0^-$, corresponding to unnatural parity exchange). We wish to determine whether the vector is produced by natural (amplitude A_N) or unnatural (amplitude A_U) parity exchange. In the center-of-mass of the produced vector particle, the momentum vectors of the beam photon and exchange particle are collinear. For circularly polarized photons, the m of the vector is the same as that of the photon. From parity conservation, the orbital angular momentum between the photon and exchange particle is $L = 0$ or $L = 2$ for natural parity exchange and $L = 1$ for unnatural parity exchange. So for circularly polarized photons, with $m = +1$, the total amplitude is $A_N + A_U$ whereas for $m = -1$, the total amplitude is $A_N - A_U$. This follows simply from the addition of angular momenta. Circularly polarized photons allow us to measure only the sum or difference of the two exchange amplitudes. If however, we have linearly polarized photons along the x-direction, we extract A_N using equation (2) and for polarization along the y-direction, we extract A_U using equation (3).

Linear polarization as an exotics filter

Using arguments similar to those above, it has been shown that linear polarization can be used

as a tool to filter exotics. For example, a $\rho\pi$ system with $I = 1$ has $C = +$. Suppose that one can determine the naturality of the exchange particle by selecting data within a range of $|t|$. For a produced $C = +$ particle with spin 1 we can have natural parity ($J^{PC} = 1^{-+}$ – exotic) or unnatural parity ($J^{PC} = 1^{++}$ – non-exotic). In the case of natural parity exchange the in-plane polarization selects the $J^{PC} = 1^{-+}$ wave while out-of-plane polarization selects $J^{PC} = 1^{++}$. For unnatural parity exchange the reverse is true. Note that in this case we are specifying the naturality of the exchange and using linear polarization to select the naturality of the produced particle. In the previous section, we specified the naturality of the produced particle and used linear polarization to select the naturality of the exchanged particle.

2.A.4 The Optimal Photon and Electron Energies

What is the optimal photon beam energy to reach the Hall D physics goals? The goal of this experiment is to search for mesons in the mass range from 1 to 2.5 GeV/c^2. An incident photon energy of just under 8 GeV is sufficient to produce a meson of mass 3 GeV/c^2. We also want to produce mesons with sufficient yield. The yield is determined by the value of $|t|_{\rm min}$ and the exponentially falling distribution in $|t|$, as discussed in the previous section. The relative yield for a slope parameter of $\alpha = 8$ (GeV/c)$^{-2}$ is shown in Fig. 21a. Another consideration is the ability to kinematically separate meson resonance production from baryon resonance production. As an example, we considered various reactions leading to a final state: $\pi^+\pi^-\pi^+n$. We enumerate the possibilities:

$$\gamma p \rightarrow X^+ n \rightarrow \rho^0\pi^+ n \rightarrow \pi^+\pi^-\pi^+ n \quad (4)$$

$$\gamma p \rightarrow \rho^0\Delta^+ \rightarrow \rho^0\pi^+ n \rightarrow \pi^+\pi^-\pi^+ n \quad (5)$$

$$\gamma p \rightarrow \pi^+\Delta^{*0} \rightarrow \pi^+\pi^-\pi^+ n \quad (6)$$

The first of these is the reaction of interest. We can reduce the other two by requiring that the effective mass of any πn or $\pi\pi n$ combination be outside the baryon resonance region (greater than 1.7 GeV/c^2 for this exercise). The fraction of events for which we are able to use kinematics to remove the offending reaction is shown in Fig. 21b as a function of beam momentum and for various m_X masses.

Whereas the considerations mentioned thus far favor higher photon beam energies, other considerations favor a lower photon beam energy. For the tagged and collimated coherent photon beam the variation in flux, for constant total hadronic rate in the detector, is plotted in Fig. 22a as a function of photon beam energy for three different values of electron energy. In Fig. 22b the degree

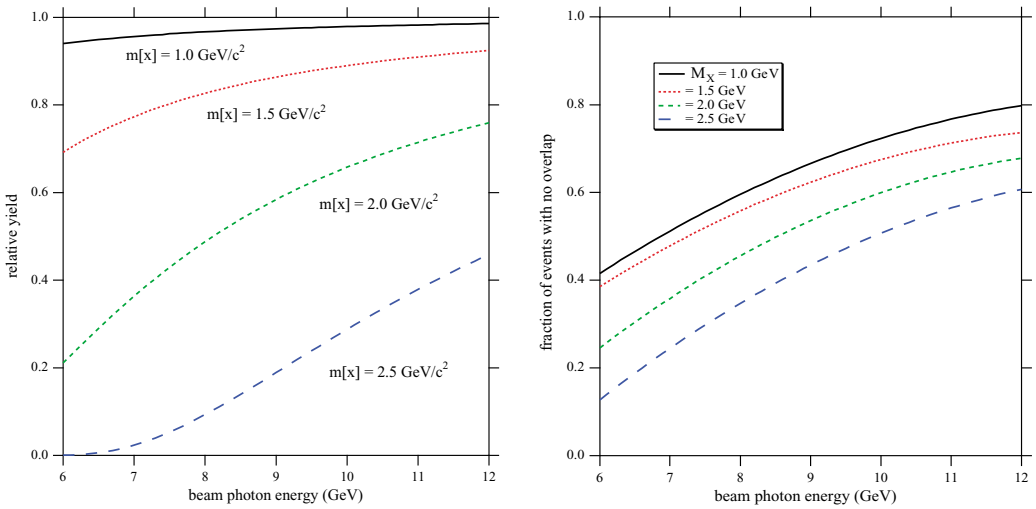

Figure 21: Various figures of merit to choose the optimal photon beam energy: (**a**) the relative meson yield as a function of photon beam energy for various meson masses (left); and (**b**) the fraction of events in which meson and baryon resonances are separated as a function of photon beam energy for various meson masses (right).

of linear polarization is plotted as a function of photon beam energy for three different values for the electron energy as well.

Finally, in Fig. 23 we plot an overall figure of merit that folds together the variation of beam flux and the degree of linear polarization with beam energy and with the effective yield (taking into account $|t|_{\rm min}$ effects and the ability to kinematically separate meson resonances from baryon resonances).

From this and other considerations we conclude that the optimum photon beam energy is between 8 and 9 GeV. The other considerations include the facts that for beam energies significantly below 8 GeV the line shape for resonances at the upper end of our mass range of interest is severely distorted, and for beam energies above 9 GeV, the momentum resolution for charged particles from two-particle decays of mesons at the lower end of our meson mass range is degraded since the transverse momentum of the decay products is small.

Taking all of these considerations into account, we find a clear *sweet spot* for the photon beam energy – 8 to 9 GeV . Of equal importance is that it is clearly desirable to have an electron energy as close as possible to the maximum energy achievable with the proposed Upgrade. The plots of Fig. 22 show the price of dropping this electron energy in terms of flux and polarization.

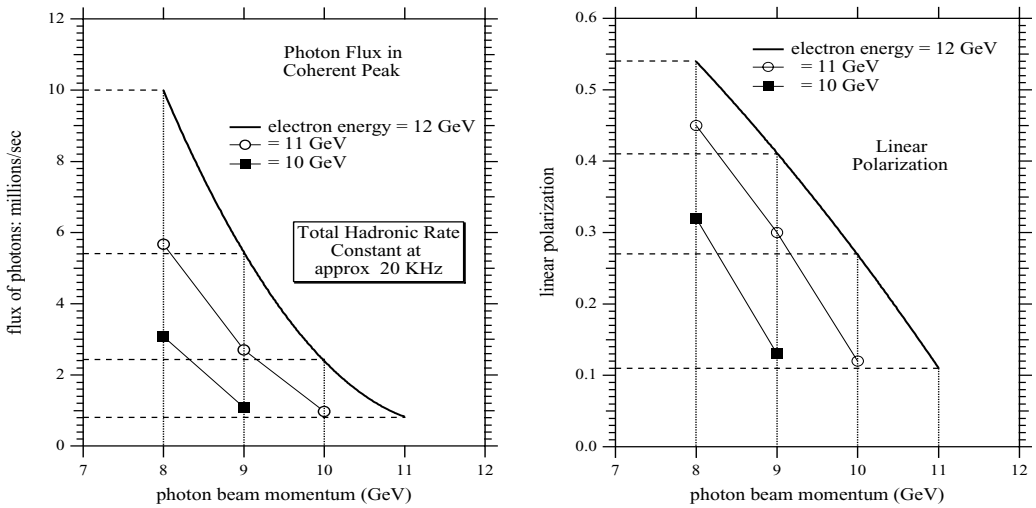

Figure 22: Photon beam flux and degree of linear polarization for various values of electron energy: (**a**) the flux dependence on photon beam energy (left); and (**b**) the degree of linear polarization dependence on photon beam energy (right).

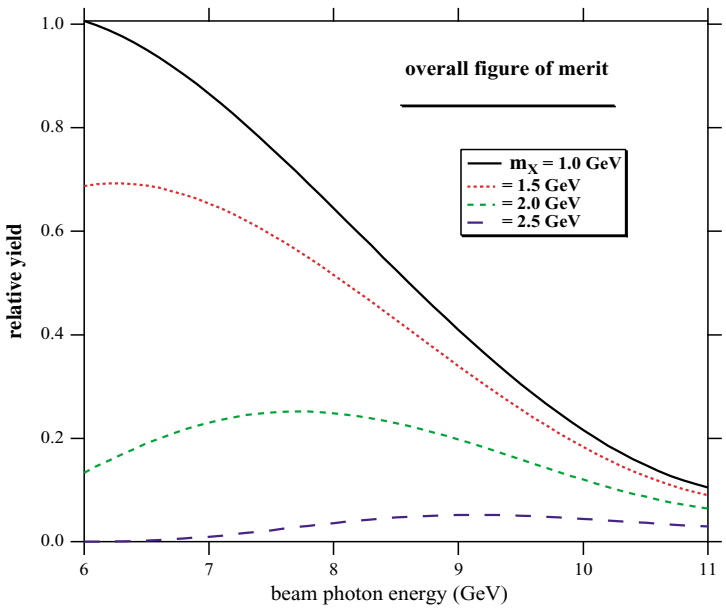

Figure 23: Figure of merit: relative meson yield as a function of photon beam energy for various meson masses and a fixed incident electron beam energy of 12 GeV.

2.A.5 External Review of the Hall D Project

The details of the civil construction, beam, detector, rates, and analysis will be presented in a later chapter of this White Paper. We point out here that a committee chaired by David Cassel (Cornell) and consisting of Frank Close (Rutherford Laboratory), John Domingo (Jefferson Lab), William Dunwoodie (SLAC), Donald Geesaman (Argonne), David Hitlin (Caltech), Martin Olsson (Wisconsin), and Glenn Young (Oak Ridge) reviewed the project plans in December 1999. The committee was asked to address three principal questions, whose answers were to be based on the answers to more detailed questions. The questions cover both the physics and the experimental technique [Ca00].

The physics motivation was described above and the technique, including the beam and detector, are discussed in greater detail in the discussion of Hall D. However, in order to provide some background to the review report summary below, we briefly point out the following about the beam and detector. The coherent bremsstrahlung technique involves passing a fine electron beam from the CEBAF accelerator though a wafer-thin diamond crystal: at special settings for the orientation of the crystal, the atoms of the crystal can be made to recoil together from the radiating electron, leading to the emission, at particular photon energies, of linearly polarized photons.

The use of a solenoidal spectrometer allows for the measurement of charged particles with excellent efficiency and momentum resolution while, at the same time, containing the shower of unwanted electron-positron pairs associated with the photon beam. One of the two largest components of the detector is the superconducting solenoid that was originally used in the LASS experiment at SLAC and later moved to LANL for the MEGA experiment. The other is the 3000-element lead glass detector originally built for the E852 experiment, which used the MPS at the Brookhaven AGS. Both components are available for use in Hall D, and their availability reduces the cost of the Hall D experimental apparatus by about $10M.

Review report summary

The questions posed to the review committee and their answers or conclusions were:

1. Evaluate the scientific opportunities presented by the Hall D project.

> *This collaboration proposes to explore systematically the light mesons (with masses up to about 2.5 GeV/c^2) with capabilities far beyond those of previous experiments. The copious spin and flavor initial states produced by photon beams will be an extremely*

useful tool in this endeavor. Thorough study of the masses, spins, parities, and charge conjugation states of these light mesons will require a complete partial wave analysis. This will provide a much deeper understanding of quark-antiquark states, and will as well permit a definitive search for mesons with exotic quantum numbers, particularly hybrid states and glueballs. This search is very high-priority physics, since the states involving excited glue, as well as quarkless glueball states, must exist if QCD is the correct theory of the strong interactions. JLab is unique in being able to provide the high-quality, low-emittance, cw photon beams that are required for this experiment. In addition, JLab and a significant segment of the JLab physics community are committed to this physics program. Together these provide a unique opportunity for exploring light meson states and making definitive searches for exotic states in this mass region.

2. Review the collaboration's approach to the realization of that facility.

The general design of the detector is technically sound. This is verified by a detailed comparison of the capabilities of the proposed Hall D detector with those of the successful LASS detector. This comparison leads to the conclusion that the proposed detector and beam combination will be able to realize the physics goals of the project. However, substantial effort must be invested to optimize the detector design and minimize the cost. The items requiring optimization that we have identified are described in detail in the report. These optimizations are part of the R&D required to prepare a conceptual design report (CDR) for the Hall D project. Preparation of a CDR with the associated work breakdown structure (WBS) and resource-loaded cost and schedule will require a project office at JLab with a project director and a well-structured organization designed to address the necessary R&D and optimization efforts.

3. Recommend R&D needed to optimize the facility design and to minimize the overall project cost.

The R&D item of greatest concern is ensuring that the magnet is still functional, particularly the fourth coil, which has not been used for at least 15 years. R&D should also include construction of prototypes to optimize detector design; to validate mechanical, electronic, and software choices; and to ensure the feasibility of the proposed coherent bremsstrahlung system.

The committee commented on the uniqueness of JLab for carrying out this search using the coherent bremsstrahlung beam:

> *JLab, with the energy upgrade, will be uniquely suited for providing such a beam. In particular, the excellent emittance of the JLab electron beam allows for strong collimation of the coherent bremsstrahlung radiation to enhance the polarization and ratio of tagged to untagged photons in the tagged photon beam. No other facility in the world will be able to provide a beam of this quality, with this combination of energy, duty factor, and emittance. If such a project were pursued at other existing high-energy facilities, either the data-taking rate would be dramatically reduced, compromising the physics goals, or a much more complicated detector would be required. We do not see any project at an existing accelerator complex (e.g., SLAC, CESR, DESY) which is likely to be able to compete with the Hall D initiative in this area.*

Since the report was issued in January 2000, the Hall D collaboration has started on an active R&D program to address issues of optimization and design. Work is underway in electronics, particle identification and tracking. The lead glass detector is now being moved from Brookhaven Lab to JLab.

Two areas of concern raised by the committee have now been addressed. An assessment team visited the Los Alamos National Laboratory (LANL) in March 2000 to examine the superconducting magnet and fourth coil. That team included the two engineers who originally designed, built, and tested the magnet for its use in the LASS spectrometer at SLAC and were also involved in the transfer of the magnet to LANL. The team found the magnet and fourth coil to be in excellent condition based on visual inspection, interviews with users and engineering and technical staff, and a review of written records. Another concern was the ability to obtain synthetic diamonds thin enough ($\approx$ 15 microns) to achieve the necessary collimation. Recently the group from the University of Glasgow has joined the Hall D collaboration. They have acquired sufficiently thin crystals and are making measurements of rocking curves with them.

In summary, the review committee recognized the uniqueness of an energy-upgraded CEBAF accelerator at JLab to carry out the *definitive searches* for the states required by QCD. The major concerns they raised have already been addressed. The program of R&D recommended for optimization and technology choices has started.

2.A.6 The Spectroscopy of $s\bar{s}$ Mesons

In order to carry out a complete search for exotic mesons, it will be necessary to understand the spectrum of normal mesons as well. They will both provide the references against which the exotic states will be observed, and mix with hybrids that have non–exotic quantum numbers. As such, understanding the normal meson spectrum will be a natural byproduct of the exotic searches in Hall D. Of particular interest with the normal mesons are the $s\bar{s}$ states, *strangeonium*.

The non-strange $n\bar{n}$ mesons (mesons built only from u and d) are fairly well established experimentally at lower masses, *albeit* with notable exceptions such as the scalar states. Taking 2.2 GeV/c^2 as a current frontier of light-meson spectroscopy, the quark model anticipates 44 $n\bar{n}$ states up to this mass. About half these mesons have been identified experimentally. Similarly we anticipate 22 kaonic J^{PC} levels ($n\bar{s}$ and $s\bar{n}$), and about two-thirds of these are known. In comparison the $s\bar{s}$ strangeonium states are a *terra incognita*: we consider only five $s\bar{s}$ states to be well established. These are the $\eta(547)$ and $\eta'(958)$ (counted as one $s\bar{s}$ state), $\phi(1019)$, $f_2'(1525)$, $\phi(1680)$, and the $\phi_3(1854)$. Other more controversial possibilities are $\eta(1295)/\eta(1440)$, $h_1'(1380)$, and $f_1(1420)$.

Photoproduction is an excellent technique for producing $s\bar{s}$ mesons, because the incident photon is, in effect, a vector-meson beam with a large ϕ-meson component. Much of the photon-hadron interaction takes place through vector dominance, in which the incident photon becomes a vector meson. The relative probability of interacting through the different light meson types is 9:1:2 for ρ°:ω:ϕ according to the quark model, and this relative coupling strength is approximately confirmed by the diffractive cross sections for vector-meson photoproduction. (There is an additional suppression of the $s\bar{s}$ cross section by about a factor of 2 that is not well understood.) Thus in photoproduction we have the opportunity to produce mesons with vector-meson beams of all diagonal light flavors $u\bar{u}$, $d\bar{d}$, and $s\bar{s}$, with a known relative luminosity between the flavors. At Hall D energies, and in the absence of a large $s\bar{s}$ component of the proton, diffractive photoproduction will presumably dominate the $s\bar{s}$ cross sections. Both of these produce exclusively $C = (-)$ states. The exception to this rule will be channels where t-channel exchanges of OZI-violating systems (like those of η-η') produce $s\bar{s}$ final states. Other mechanisms such as t-channel vector exchange can be expected to lead to photoproduction of $C = (+)$ $s\bar{s}$ states, albeit at a lower level. In contrast, hadronic production of $s\bar{s}$ states is suppressed because the initial hadrons provide, at most, one strange valence quark.

If these $s\bar{s}$ states were expected to be simple copies of the $n\bar{n}$ states, with the mass of each state simply shifted up by about 250 MeV/c^2, establishing the $s\bar{s}$ spectrum might be considered

a mundane exercise. However, recent studies within the context of Heavy Quark Effective Theory have shown that while sometimes u, d, s behave like an $\mathrm{SU(3)_{light}}$ multiplet (the Eightfold Way) and therefore do display such symmetry with respect to $n\bar{n}$ states, in other cases the s quark behaves like a heavy quark (s, c, b) and behaves like it is part of an $\mathrm{SU(3)_{heavy}}$ symmetry. One dramatic example of this occurs for the $Q\bar{d}$ mesons with $Q = b, c, s$, where the two L=1 states with J=1 (namely the $^3\mathrm{P}_1$ and $^1\mathrm{P}_1$ states) are measured to have the heavy-quark mixing angle of about 35° for not only $b\bar{d}$ and $c\bar{d}$ as expected, but also for $s\bar{d}$. That the s quark might have such a schizophrenic character was pointed out long ago by Gell-Mann: a light quark is defined to be one with a mass $\ll \Lambda_{\mathrm{QCD}}$, while a heavy quark is one with a mass $\gg \Lambda_{\mathrm{QCD}}$. Since $m_s \simeq \Lambda_{\mathrm{QCD}}$, the s quark straddles the border between these two worlds. Exploring the similarity between the $\bar{s}s$ spectrum and the $Q\bar{Q}$ systems needs to be understood to bridge the gap between Heavy Quark Effective Theory and the light-quark world in which we live.

The $s\bar{s}$ sector has other interesting features. For example, some decay modes should be very clean. These include channels such as $\phi\eta$, $\phi\eta'$, and $\phi\phi$, which, according to the Zweig rule, should only arise from $s\bar{s}$ initial states. One may also study channels such as $\phi\pi$, which are *not* expected as decays of $q\bar{q}$ states. One might find evidence for molecular states or Zweig-rule violation in this channel. Observation of both the $n\bar{n}$ and $s\bar{s}$ partners of a flavor nonet would be useful for establishing the $q\bar{q}$ (and $q\bar{q}g$ hybrid) spectrum, since the relative photoproduction amplitudes can be estimated. This would distinguish a $q\bar{q}$ or hybrid flavor nonet from a meson-meson molecule or a glueball, as molecules and glueballs do not span nonets.

The discovery of the CERN glueball candidate has emphasized the puzzling behavior of $s\bar{s}$ systems [Ba93, Se95, We94, Am95, Am96]. The observed decays of the $f_0(1500)$ are far from the flavor-symmetric pattern of: $\pi\pi : KK : \eta\eta : \eta\eta' = 3 : 4 : 1 : 0$ (for branching fraction divided by phase space) that one would expect from a simple model of glueball decay, and instead strongly favor $\pi\pi$. This may be due to an intrinsic quark mass dependence of these couplings (as suggested by the LGT results of Weingarten *et al.* [We94]), or (as suggested by Close and Amsler [Am95]) it may be due to a large $n\bar{n} \leftrightarrow G \leftrightarrow s\bar{s}$ mixing similar to the $n\bar{n} \leftrightarrow s\bar{s}$ mixing in the $\eta - \eta'$ system. While all J^{PC} channels will provide important information regarding $n\bar{n} \leftrightarrow s\bar{s}$ mixing, the most likely *a priori* to show a significant effect are the radial pseudoscalars (perhaps the $\eta(1295)$ and the $\eta(1440)$) and the 2^{-+} pseudotensors. The 2^{-+} states are interesting because some models predict this to be one of the lighter glueball channels. In addition, there are η_2 states at about 1.65 and 1.87 GeV/c^2 (reported by Crystal Barrel [Ad96]), both of which couple strongly to modes forbidden to $s\bar{s}$ by the Zweig rule. Understanding the $s\bar{s}$ states and how they are mixed is likely to provide a significant constraint on our understanding of QCD.

2.B Campaign 2: How are the Nuclear Building Blocks Made from Quarks and Gluons?

This section describes the dramatic progress that can be achieved in our understanding of the fundamental structure of the nuclear building blocks. One glaring gap in our knowledge exists in the region of the three basic "valence" quarks that mainly contribute at large x_{Bj}. Section 2.B.1 highlights the substantial improvements that can be reached probing parton distributions at large x_{Bj} using the deep inelastic scattering process.[1] Such a process measures a diagonal matrix element (*i.e.*, initial and final state are the same) of QCD field operators. Recently, a generalization of these parton distributions encompassing the description of exclusive processes was developed. Section 2.B.2. describes the strategy needed to verify that one is in the domain where these generalized distributions can be accessed. In the most straightforward example, deeply virtual Compton scattering, one can gain supplementary information on partons in the intermediate and large x_{Bj} region. Here one accesses non-diagonal matrix elements of QCD field operators. Similarly, in this framework hadronic form factors access a non-diagonal matrix element of local QCD field operators. Thus, hadronic form factors are related to the same generalized parton distribution functions. As such, we highlight in Section 2.B.3 the substantial progress one can reach in hadronic form factor measurements.

Deep inelastic inclusive scattering shows that scaling at modest Q^2 and ν already arises from very few resonance channels. This duality reflects the transition from strongly interacting matter to a quark-gluon theory, and thus is of fundamental importance. If quantitatively understood, low-energy quark-hadron duality can be used to obtain precise constraints for parton distributions at even larger x_{Bj}. This is described in Section 2.B.4. Lastly, in semi-inclusive meson production the scattering and production mechanisms factorize at high energy. To what extent this factorization applies at lower energy is an open question. Confirmation of factorization at lower energies would open a rich semi-inclusive program, as discussed in Section 2.B.5, allowing an unprecedented spin/flavor decomposition of parton distributions.

[1] In this section x_{Bj} is used for "Bjorken-x", the deep inelastic scattering scaling variable (which ranges from $0 \to 1$) rather than the simpler notation, x, used in the executive summary. This has been done to avoid confusion with the variable x used in the Generalized Parton Distributions (GPD's) discussed in this section; for the GPD's, x denotes the generalized parton momentum distribution (which ranges from $-1 \to 1$ because it includes the antiquark distribution).

2.B.1 Valence Quark Momentum Distributions

One of the most fundamental properties of the nucleon is the structure of its valence quark distributions, since they are the irreducible kernel of each hadron. Sea quarks, which at very high Q^2 are largely generated in perturbative QCD through gluon bremsstrahlung and subsequent splitting into quark-antiquark pairs, at low Q^2 represent one source of the nonperturbative "meson cloud contributions" that act as "dressing" on the valence quarks. At higher x values these $q\bar{q}$ complications drop away, and the simple physics of the valence quark model is exposed [Is99].

Experimentally, most of the recent studies of nucleon structure have emphasized the small-x_{Bj} region populated mainly by sea quarks (x_{Bj} being the fraction of momentum of the nucleon carried by the quark), while the valence quark structure has for some time now been thought to be understood. Three decades of deep inelastic and other high-energy scattering experiments have provided a detailed map of the nucleon's quark distributions over a large range of kinematics with one major exception – the deep valence region, at very large x_{Bj} ($x_{Bj} \gtrsim 0.5$). In this region the valence structure of the nucleon can be probed most directly, since sea quark distributions, which must be subtracted from the measured cross sections to reveal the valence structure, are negligibly small beyond $x_{Bj} \sim 0.2 - 0.3$. It is both surprising and unfortunate that the large-x_{Bj} region has been so poorly explored experimentally.

This situation is clearly evident in the valence u and d quark distributions, which are usually obtained from measurements of the proton and neutron structure functions, F_2^p and F_2^n, respectively. At leading order these functions are defined as the charge-squared weighted sums of the quark and antiquark distributions of various flavors ($q = u, d, s, \ldots$):

$$F_2(x_{Bj}) \;=\; 2x_{Bj}F_1(x_{Bj}) \;=\; x_{Bj} \sum_q e_q^2 \left(q(x_{Bj}) + \bar{q}(x_{Bj})\right) \;. \tag{7}$$

While the u quark distribution is relatively well constrained by the F_2^p data for $x_{Bj} < 0.8$, the absence of free neutron targets has left large uncertainties in the d quark distribution beyond $x_{Bj} \sim 0.5$ arising from incomplete understanding of the nuclear medium modifications in the deuteron, from which F_2^n is extracted. For instance, depending on whether one does or does not correct for Fermi motion and binding (off-shell) effects in the deuteron, the extracted $R^{np} \equiv F_2^n/F_2^p$ ratio can differ by $\sim 50\%$ already at $x_{Bj} \sim 0.75$ [Me96, Wh92] (see Fig. 24).

These large uncertainties have prevented answers to such basic questions as why the d quark distribution at large x_{Bj} appears to be smaller (or "softer") than that of the u, softer even than what would be expected from flavor symmetry. Furthermore, since the precise $x_{Bj} \to 1$ behavior of the d/u ratio is a critical test of the mechanism of spin-flavor symmetry breaking, the large errors on

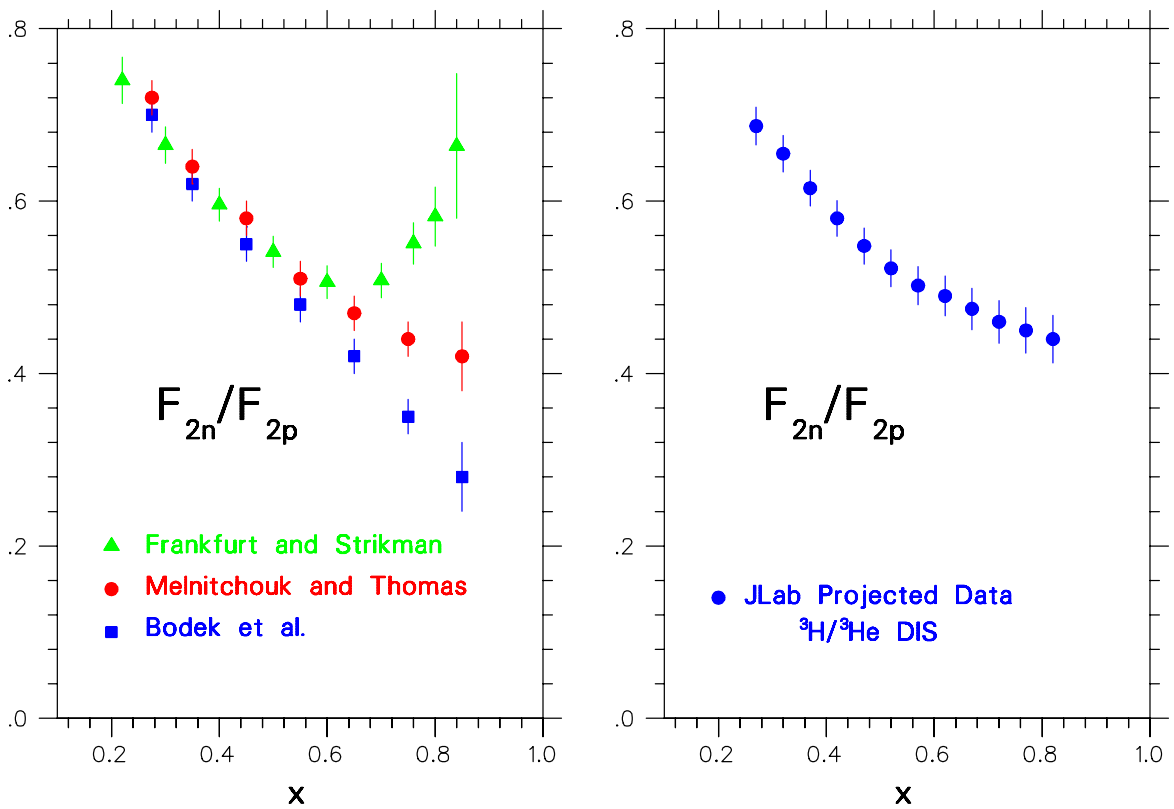

Figure 24: Ratio R^{np} of neutron to proton structure functions as a function of x_{Bj}, extracted from the SLAC data on the deep inelastic proton and deuteron structure functions. The left panel represents R^{np} extracted according to different prescriptions for treating nuclear effects in the deuteron: Fermi smearing only [Bo81, Wh92], Fermi motion and nuclear binding corrections [Me96], and assuming the nuclear EMC effect in the deuteron scales with nuclear density [Fr88]. The right panel shows the projected data with total (statistical, systematic, and model-dependent) errors for the proposed ^{3}H and ^{3}He JLab experiment.

the current data preclude any definitive conclusions about the fundamental nature of quark-gluon dynamics in the valence quark region. From another perspective, knowledge of quark distributions at large x_{Bj} is also essential for determining high-energy cross sections at collider energies, such as in searches for new physics beyond the standard model [Ku00], where structure information at $x_{Bj} \sim 0.6 - 0.8$ feeds down to lower x_{Bj} at higher values of Q^2 through perturbative Q^2 evolution.

The need for reliable large-x_{Bj} data is even more pressing for the spin-dependent quark distributions. Spin degrees of freedom allow access to information about the structure of hadrons not available through unpolarized processes. Spin-dependent quark distributions are usually extracted from measurements of the spin-polarization asymmetry, A_1, which is approximately given by the ratio of spin-dependent to spin-averaged structure functions:

$$A_1(x_{Bj}) \approx \frac{g_1(x_{Bj})}{F_1(x_{Bj})} , \tag{8}$$

where, to leading order,

$$g_1(x_{Bj}) = \sum_q e_q^2 \ (\Delta q(x_{Bj}) + \Delta\bar{q}(x_{Bj})) \ , \tag{9}$$

with Δq defined as the difference between quark distributions with spin aligned and anti-aligned with the spin of the nucleon, $\Delta q = q \uparrow - q \downarrow$. The first spin structure function experiments at CERN [As88] on the moment, or integral, of g_1, suggested that the total spin carried by quarks was very small, or even zero, prompting the so-called "proton spin-crisis". A decade of subsequent measurements of spin structure functions using proton, deuteron, and ^{3}He targets have determined the total quark spin much more accurately, with the current world average value being $\sim 30\%$ [La98a], which is still considerably less than the value expected from the most naïve quark model in which valence quarks carry all of the proton spin.

While the spin fractions carried by quarks and gluons (or generically, partons) are obtained by integrating the spin-dependent parton momentum distributions, the distributions themselves, as a function of the momentum fraction x_{Bj}, contain considerably more information about the quark-gluon dynamics than their integrals do. Furthermore, the spin-dependent distributions are generally even more sensitive than the spin-averaged ones to the quark-gluon dynamics responsible for spin-flavor symmetry breaking. Considerable progress has been made in measuring spin-dependent structure functions over the last decade, especially in the small x_{Bj} region. However, relatively little attention has been paid to the polarized structure functions in the pure valence region at large x_{Bj}. The lack of data in the valence region is particularly glaring in the case of the neutron, where there is no information at all on the polarization asymmetry A_1^n for $x_{Bj} \geq 0.4$. This is unfortunate, since there are rigorous QCD predictions for the behavior of A_1 as $x_{Bj} \to 1$ that have never been tested.

Theoretical predictions for large-x_{Bj} distributions

The simplest model of the proton, polarized in the $+z$ direction, has three quarks described by a wavefunction that is symmetric in spin and flavor [Cl73]:

$$\begin{aligned} |p\uparrow\rangle \;\; = \;\; & \frac{1}{\sqrt{2}}\,|u\uparrow(ud)_{S=0}\rangle \;+\; \frac{1}{\sqrt{18}}\,|u\uparrow(ud)_{S=1}\rangle \;-\; \frac{1}{3}\,|u\downarrow(ud)_{S=1}\rangle \\ & -\frac{1}{3}\,|d\uparrow(uu)_{S=1}\rangle \;-\; \frac{\sqrt{2}}{3}\,|d\downarrow(uu)_{S=1}\rangle\;, \end{aligned} \tag{10}$$

where $q\uparrow\downarrow$ represents the active quark that undergoes the deep inelastic collision, and $(qq)_S$ denotes the two-quark configuration with spin S that is a spectator to the scattering. (The neutron wavefunction can be obtained by simply interchanging the u and d quarks in this expression.) On the basis of exact spin-flavor symmetry, which is described by the group SU(6), the $S=0$ and $S=1$ "di-quark" states contribute equally, giving rise to simple relations among the quark distributions, such as $u=2d$ and $\Delta u=-4\Delta d$, which in terms of the structure functions correspond to:

$$R^{np}\equiv F_2^n/F_2^p=\frac{2}{3};\quad A_1^p=5/9;\quad \text{and}\quad A_1^n=0. \tag{11}$$

In nature the spin-flavor SU(6) symmetry is, of course, broken. It has been known for some time that the d quark distribution is softer than the u quark distribution, reflecting the fact that the neutron-to-proton ratio R^{np} (shown in Fig. 24) deviates strongly from the SU(6) expectation beyond $x_{Bj}\sim 0.4$. On the other hand, the data for the polarization asymmetries A_1^p and A_1^n (shown in Fig. 25) are so poor in the valence region that it is presently not possible to discern whether the SU(6) predictions are borne out for the spin-dependent distributions.

A number of models have been developed for quark distributions that incorporate mechanisms for the breaking of the SU(6) symmetry; some of these models can be linked directly to phenomena such as the hyperfine splitting of the baryon and meson mass spectra. Feynman and others [Fe72, Cl73, Ca75a] observed that there was a correlation between the nucleon and Δ mass difference and the suppression of R^{np} at large x_{Bj}. A quark hyperfine interaction, such as that due to one-gluon exchange, instantons or pion exchange (which can induce a higher energy for the $S=1$ spectator "di-quark" in Eq.(10)) will necessarily give rise to a larger mass for the Δ since the quark wavefunction for the Δ has all "di-quark" configurations with $S=1$. If the $S=0$ states are dominant at large x_{Bj}, Eq.(10) implies that the d quark distribution will be suppressed relative to that of the u in the valence quark region. This expectation has, in fact, been built into most phenomenological fits to the parton distribution data [Ei84, Di88, Ma94a, La95]. This mechanism also leads to specific predictions for the polarization asymmetries as $x_{Bj}\to 1$:

$$R^{np}\to\frac{1}{4};\quad A_1^p\to 1;\quad \text{and}\quad A_1^n\to 1\;. \tag{12}$$

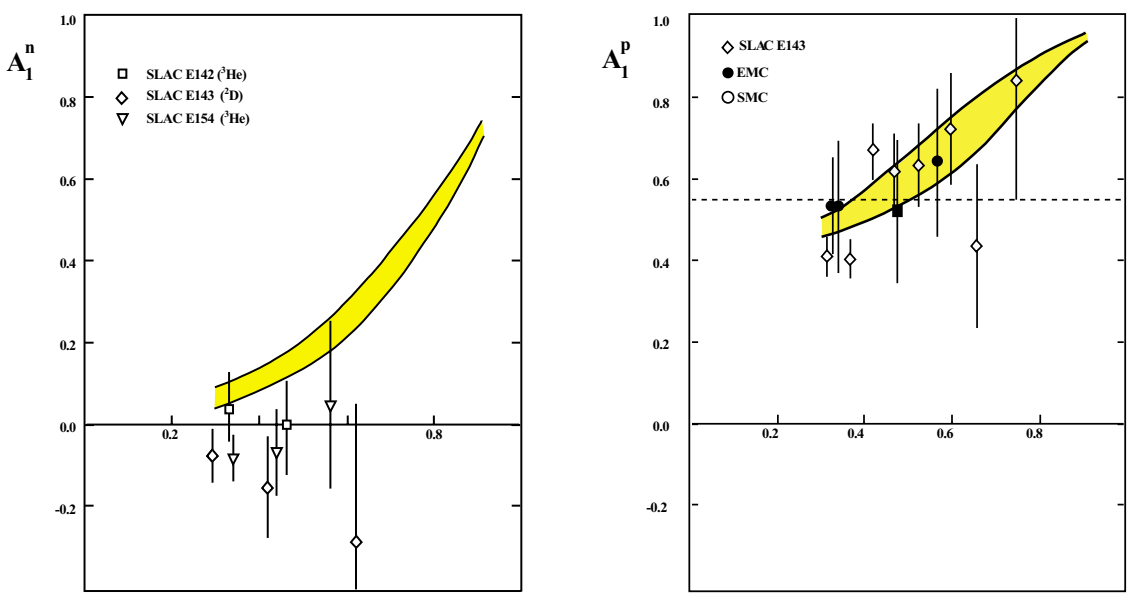

Figure 25: Sample of large-x_{Bj} data for A_1^n (left) and A_1^p (right). The predictions of SU(6) for $x_{Bj} \to 1$ are $A_1^n = 0$ and $A_1^p = 5/9$ (dashed line). The shaded bands are broken SU(6) valence quark model predictions versus x_{Bj} for A_1^n and A_1^p, as evaluated in Ref. [Is99].

More radical nonperturbative models of SU(6) breaking, such as those which include instantons as important degrees of freedom, predict dramatically different behavior for A_1^n as $x_{Bj} \to 1$; *i.e.*, that it goes to a low value close to zero [Ko97, Kopc].

Arguments based on perturbative QCD, on the other hand, predict that the dominant components of the proton valence wavefunction at large x_{Bj} are those associated with states in which the total "di-quark" spin projection, S_z, is zero [Fa75]. Consequently, scattering from a quark polarized in the opposite direction to the proton polarization is suppressed relative to the helicity-aligned configuration. From Eq.(10) this leads to the predictions in the $x_{Bj} \to 1$ limit:

$$R^{np} \to \frac{3}{7}; \quad A_1^p \to 1; \quad \text{and} \quad A_1^n \to 1 \; . \tag{13}$$

The novelty of these predictions, especially for A_1^p and A_1^n, is that they follow essentially directly from perturbative QCD in the limit of $Q^2 \to \infty$ and $x_{Bj} \to 1$. However, it is not clear *a priori* at which x_{Bj} and Q^2 the transition from the nonperturbative dynamics, embodied in the predictions (12), to perturbative QCD takes place, so experimental guidance on this issue is essential.

While the trend of the existing R^{np} data is consistent with models with broken SU(6) symmetry, they cannot discriminate between the competing mechanisms of SU(6) breaking (as evident from Fig. 24) because of uncertainties in the extraction procedure associated with nuclear corrections. For the asymmetries A_1^n and A_1^p, while we do not expect the SU(6) predictions to be accurate, the existing measurements at high x_{Bj} lack the precision to even distinguish any of the predictions from the naïve SU(6) result.

The ratio $R^{np} = F_2^n/F_2^p$ of the neutron and proton structure functions

If the nuclear EMC effect (the modification of the free nucleon structure function in the nuclear environment) in deuterium were known, one could apply nuclear smearing corrections directly to the deuterium data to obtain the free neutron F_2^n. However, the EMC effect in the deuteron requires knowledge of the free neutron structure function itself, so the argument becomes cyclic. The best way to reliably determine R^{np}, free of the large uncertainties associated with nuclear corrections at large x_{Bj}, is through simultaneous measurements of the inclusive ^{3}He and ^{3}H structure functions, maximally exploiting the mirror symmetry of $A = 3$ nuclei. Regardless of the absolute value of the nuclear EMC effect in ^{3}He or ^{3}H, the differences between the EMC effects in these nuclei will be small (on the scale of charge symmetry breaking in the nucleus).

In the absence of a Coulomb interaction, and in an isospin-symmetric world, the properties of a proton (neutron) bound in the ^{3}He nucleus would be identical to those of a neutron (proton) bound

in the ^{3}H nucleus. If, in addition, the proton and neutron distributions in ^{3}He (and in ^{3}H) were identical, the neutron structure function could be extracted with no nuclear corrections, regardless of the size of the EMC effect in ^{3}He or ^{3}H separately.

In practice, ^{3}He and ^{3}H are of course not perfect mirror nuclei – their binding energies for instance differ by some 10% – and the proton and neutron distributions are not quite identical. However, the $A = 3$ system has been studied for many years, and modern realistic $A = 3$ wavefunctions are known to rather good accuracy. Using these wavefunctions, together with a nucleon spectral function, the difference in the EMC effects for the ^{3}He and ^{3}H nuclei has been calculated [Af00b, Pa00, Ci90, Uc88] to be less than 2% for $x_{Bj} < 0.85$. More importantly, the actual model dependence of this difference is less than 1% for all x_{Bj} values accessible experimentally with an 11 GeV beam.

By performing the tritium and helium measurements under identical conditions, the ratio of the deep inelastic cross sections for the two nuclei can be measured with 1% experimental uncertainty (SLAC Experiments E139 [Go94] and E140 [Da94, Ta96] have quoted 0.5% uncertainties for measurements of ratios of cross sections). Deep inelastic scattering with the proposed 11 GeV JLab electron beam can therefore provide precise measurements for the $F_2^{^3\mathrm{He}}/F_2^{^3\mathrm{H}}$ ratio, from which R^{np} can be extracted essentially free of nuclear corrections at the 1% level over the entire range $0.10 \leq x_{Bj} \leq 0.82$. In addition, it will for the first time enable the size of the EMC effect to be determined in $A = 3$ nuclei, which to date has been measured only for $A \geq 4$ nuclei. The key issue for this experiment will be the availability of a high-density tritium target, comparable with the previously used Saclay [Am94] and MIT-Bates [Be89] tritium targets. The quality of the projected data is highlighted in Fig. 24 and in Fig. 6 of the executive summary.

The neutron spin structure function A_1^n

While data on R^{np} and A_1^p give some indication of the large-x_{Bj} behavior of the valence quark distributions at $x_{Bj} \lesssim 0.5$, the experimental situation for the neutron A_1^n at large x_{Bj} is totally unclear. The statistical precision of the data available does not even allow a meaningful statement about the qualitative behavior of A_1^n for $x_{Bj} > 0.4$. The experiment proposed here, as outlined in the executive summary, will use the 11 GeV JLab electron beam to perform a precision measurement of A_1^n, utilizing the Hall A polarized ^{3}He target and the proposed MAD (Medium-Acceptance Device) spectrometer. Because the neutron in ^{3}He carries almost 90% of the nuclear spin, polarized ^{3}He is an ideal source of polarized neutrons [Fr90].

The experiment involves measurement of the polarization asymmetry, $A_1^{^3\mathrm{He}}$, defined as:

$$A_1^{^3\mathrm{He}}(x_{Bj}) \approx \frac{1}{D}\frac{d\sigma^{\uparrow\downarrow} - d\sigma^{\uparrow\uparrow}}{d\sigma^{\uparrow\downarrow} + d\sigma^{\uparrow\uparrow}} \ , \tag{14}$$

where $d\sigma^{\uparrow\uparrow}$ ($d\sigma^{\uparrow\downarrow}$) is the cross section for scattering polarized electrons from a polarized ^{3}He target with the beam and target helicities parallel (antiparallel) and D is a kinematic factor relating the virtual photon polarization to that of the electron. The neutron asymmetry A_1^n is extracted from $A_1^{^3\mathrm{He}}$ after correcting for residual nuclear effects in ^{3}He associated with Fermi motion and binding, using modern three-body wavefunctions [Wo89, Ci93a, Sc93], similar to those used in correcting for nuclear effects in $F_2^{^3\mathrm{He}}$ discussed in the previous section. Furthermore, because the asymmetry is a ratio of nuclear structure functions, the nuclear effects on A_1^n will be considerably smaller than those associated with absolute structure functions. In addition to the use of the polarized ^{3}He target, other polarized targets (ND_3 and NH_3)will be used for cross checks and for the investigation of the nuclear effects.

An example of the kinematics relevant for this experiment is given in Table 2. (Note that substantial improvements in the measurement of A_1^p at large x_{Bj}, or A_1^n at large x_{Bj} using polarized solid-state NH_3 and ND_3 targets, would also be possible with an 11 GeV cw beam). To illustrate the improvement of the projected results obtainable with JLab at 11 GeV compared with previously measured data from other facilities we introduce a figure of merit (FOM) $= D^2 \times \mathrm{Rate} \times f^2$, which allows a meaningful comparison between different laboratories. Here "Rate" takes into account the use of the proposed Medium-Acceptance Device spectrometer, and f is the dilution factor defined as the ratio of polarized nucleons to the total number of nucleons in the target. Table 2 shows the comparison between the relevant parameters at competitive existing laboratories at comparably large x_{Bj} and Q^2. Note that with increasing beam energy the depolarization factor decreases. The lowest beam energy, therefore, which guarantees access to the large-x_{Bj} region in the Bjorken limit is optimal. The anticipated data are shown in Fig. 26. JLab at 11 GeV would enable access to $x_{Bj} \lesssim 0.8$ at $W^2 \approx 4$ GeV.

Higher-twist effects and the g_2^n structure function

While the g_1 structure function has a simple interpretation in the quark-parton model in terms of quark helicity distributions and has been the focus of extensive experimental programs over the last decade, there have been few dedicated experimental studies of the g_2 structure function. The g_2 structure function is related to the transverse polarization of the nucleon, and although it does not have a simple quark-parton model interpretation, it contains important information about quark-gluon correlations within the nucleon.

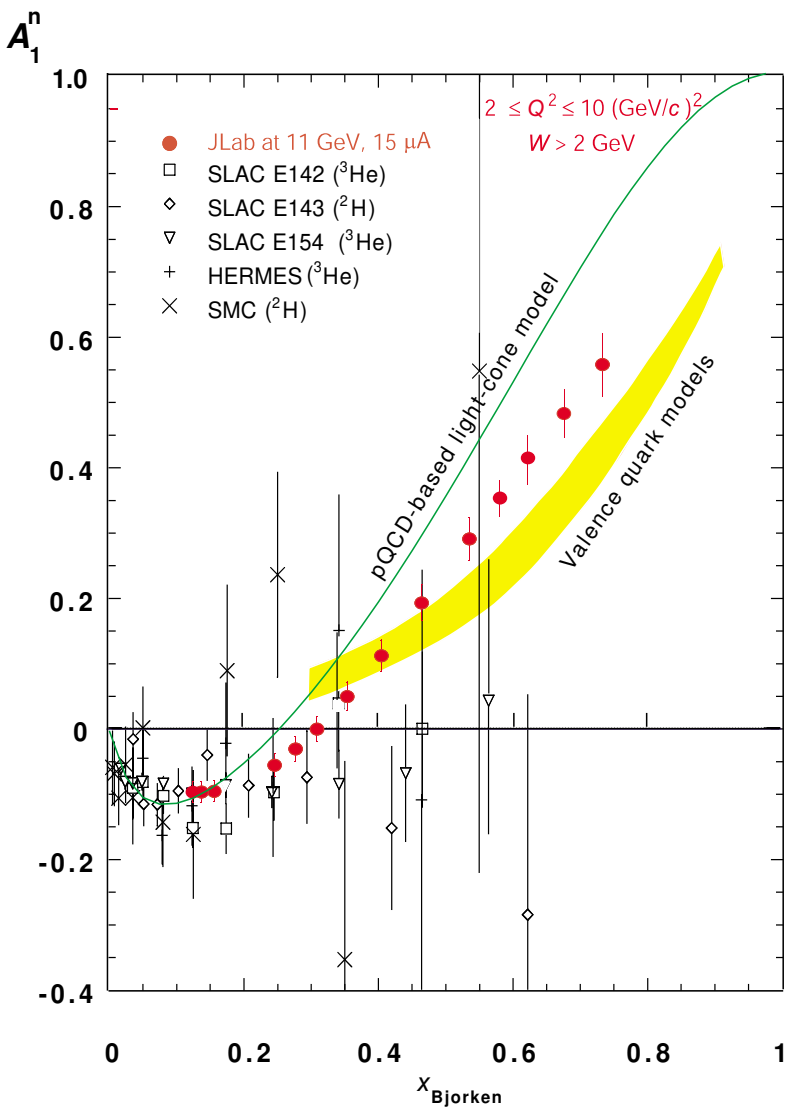

Figure 26: Simulated data for a measurement of A_1^n in the large Bjorken-x region, where it is determined by the spin structure of the valence quarks, made possible by the proposed 12 GeV Upgrade.

Table 2: Comparison of the figure of merit (FOM) for large x_{Bj} measurements of the A_1^n structure function at HERA, SLAC, and JLab.

Expt. name	E_i (GeV)	E' (GeV)	θ (deg.)	x_{Bj} bin	Q^2 $(\mathrm{GeV}/c)^2$	D	f	Rate (Hz)	FOM (10^{-4})
HERMES	35.0	17.0	5.2	0.60-0.70	9.1	0.22	0.3	0.05	2
SLAC E143	29.13	25.5	7.0	0.60-0.70	9.1	0.29	0.2	0.3	10
JLab	11.0	4.4	25	0.60-0.70	8.5	0.67	0.3	2.7	1000

In QCD the quark-gluon correlations are associated with so-called higher twist operators (where "twist" is defined as the difference between dimension and spin of an operator), which are suppressed by additional factors of $1/Q$ relative to the leading twist contribution (which is associated with free quark scattering). At large values of Q^2, QCD allows one to relate moments of spin structure functions to the matrix elements of operators of given twist. The simplest twist-3 matrix element that contains information on quark-gluon correlations is given by:

$$d_2(Q^2) \;=\; \int_0^1 dx_{Bj}\; x_{Bj}^2 \Big[2g_1(x_{Bj},Q^2) + 3g_2(x_{Bj},Q^2)\Big] \tag{15}$$

Note that because of the x_{Bj}^2 weighting in Eq.(15), d_2 is dominated by the large-x_{Bj} behavior of g_1 and g_2. The physical significance of d_2 is that it reflects the response of a quark to the polarization of the gluon color field in the nucleon, $d_2 = (2\chi_B + \chi_E)/3$, with χ_B (χ_E) the gluon-field polarizability in response to a color magnetic (electric) field $\vec{B}$ ($\vec{E}$) [St95].

Published data for g_2 were obtained from experiments E142-E155 at SLAC [Ab96] and the SMC experiment at CERN [Ad93]. The world's best data will soon be published from the recent E155x experiment at SLAC, which measured g_2 for proton and deuteron. Using preliminary results from this experiment [Bo00], values for g_2 for the neutron were extracted and are shown in Fig. 27. The curve labeled "g_2^{WW}" represents the leading twist contribution to g_2 [Wa77]. Using these data, a nonzero positive value for d_2^n has been extracted that is in disagreement with all of the theoretical calculations. However, in most cases, the disagreement is less than 1σ, and the size of the experimental error does not allow one to make a conclusive statement about the importance of higher-twist effects in the nucleon.

A 12 GeV JLab experiment will make a factor of 10 statistical improvement in the error on d_2^n, by taking advantage of the high-luminosity 11 GeV beam and the large-acceptance MAD spectrometer. Precision data for g_2 will be obtained in the range $0.15 \le x_{Bj} \le 0.8$, $W > 2$ GeV, for example at $Q^2 = 5$ $(\mathrm{GeV}/c)^2$, with special focus on the high-x_{Bj} region which dominates d_2. Projected uncertainties for such an experiment are indicated by the squares in Fig. 27.

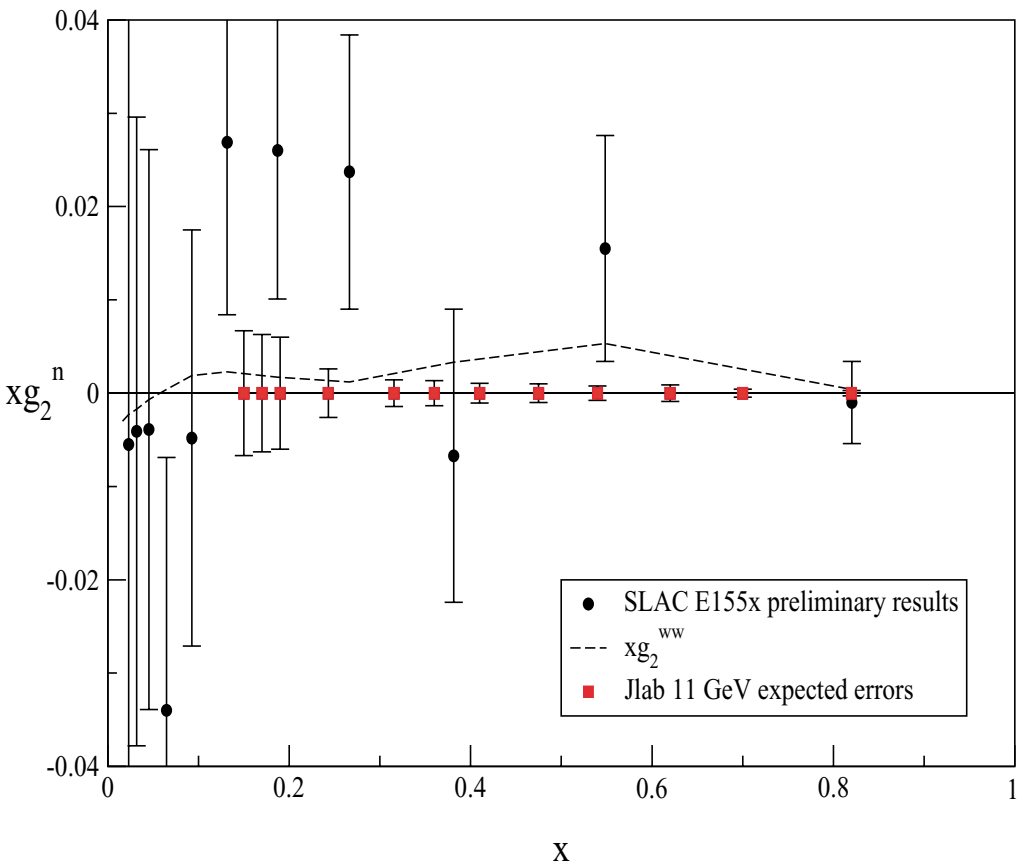

Figure 27: The preliminary results for the g_2^n spin structure function from SLAC experiment E155x. The dashed curve shows the Wandzura-Wilczek [Wa77] calculation of the leading twist contribution to g_2^n. The open squares are the expected uncertainties from an 11 GeV JLab measurement.

2.B.2 Deep Exclusive Scattering (DES) Cross Sections and Generalized Parton Distributions

Exclusive reactions allow us to determine new aspects of the nucleon structure which can be understood within the formalism of Generalized Parton Distributions. Inclusive measurements probe the longitudinal momentum distribution of quarks inside the nucleon. The exclusive measurements of photons and mesons probe the full nucleon wavefunction at the amplitude level and, for example, will shed light on the distribution of the transverse momentum of quarks, determine the contribution of the quark angular momentum to the spin of the proton, and measure quark-quark correlations through non-diagonal matrix elements.

The standard feature of applications of perturbative QCD to hard processes is the introduction of phenomenological functions describing nonperturbative long-distance dynamics. Thus, much of the internal structure of the nucleon, in the form of parton distribution functions, was revealed over the past three decades through the inclusive scattering of high-energy leptons on the nucleon in the Bjorken or "Deep Inelastic Scattering" (DIS) regime (Q^2 and ν large, with $x_{Bj} = Q^2/2M\nu$ finite). Simple theoretical interpretations of the experimental results and quantitative conclusions were reached in the framework of the parton model and QCD when summing over all possible hadronic final states. The parton distribution DIS functions inferred from DIS data are probabilities, and, for example, unpolarized (polarized) DIS revealed that the quarks carry about 50% (25%) of the nucleon's momentum (spin).

In contrast, in the asymptotic QCD regime one can extract information from exclusive processes on distribution amplitudes $\varphi(x)$ [Ch77, Fa79, Ra77, Ef80, Br79a, Br80]. For instance, $\varphi_{\pi^+}(x)$ gives the probability amplitude of finding a (positive) fast-moving pion in a quark-antiquark state $u\bar{d}$, with the longitudinal pion momentum p shared in fractions x and $1-x$:

$$\varphi_{\pi^+}(x) \sim \Psi\{\pi^+(p) \to u(xp) + d((1-x)p)\} \ . \tag{16}$$

The two types of nonperturbative functions, parton distribution functions and distribution amplitudes (Fig. 28), provide complementary information about the hadronic structure. These latter functions are wavefunctions, not probabilities.

Recently the formalism of the Generalized Parton Distributions (GPD's) has been developed [Ji97, Ra96]. These hybrid functions generalize the features of the usual parton distribution functions, the hadron distribution amplitudes, and the electromagnetic form factors, and provide a unifying description for these fundamental quantities of hadronic structure. The GPD's contain a wealth of information about the transverse momentum and angular momentum carried by the

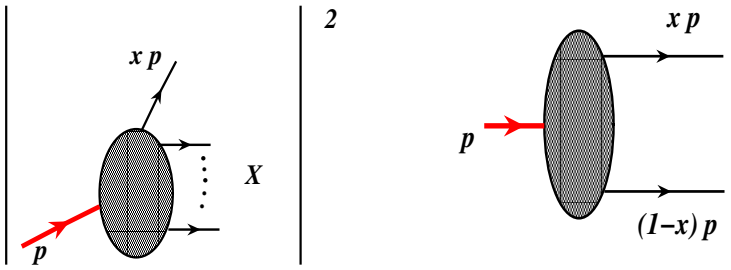

Figure 28: The parton distribution function (left) and the pion distribution amplitude (right).

quarks in the proton, and can be accessed through hard exclusive electroproduction of mesons and photons.

The GPD's $\tilde{H}^a(x,\xi;t)$, $\tilde{E}^a(x,\xi;t)$, $H^a(x,\xi;t)$, and $E^a(x,\xi;t)$, where $a = u, d, \ldots$ denotes the quark flavor, were called off-forward parton distributions when first introduced by X. Ji [Ji97]. [2] They correspond to a description (Figs. 29 and 30) in which the initial (h_i) and final (h_f) hadrons are treated in a symmetric way: the longitudinal momentum of the initial hadron is written as $p = (1+\xi)P$ and that of the final one as $p' = (1-\xi)P$. Here, the skewedness parameter ξ, or the longitudinal-momentum fraction of the transfer Δ, is related to x_{Bj} by

$$\xi = \frac{x_{Bj}}{2 - x_{Bj}} \tag{17}$$

and $P = (p+p')/2$ is the average momentum of the initial and final hadron.

The longitudinal momentum of the initial, struck, parton in Figs. 29 and 30 is written as $(x+\xi)P$ and that of the final parton as $(x-\xi)P$. Note that ξ varies between 0 and 1, and x, the momentum fraction of the struck quark in the quark loop, varies between -1 and 1. As such, x is not directly accessible experimentally. Lastly, $t = \Delta^2$ is the standard momentum transfer between the virtual photon and the final-state meson. Thus,

$$H^a(x,\xi;t) \sim \sum_X \Psi\{h_i(1+\xi) \to a(x+\xi) + \text{“}X\text{”}\} \times \Psi^*\{h_f(1-\xi) \to a(x-\xi) + \text{“}X\text{”}\}\ , \tag{18}$$

where “X” denotes all the intermediate states in the “soft” blob of Fig. 30. In the forward limit, when $p = p'$ [*i.e.*, $t = 0$ and $\xi = 0$], the GPD's H^a ($\tilde{H}^a$) collapse to the usual spin-independent

[2] A. Radyushkin [Ra96] introduced similar functions, which he called nonforward parton distributions (NFPD's; see also [Co97]). OFPD's and NFPD's can be treated as specific cases of skewed or generalized parton distributions.

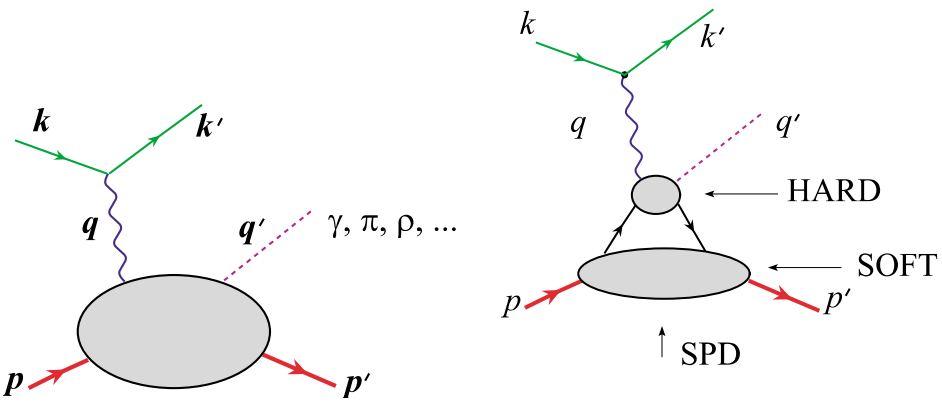

Figure 29: Hard electroproduction processes: the general structure (left); and perturbative QCD factorization (right).

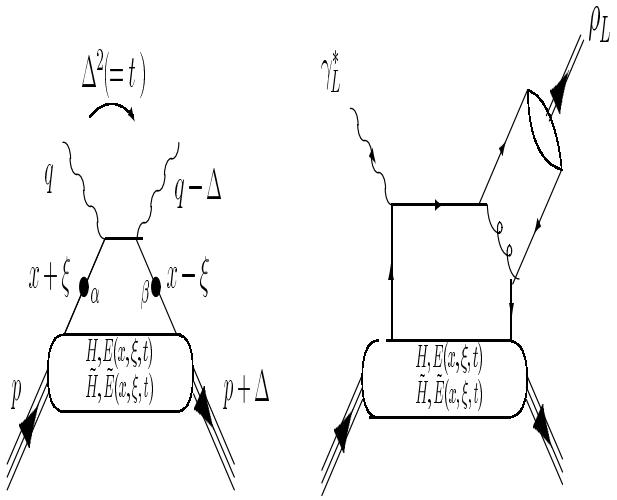

Figure 30: "Handbag" diagrams for DVCS (left) and meson production (right).

(spin-dependent) parton distribution functions measured in inclusive processes such as deep inelastic scattering. Furthermore, in a nonforward kinematics (a non-inclusive process), GPD's contain much richer information about the parton correlations. The latter can be nondiagonal in hadron/parton momenta and in hadron/parton spin, and can even correspond to different hadrons in the initial and final state (*e.g.*, one can consider matrix elements corresponding to $p \to n$, $N \to \Delta$, $N \to \Lambda$, etc. transitions).

The spin-independent (spin-dependent) GPD's H, E ($\tilde{H}, \tilde{E}$) provide detailed information about the nucleon structure: they are sensitive not only to probabilities but also to interference between different components of the nucleon wavefunction. The GPD's reflect the structure of the nucleon independent of the reaction that probes the nucleon. They can be accessed through the hard exclusive electroproduction of mesons ($\pi^{0,\pm}$, $\rho^{0,\pm}$, ω, ϕ,... ; see Fig. 30b) for which a QCD factorization proof has been given [Co97]. In this proof it was shown that factorization applies when the virtual photon is longitudinally polarized because, in this case, the end-point contributions to the meson wavefunction are power suppressed. It was also shown that the cross section for a transversely polarized photon is suppressed by $1/Q^2$ compared to a longitudinally polarized photon, so that asymptotically, only σ_L survives. Collins *et al.* [Co97] showed that leading-order pQCD also predicts that the vector-meson channels ($\rho_L^{0,\pm}$, ω_L, ϕ_L) are sensitive only to the unpolarized GPD's (H and E), whereas the pseudoscalar channels ($\pi^{0,\pm}$, $\eta, ...$) are sensitive only to the polarized GPD's ($\tilde{H}$ and $\tilde{E}$). In contrast, Deeply Virtual Compton Scattering (DVCS) depends on *both* the polarized and unpolarized GPD's. Therefore, by selecting specific mesons in the final state one selects the spin-dependent or spin-independent generalized parton distributions. Note that in this latter case, one can access polarized nucleon structure information without any polarization of external particles. To explore what can be done, real photon, vector meson, and charged pion channels will be discussed since they have relatively high cross sections. In a later section we will come back to measuring nucleon elastic form factors (corresponding to the $< x^0 >$ moment of the GPD's) nucleon transition form factors, and Real Compton Scattering (RCS) (measuring the $< x^{-1} >$ moment of the GPD's). Note that while the elastic form factors at large t become increasingly sensitive to high $x \to 1$, RCS is more sensitive to the medium x-region due to the $1/x$ weighting in the integral.

DVCS and hard meson electroproduction processes have the following features:

1. **Scaling.** DVCS and hard meson electroproduction processes depend on three invariants: the initial photon virtuality $q^2 = -Q^2$, the initial photon energy in the lab frame ν: $p \cdot q = m\nu$, and the invariant momentum transfer $t = (p - p')^2$. The nontrivial prediction of perturbative QCD is that for fixed t and sufficiently large Q^2 and pq, the hard exclusive electroproduction

amplitudes have a simple scaling structure $T(x_{Bj})/Q^N$, with a calculable integer power N (determined by dimensional analysis) and the function $T(x_{Bj})$ depending only on the Bjorken ratio $Q^2/2p\cdot q) \equiv x_{Bj}$. This prediction reflects the basic pointlike nature of the quarks and the fundamental short-distance properties of quantum chromodynamics such as asymptotic freedom.

2. **Exclusive-inclusive connection.** As already emphasized, another nontrivial prediction of QCD is that the generalized parton distributions $H(x,\xi;t)$ describing the amplitudes of purely exclusive processes like DVCS process $\gamma^* N \to \gamma N$ are directly related to the usual parton distribution functions describing the cross sections of inclusive processes like DIS process $\gamma^* N \to X$.

3. **Electroproduction–form factor connection.** Since the integrals of GPD's are related to hadronic form factors, the t-dependences of hard electroproduction amplitudes and elastic form factors are interconnected.

It is important to measure the Q^2-dependence of the nearly forward differential cross section at fixed x_{Bj}. It is still uncertain at which Q^2 value one will reach the scaling regime, where the leading-order pQCD domain applies fully for meson electroproduction. However, it is expected to be between 5 and 10 $(\mathrm{GeV}/c)^2$, which is attainable with a 12 GeV beam. In any case, the way the asymptotic $1/Q^6$ behavior is approached is an important source of information on pre-asymptotic effects. "Soft" contributions are expected to drop as $1/Q^8$. An estimate of these pre-asymptotic effects in hard electroproduction reactions in the valence region is given in Ref. [Va99], where the effects of the intrinsic transverse momentum dependence of the quarks in the nucleon and in the meson are quantified. We may also note that reaching the fully asymptotic regime is not necessary as long as the corrections can be controlled by perturbative QCD methods. For example, if one is in a region of pre-asymptotic scaling a ratio of two production channels may lead to a nearly complete cancelation of "soft" contributions. Eides, Frankfurt, and Strikman [Ei99] point out that "It seems likely that a *precocious factorization* ... could be valid already at moderately high Q^2 $[\geq 5\ (\mathrm{GeV}/c)^2]$, leading to *precocious scaling of the spin asymmetries and of the ratios of the cross sections* as a function of Q^2, and x_{Bj}".

The complete extraction of the GPD's presents an extensive program, not a single experiment, involving the measurement of a variety of channels and observables. As the GPD's also depend on the unmeasurable momentum fraction of the struck quark in the quark loop (see Fig. 30), a global analysis will be required to extract the GPD's definitively from a large set of measurements.

The goal is to simultaneously measure the Q^2, x_{Bj} and t-dependences of cross sections, beam

asymmetries (for DVCS) and transverse polarized target asymmetries (for meson production). These observables involve the leading-order pQCD amplitudes, which are directly related to the GPD formalism. Toward this end, a large-acceptance spectrometer is highly desirable, as it will allow mapping the various dependences for all channels, simultaneously.

At JLab, one may begin to explore GPD's over a wide range of kinematics, for example $0.1 \lesssim x_{Bj} \lesssim 0.9$, $Q^2 > 2$ (GeV/c)^2, and -t <1.5 (GeV/c)^2. This program requires:

- high energy to reach the required high Q^2 at small x_{Bj},
- high luminosity to compensate for the typical fast drop of exclusive cross sections with Q^2 and hadronic center-of-mass system energy,
- good detector resolution to identify exclusive channels, and
- large acceptances for charged particle and neutral particle detection to measure various channels simultaneously, and over a large kinematic range, and to guarantee the exclusivity of the process.

JLab at 12 GeV, with the proposed CLAS detector upgrade, or, in specific cases, a high-luminosity spectrometer and calorimeter setup (DVCS) or two spectrometers (*e.g.*, hard charged pion electroproduction), will meet most of these requirements. Of course the beam energy will limit the kinematic range accessible, but given the rapid rate of cross section fall-off, this is not as serious a constraint as is commonly believed.

Deeply virtual Compton scattering

An important practical question is: what Q^2 is large enough to ensure the dominance of the lowest-twist handbag contribution? Guidance for DVCS can come from experimental data for the exclusive process $\gamma(q_1)\gamma^*(q_2) \to \pi^0$ studied on e^+e^- colliders. If one of the photons is highly virtual $q_1^2 = -Q^2$ while another is (almost) real $q_2^2 \sim 0$, the process is kinematically similar to DVCS. In the leading order of QCD, the $F_{\gamma\gamma^*\pi^0}(Q^2)$ transition form factor is given by a handbag diagram. The recent measurements by CLEO [Gr98] show that the pQCD prediction $F_{\gamma\gamma^*\pi^0}(Q^2) \sim 1/Q^2$ seems valid for $Q^2 \sim 2\,(\mathrm{GeV}/c)^2$ (see Fig. 31).

The $\gamma\gamma^*\pi^0$ vertex (for a virtual pion) can also be measured on a fixed-target machine, in which case it is just a part of the DVCS amplitude corresponding to the $\tilde{E}(x,\xi;t)$ generalized

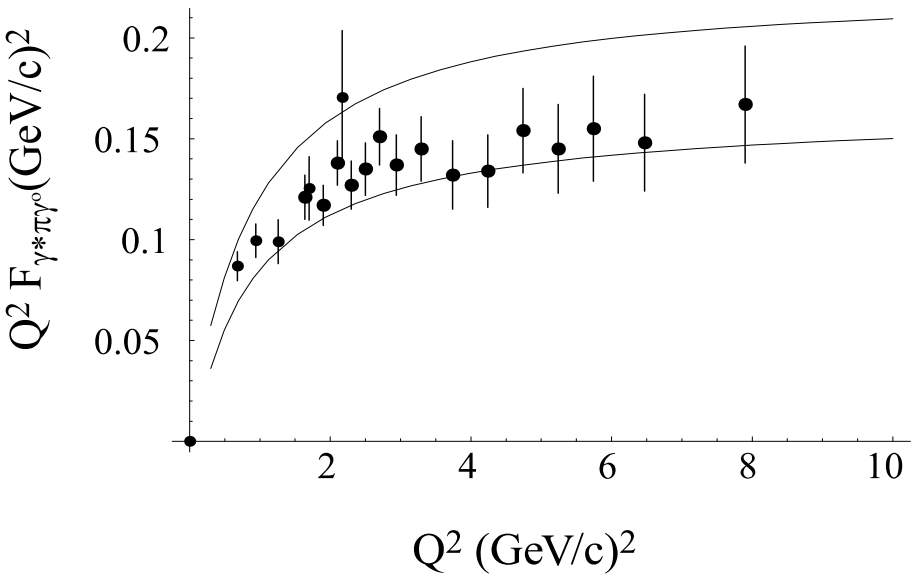

Figure 31: Comparison of experimental data on the $\gamma^*\gamma\pi^0$ form factor with quark transverse momentum power-corrected pQCD predictions using the asymptotic shape for the pion distribution amplitude (lower curve) and the Chernyak-Zhitnitsky model (upper curve).

parton distribution. Hence, CLEO data indicate that DVCS may be handbag-dominated for Q^2 as low as 2 $(\mathrm{GeV}/c)^2$.

One complication with experimentally studying DVCS is the competing Bethe-Heitler (BH) process. Here higher energies are an advantage, since the relative strength of DVCS increases with increasing beam energy. One can either select kinematics where the DVCS contributions dominate the BH contributions, or, alternatively, measure an interference term between the BH and DVCS contributions, thus benefitting from the strong BH term.

Thus, DVCS contributions can be extracted in various ways:

- Direct measurements of the absolute DVCS amplitude in the region where the BH contribution is small and can be calculated.
- Extracting the imaginary part of the DVCS amplitude by measuring the single-spin asymmetry with longitudinally polarized beam.

Studies of all three processes are needed over a wide kinematic range for a complete understanding of GPD's. The first two can be achieved with the electron beams that will be available

after the 12 GeV Upgrade, while the third requires use of positron beams. Note that the availability of JLab's highly polarized electron beam will especially allow unprecedented measurements of beam spin asymmetries, and the proposed upgraded CLAS detector in Hall B would be well suited to conduct these studies. Figure 32 shows the kinematic range in Q^2 and W accessible with CLAS for a beam energy of 11 GeV. Systematic studies in the range of Q^2 up to 6 $(\mathrm{GeV}/c)^2$ and for x_{Bj} from 0.15 to 0.45 will be possible. Such a DVCS program would be complementary to a program with a high-momentum spectrometer detecting the scattered electron and the (upgraded) Hall A "RCS calorimeter" to detect the hard photon. In either case, one would measure the recoiling nucleon in coincidence to guarantee the full-exclusiveness of the reaction. This is important, as separating a single photon from π^o production becomes more problematic at higher beam energies.

For the upgraded CLAS (capable of running at a luminosity of $L = 10^{35}$ cm^{-2} s^{-1}), count rates are estimated using the cross sections calculated by [Gupc]. Figure 33 shows, as an example, the high-quality single-spin asymmetries one could obtain at $Q^2 = 3$ $(\mathrm{GeV}/c)^2$, for a 500 hour run.

Hard meson electroproduction

The GPD's can also be measured in hard meson electroproduction processes. The leading-twist pQCD contribution in this case involves an additional one-gluon exchange, which means that the hard subprocess is suppressed by a factor of $\alpha_s/\pi \sim 1/10$ with respect to soft processes.

Calculating the one-gluon-exchange amplitude perturbatively, one obtains the hard contribution in the form of a product of two nonperturbative functions: the distribution amplitude $\phi(\tau)$ of the relevant meson [integrated with $1/\tau$] and a generalized parton distribution $H(x,\xi;t)$ (or $E, \tilde{H}, \tilde{E}$) integrated with $1/(x-\xi+i0)$ or $1/(x+\xi-i0)$, the same integrals as in DVCS. In distinction to the DVCS amplitude, which contains four GPD's $H(x,\xi;t)$, $E(x,\xi;t)$, $\tilde{H}(x,\xi;t)$ and $\tilde{E}(x,\xi;t)$, the nature of the produced meson "filters" the participating GPD's: vector-meson production is sensitive to $H(x,\xi;t)$ and $E(x,\xi;t)$, while the amplitude of the hard pion electroproduction is expressed in terms of $\tilde{H}(x,\xi;t)$ and $\tilde{E}(x,\xi;t)$ only.

As mentioned, $\tilde{H}(x,\xi;t)$ reduces to a spin-dependent parton distribution function in the forward limit. By taking advantage of this fact one can measure polarized parton distributions in this process without polarizing any participating particle. Note that polarization observables are expected to show precocious scaling already at $Q^2 = 3$ – 4 $(\mathrm{GeV}/c)^2$.

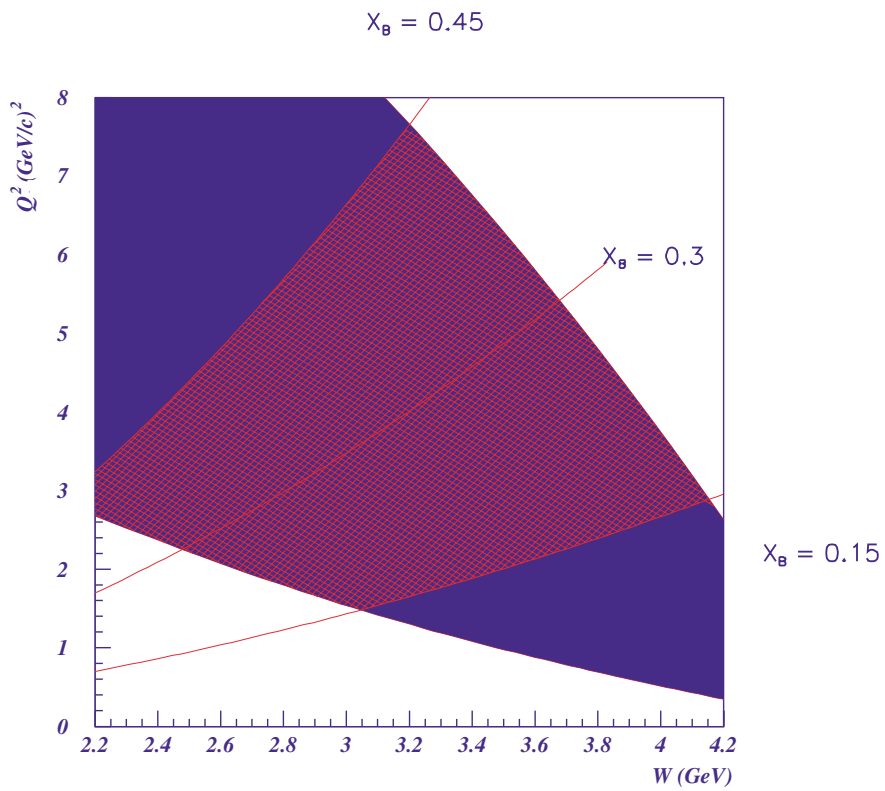

Figure 32: The accessible range of Q^2 and W at 11 GeV beam energy with the upgraded CLAS detector. The filled region is defined by detection of the scattered electron. The shaded region is the favorable kinematic range, accessible for DVCS measurements. The lines represent fixed values of x_{Bj}.

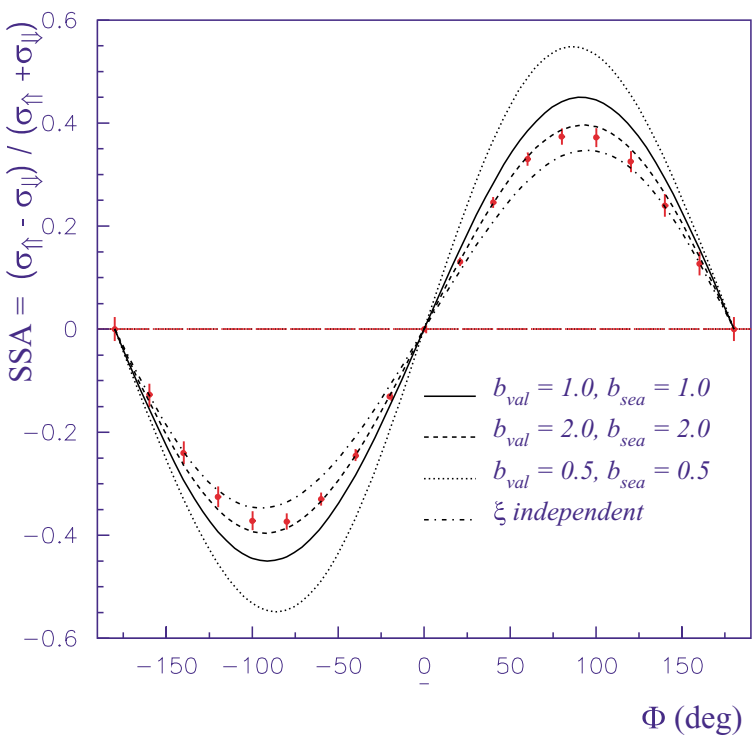

Figure 33: Single-spin asymmetry of the $ep \to ep\gamma$ reaction measured with a longitudinally polarized 11 GeV electron beam. Uncertainties correspond to a 500 hour run with CLAS operating at a luminosity of 10^{35} cm^{-2} sec^{-1}. Pseudo-data were integrated in the bins of $Q^2 = (3 \pm 0.1)$ (GeV/c)^2 and $W = (2.8 \pm 0.15)$ GeV and $-t = (0.3 \pm 0.1)$ (GeV/c)^2. The curves indicate various models of Generalized Parton Distributions, all of which are compatible with the known longitudinal parton momentum distributions.

The $ep \to e'\rho p$ channel We recall that an experimental program aiming to study the GPD's must begin by identifying the longitudinal part of the cross section for which the factorization theorem applies and the connection with the GPD formalism can be made. Longitudinal ρ^0_L's can be identified through the angular distribution of the vector-meson decay. Assuming s-channel helicity conservation, or SCHC, the desired cross section: $\gamma^*_L p \to p(\rho^0_L, ...)$ can be extracted by analyzing the angular distribution.[3]

The angular distribution of the decay products of the ρ reflects its polarization state. Assuming the outgoing electron and proton are detected, measurement of only one decay pion is sufficient to determine the decay angular distribution. The decay pion defines an angle, θ_{cm}, which is the polar angle relative to the direction opposite to the recoiling target in the ρ center-of-mass frame. The $\cos(\theta_{cm})$ distribution follows the form:

$$W\left(\cos(\theta_{cm})\right) = \frac{3}{4}\left\{1 - r^{04}_{00} + (3r^{04}_{00} - 1)\cos^2(\theta_{cm})\right\}. \tag{19}$$

The matrix element r^{04}_{00} depends on Q^2 and W, and is linked to the longitudinal polarization state of the ρ. For example, r^{04}_{00}=1 (0) corresponds to pure longitudinal (transverse) polarization of the ρ, respectively, and, in terms of angular distribution, to $\frac{3}{2}\cos^2\theta_{cm}$ ($\frac{3}{4}\sin^2\theta_{cm}$), respectively. Assuming SCHC, one often links the ρ polarization to the virtual photon polarization, and defines:

$$R = \frac{\sigma_L}{\sigma_T} = \frac{1}{\epsilon}\frac{r^{04}_{00}}{1 - r^{04}_{00}}. \tag{20}$$

The link is obvious: as r^{04}_{00} represents the longitudinal degree of polarization, $1 - r^{04}_{00}$ represents the transverse degree of polarization, and the factor $1/\epsilon$ accounts for the degree of longitudinal polarization of the virtual photons.

R has been measured in many experiments. It is displayed in Fig. 34 as a function of Q^2, though for a mixture of W values. (The HERMES collaboration recently reported a slight dependence on W, for $W > 4$ GeV [Ac00].) The observed increase of R with Q^2 means that longitudinal ρ's are dominant at large Q^2. However, there are no data in the region of interest for this study ($Q^2 \approx 3$ (GeV/c)^2 and $2 < W < 3$ GeV).

To estimate the accuracy we will be able to achieve for a measurement of R, events were

[3]The SCHC hypothesis can actually be tested by considering the interference response functions R_{TT} and R_{TL}, which are accessible with a large-acceptance detector such as CLAS.

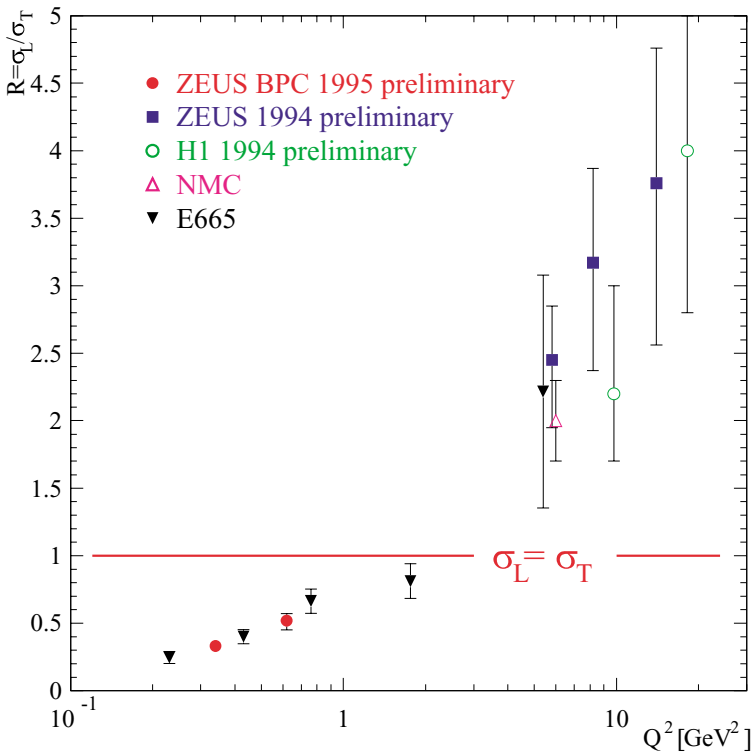

Figure 34: World data for $R = \sigma_L/\sigma_T$ as a function of Q^2 (assuming SCHC) [Cr97].

generated with the ratio R using the relationship:

$$R = \xi^2 \frac{Q^2}{M_\rho^2} \tag{21}$$

This formula is based on the Vector Meson Dominance (VMD) approach [Sa69], and describes the data of Fig. 34 at intermediate Q^2 [≈ 3 (GeV/c)^2] with a value $\xi^2 = 0.3$.

The θ_{cm} angular distribution of the decay π^+ has been simulated for different Q^2 bins, taking the acceptance of the upgraded CLAS into account. We assumed a luminosity of 10^{35} cm^{-2} s^{-1}, a beam energy of 11 GeV, and a 400 hour run time. Bin sizes of $0.3 < x_{Bj} < 0.4$, $-0.2 < -t < 0.4$ (GeV/c)^2, and $\Delta Q^2 = 1$ (GeV/c)^2 were assumed. The ratio R=σ_L/σ_T has been extracted from the simulated θ_{cm} distribution as described above. Figure 35 shows the separated cross sections for ρ electroproduction, with the anticipated statistical uncertainties. If it is found that the trend of the current data is confirmed with high precision at the upgraded CEBAF machine, corrections for σ_T maybe applied to $\sigma_{\rm tot}$ without performing an L/T separation. In this case the data can be extended to even higher Q^2.

Hard pion electroproduction The L/T separation for pions obviously can be accomplished using the Rosenbluth technique. In order to separate σ_T and σ_L, it is necessary to vary the virtual photon polarization parameter ϵ, which can only be done, keeping x_{Bj} and Q^2 fixed, by varying the beam energy (Rosenbluth separation). In the following, we will assume 6, 8, and 11 GeV incident beams. For the identification of the reaction, it is sufficient to detect the scattered electron and the charged pion, the neutron being reconstructed by the missing-mass technique.

Figure 36 shows the anticipated data; separated cross sections can be obtained up to $Q^2 \approx 6$ (GeV/c)^2. Obviously, the unseparated cross-section estimates reach a higher Q^2 value as one does not require a range in ϵ for L/T separation. For the case of Hall B, the maximum Q^2 attainable would be ≈ 8 (GeV/c)^2. In principle, Halls A and/or C could extend these Q^2 ranges utilizing their high-luminosity capabilities. For example, using the HMS-SHMS combination in Hall C (the existing High-Momentum Spectrometer and the planned Super-High-Momentum Spectrometer), one could do precise measurements of $R = \sigma_L/\sigma_T$ in $H(e, e'K^+)\Lambda$ electroproduction up to Q^2 of 10 (GeV/c)^2.

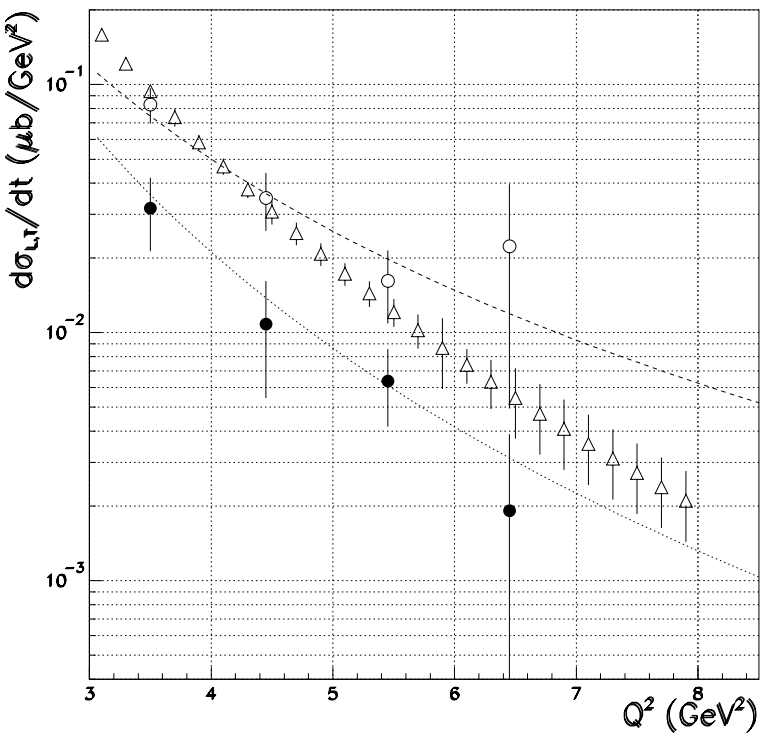

Figure 35: Simulation of the L/T separated cross section $d\sigma/dt$ for ρ electroproduction with an 11 GeV electron beam. Open triangles are the total (unseparated) cross section ($\sigma_{\rm tot} = \sigma_T + \epsilon\sigma_L$). Full circles are σ_T, decreasing like $1/Q^8$ (dotted line). Empty circles are σ_L, decreasing like $1/Q^6$ (dashed line).

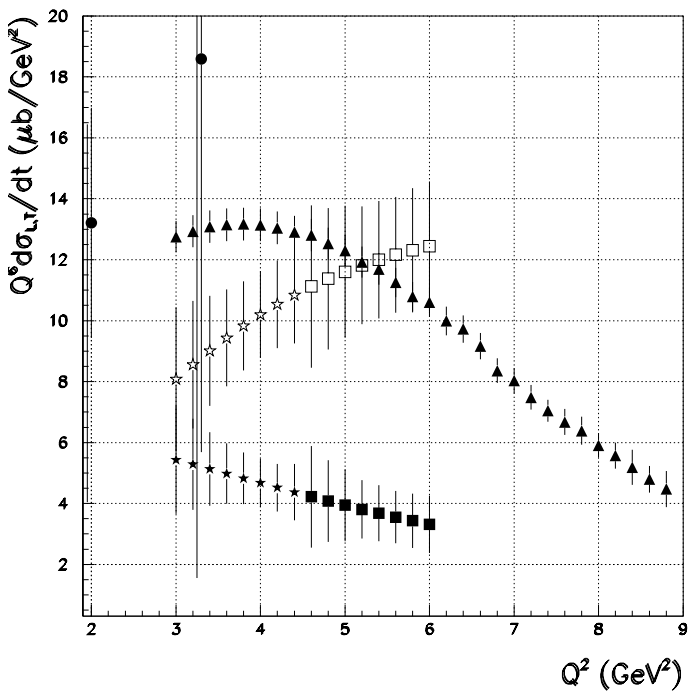

Figure 36: Separated and unseparated differential cross section $d\sigma/dt$ (multiplied by Q^6) for $ep \to \pi^+ n$ as a function of Q^2. Circles are the existing data points of Bebek *et al.* [Be78]. Open (filled) stars and squares correspond to projected σ_L (σ_T) data. Projected data at lower Q^2 use a 6 GeV-11 GeV beam energy combination, data at higher Q^2 an 8 GeV-11 GeV beam energy combination. The solid triangles are the unseparated differential cross sections. Bins of x_{Bj} = 0.4 – 0.5, and $-t = 0.2-0.4$ (GeV/c)^2 are used. An upgraded CLAS acceptance and a luminosity of 10^{35} cm^{-2}s^{-1}, and 1600 hours of beam time have been assumed.

2.B.3 Form Factors

Hadron form factors are fundamental quantities in nuclear physics. They are the most basic observables which reflect the composite nature of the hadrons. Indeed, the first indication that the nucleon is a composite object came from measurements of the proton form factors in elastic electron-proton scattering [Ho55].

Nucleon elastic and transition form factors

Measurements of nucleon elastic and transition form factors have become very interesting in recent years due to the development of a variety of precise, new measurement techniques. At small Q^2, below 1 $(\mathrm{GeV}/c)^2$, precise measurements of the neutron charge form factor show values statistically significantly different from 0; the neutron magnetic form factor remains controversial due to disagreements between precise experiments in excess of their stated uncertainties. Next to this, few precise measurements exist beyond $Q^2 = 1$ $(\mathrm{GeV}/c)^2$. For the proton, recent JLab polarization measurements [Jo00] have shown that the electric form factor falls much faster than the magnetic form factor. Lastly, the $E2/M1$ ratio for the $N \to \Delta$ transition has remained near 0 over the entire range of momentum transfer explored [up to $Q^2 = 4$ $(\mathrm{GeV}/c)^2$] [Fr98a], whereas the perturbative QCD expectation for this ratio is unity.

JLab at 12 GeV would provide the opportunity to measure many important form factors precisely: the proton electric and magnetic form factor, the neutron magnetic form factor, the $N \to \Delta$ and $N \to S_{11}$ transition form factors, and Real Compton Scattering (RCS) up to momentum transfers of $Q^2 = -t = 10 - 15$ $(\mathrm{GeV}/c)^2$. Precise measurements above a few $(\mathrm{GeV}/c)^2$ are available only for the proton magnetic form factor. (We have listed RCS within the GPD framework, as it is the $< x^{-1} >$ moment of the $H(x, \xi, t)$ GPD, whereas the Dirac form factor $F_1(Q^2)$ is the $< x^0 >$ moment of the same GPD.) Baryon resonance structure generalizes the elastic nucleon structure studies, providing a bridge between the elastic and deep inelastic regimes. The Δ resonance is especially significant for its role in hadron structure [Th84], and for the qualitatively different Q^2-dependence of its form factor from the elastic and other resonant form factors [St93]. Moreover, the contribution of the $N \to \Delta$ transition to polarization asymmetry is known to be large and negative at low Q^2, while the same asymmetry is positive at large Q^2. Understanding this transition, and the related nontrivial Q^2-dependence of the evolution of the Gerasimov-Drell-Hearn integral at intermediate Q^2, requires a precise determination of the $N \to \Delta$ transition form factor over a large range in Q^2. The S_{11} may be considered the negative parity partner of the nucleon: in the limit of exact chiral symmetry the masses of the nucleon and the S_{11} would be degenerate, so the properties

of the S_{11} form factor reveal fundamental aspects of dynamical chiral symmetry breaking in QCD.

Understanding the transition from low to high Q^2 is vital for other reasons as well. Form factors in the transition region are very sensitive to mechanisms of spin-flavor symmetry breaking, some of which can not be described in principle within perturbation theory. A classic example is the electric form factor of the neutron, which is identically 0 in a simple valence quark picture. A nonzero value for the neutron form factor can only be understood in terms of nonperturbative mechanisms such as the hyperfine interaction between quarks [Is81] or in terms of a pion cloud [Th84]. Similarly, in the purely asymptotic picture the proton electric form factor is identically 0 in a simple valence quark picture, and a non-vanishing form factor again requires a nonperturbative wavefunction.

To summarize, the nucleon elastic form factors (G_M^n, G_E^p, and G_M^p), the nucleon transition form factors (*e.g.*, the $N \to \Delta$ and $N \to S_{11}$), and wide-angle Real Compton Scattering can be measured precisely out to large Q^2. As examples we highlight: (i) a measurement of the $D(e,e'n)/D(e,e'p)$ ratio in CLAS to extract $G_M^n(Q^2)$ (Fig. 37); (ii) the expected behavior of the ratio of $E2/M1$ in the $N \to \Delta$ transition, a ratio that can be precisely measured up to $Q^2 \approx 15$ $(\mathrm{GeV}/c)^2$ with the Hall C HMS-SHMS spectrometer combination (Fig. 39); and (iii) a projected measurement of the RCS vector form factor $R_V(t)$ in Hall A using the (upgraded) RCS calorimeter and the MAD spectrometer (Fig. 38). Each of these measurements would take of order one month of 12 GeV beam time.

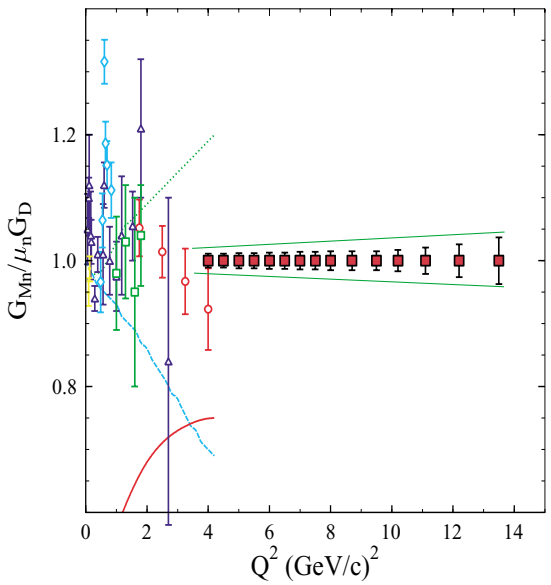

Figure 37: Projected statistical and systematic uncertainties versus Q^2 for the proposed measurements of $G_M^n(Q^2)$, contrasted with previous data.

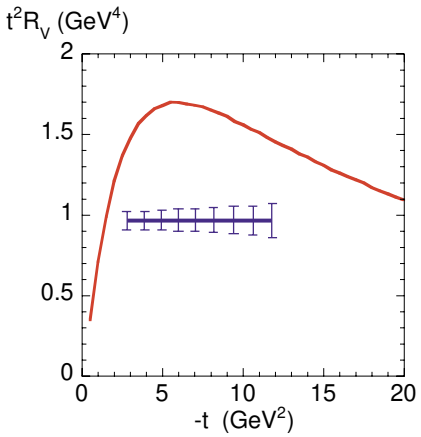

Figure 38: The RCS vector form factor $R_V(t)$, multiplied with t^2, versus t. The projected uncertainties attainable with a 12 GeV JLab are shown. The theoretical form factor is due to a calculation of Radyushkin [Ra98a].

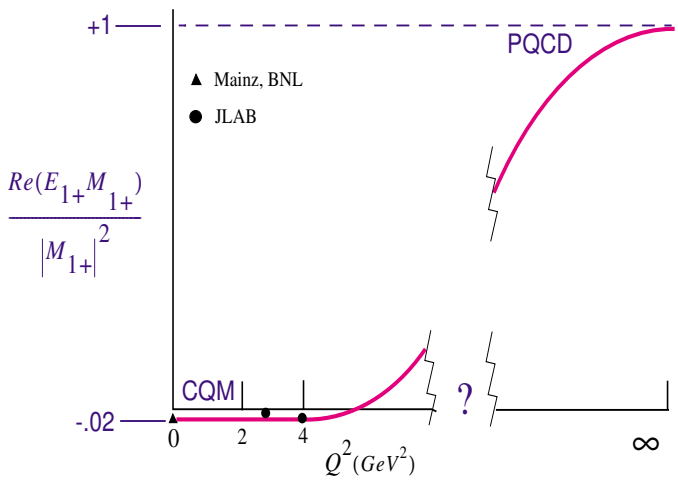

Figure 39: $Re(E^*_{1+}M_{1+})/|M_{1+}|^2$ for excitation of the $\Delta(1232)$ as a function of Q^2. The datum at $Q^2 = 0$ is the result of experiments at Mainz and BNL. The data points at $Q^2 = 2.8$ and 4.0 $(\mathrm{GeV}/c)^2$ are the JLab results. The unmodified $SU(6)$ value is 0, while the pQCD prediction is +1. The curve is a suggestion of what may be expected. The break in the abscissa indicates our lack of knowledge about where in Q^2 the transition to hard processes occurs. JLab at 12 GeV would provide precise measurements up to $Q^2 \approx 15$ $(\mathrm{GeV}/c)^2$.

The pion form factor

The π^+ electric form factor is a topic of fundamental importance to our understanding of hadronic structure. It is well known [Ch77, Fa79, Ra77, Ef80, Br79a] that the asymptotic behavior is rigorously calculable in perturbative QCD (pQCD), and takes the form

$$F_\pi \rightarrow \frac{8\pi\alpha_s f_\pi^2}{Q^2} \tag{22}$$

at high Q^2, where $f_\pi = 133$ MeV is the π^+ axial-vector decay constant.

The theoretical prediction for F_π at experimentally accessible Q^2 values is less certain, as soft scattering contributions must be taken into account explicitly. For example, in Ref. [Ja93] it was found that the inclusion of both Sudakov corrections and the transverse momenta of the quarks leads to values too small with respect to the data, thus leaving room for an important role of other, soft, contributions. A recent study [Br00a] based on a light-cone sum rule calculation found that the nonperturbative hard contributions of higher twist strongly cancel the soft components, even at relatively modest Q^2. Other models [Ja90, Ti92, It92] obtain good agreement with the experimental data over a broad region of Q^2 by incorporating a confining potential (which dominates at low Q^2) and a QCD-based interaction (which dominates at high Q^2) that takes the form of a one-gluon exchange potential or dynamic chiral symmetry breaking. Finally, Bethe-Salpeter plus Schwinger-Dyson equations were used in Ref. [Ma00] to determine the pion form factor. In this case, the model's parameters were adjusted to reproduce m_π, f_π, and $< \bar{q}q >$, and then the predicted F_π is found to be in reasonable agreement with the existing data. Reliable experimental data at intermediate Q^2 are clearly needed to delineate the role of hard versus soft contributions and aid the further development of these models.

Unfortunately, our experimental knowledge of F_π is poor. Many of the experimental difficulties in extracting the pion form factor are well understood. One must obtain high-quality $p(e, e'\pi^+)n$ data, in which the contribution of the pion pole diagram is optimized by measuring the π^+ in parallel kinematics at the smallest possible $|t|$ and performing an L/T separation. The complications of the proton target are taken into account by using a model, such as that of Ref. [Va98]. The value of $F_\pi(Q^2)$ is obtained via a fit of the σ_L model to the data. This procedure renders experimental values of $F_\pi(Q^2)$ with far smaller systematic uncertainties than the previous Chew-Low extrapolations. The high-quality, continuous electron beam of CEBAF is essential for these measurements. In 1997, E93-021 obtained data up to $Q^2 = 1.6$ $(\mathrm{GeV}/c)^2$ in Hall C [Vo00], and expects to extend these measurements to $Q^2 = 2.6$ $(\mathrm{GeV}/c)^2$ in 2002. As can be seen from Fig. 40, 2.6 GeV^2/c^2 will not be a high enough Q^2 value to determine the soft-to-hard transition definitively. Given its importance, measuring $F_\pi(Q^2)$ well at the highest possible Q^2 is warranted.

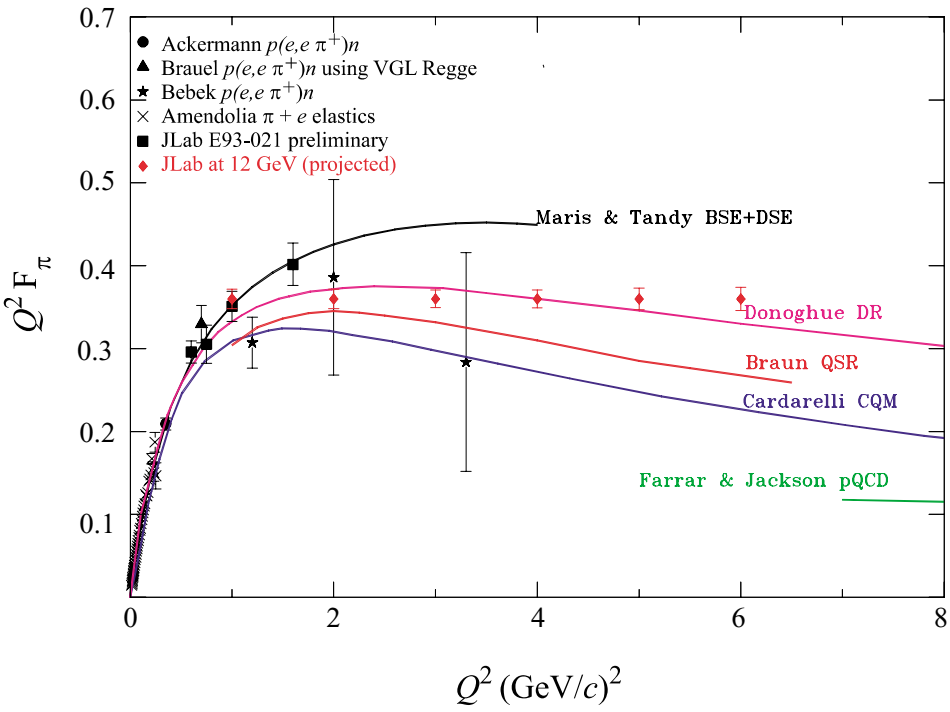

Figure 40: The measurements of the pion elastic form factor through the expected transition region from confinement-dominated dynamics to perturbative-dominated dynamics made possible by the proposed 12 GeV Upgrade. Systematic errors are estimated to be comparable to the statistical errors shown for the projected 12 GeV data. Also shown are a few of the dozens of model predictions, all characterized by being confinement-dominated below about 2 $(\mathrm{GeV}/c)^2$ and making a transition to being perturbative-dominated with a value of $Q^2 F_\pi \simeq 0.1\ (\mathrm{GeV}/c)^2$ in the region of 10 $(\mathrm{GeV}/c)^2$.

The 12 GeV Upgrade will allow one to obtain data at a higher value of the invariant energy W, resulting in lower values of $|t|$, thus enhancing the t-pole part of the cross section and the L/T ratio. Also the models used to extract the pion form factor from data on the proton are believed to be more reliable at higher values of W.

Since the pion will be emitted at rather small angles with the beam, the proposed SHMS spectrometer is essential for this measurement because of its 5.5° forward angle capability, combined with its good angular resolution (to control systematic errors in the L/T separation) and sufficient missing-mass resolution to cleanly separate $p(e,e'\pi^+)n$ events from $p(e,e'\pi^+)N\pi$. Figure 40 shows the expected error bars that could be obtained with the SHMS+HMS combination and an 11 GeV beam after 100 days of running time. It is clear that the CEBAF Upgrade would allow a significant advance in the understanding of the pion form factor.

Primakoff photo- and electro-production

One can exploit the high-energy electro- and photo-production of pseudoscalar mesons in the Coulomb field of a nucleus, the Primakoff effect, to study the two-photon decay widths, $\Gamma_{\gamma\gamma}$, and the transition form factors, $F_{\gamma\gamma^* P}$, where P represents the π°, η, and η' pseudoscalar mesons.

In the chiral limit, the classical QCD Lagrangian,

$$\mathcal{L}_{\rm QCD} = \sum_{i=u,d,s} \bar{\psi}_i (i\partial\!\!\!/ - gA\!\!\!/ - m_i)\psi_i - \frac{1}{4} G^a_{\mu\nu} G^{\mu\nu}_a, \tag{23}$$

is invariant under both chiral $SU_L(3) \times SU_R(3)$-flavor and axial $U_A(1)$ transformations. The chiral $SU_L(3) \times SU_R(3)$ symmetry is also a symmetry of the full quantum field theory, but is spontaneously broken to $SU(3)$ in the ground state. As a result, there are eight massless Goldstone bosons corresponding to the eight spontaneously broken degrees of freedom in the symmetry transformations: the octet pseudoscalar mesons (π°, η, K, etc.). In reality, these Goldstone mesons are not massless because the quark masses are nonzero (albeit small), thus breaking the symmetry explicitly.

Unlike chiral $SU_L(3) \times SU_R(3)$, the axial $U_A(1)$ is not a symmetry of the full quantum theory because of the chiral anomaly [Be69]:

$$\partial_\mu j^\mu_A = \frac{N_F \alpha_s}{8\pi} \varepsilon^{\mu\nu\lambda\sigma} G^a_{\mu\nu} G_{a\lambda\sigma} \tag{24}$$

and the existence of topologically distinct QCD vacua that make the right-hand side of Eq. 24 nonzero. (Here $N_F = 3$ is the number of flavors appearing in the axial current, and G is the gluon field.) The existence of such "Θ-vacua", which lead to the strong CP problem, and the mechanisms by

which topological transitions occur (instantons or confinement-driven vacuum fluctuations) remain one of the most profound issues in QCD. Moreover, the nature of the η' as an "almost Goldstone boson", which gets its mass from vacuum gluonic interactions, stands as one of the most interesting questions in hadron dynamics.

There is a second type of $U_A(1)$ anomaly that involves the coupling of the quarks to the photon fields. This leads to similar non-vanishing divergences:

$$\partial_\mu j^\mu_{A3} = \frac{N_c \alpha_{em}}{3\pi} \epsilon^{\mu\nu\rho\sigma} F_{\mu\nu} F_{\rho\sigma}$$

$$\partial_\mu j^\mu_{A8} = \frac{N_c}{\sqrt{3}} \frac{\alpha_{em}}{3\pi} \epsilon^{\mu\nu\rho\sigma} F_{\mu\nu} F_{\rho\sigma} \tag{25}$$

where the F's are the electromagnetic fields and N_c is the number of colors in QCD. This anomaly is directly responsible for the decay of the π°, η, and η' mesons into photon pairs, leading to a rigorous prediction in the chiral limit.

In the real world the current quark masses are non-vanishing, and have values of order $m_u \sim 5$ MeV, $m_d \sim 10$ MeV, and $m_s \sim 150$ MeV. These masses make the π° and the η massive, and shift the mass of the η' due to explicit breaking of chiral symmetry, while SU(3) and isospin breaking induce mixing among the three mesons. The mixing is expressed in terms of three mixing angles. Writing on the left the eigenstates of the chiral limit, we have:

$$\pi^\circ_8 = \pi^\circ - \epsilon\eta - \epsilon'\eta'$$

$$\eta_8 = (\eta + \epsilon\pi^\circ)\cos\theta + (\eta' + \epsilon'\pi^\circ)\sin\theta$$

$$\eta_\circ = -(\eta + \epsilon\pi^\circ)\sin\theta + (\eta' + \epsilon'\pi^\circ)\cos\theta. \tag{26}$$

The mixing angle, ϵ, is predicted in ChPT to be approximately -0.55°. There are no rigorous predictions for the other two angles. In the large N_c limit they become: $\epsilon' \sim -0.25^\circ$ and $\theta \sim -22^\circ$, but the size of deviations from this limit is unknown. The 12 GeV Upgrade will allow significantly improved measurements of some of the parameters of this fundamental system of QCD.

Figure 41 (left) shows a Monte Carlo simulation of the expected angular distribution of $\eta \to \gamma\gamma$ events on ^{12}C, where the resolution and geometrical acceptance of the anticipated PRIMEX hybrid calorimeter were taken into account. A target thickness of 2×10^{19} carbon atoms/cm^2 was assumed, a beam current of 5 μA, and 30 days of data-taking. The simulation yields 72,500 $\eta \to \gamma\gamma$ events and a 0.7% statistical uncertainty on the width. The estimated systematic uncertainty is of order 2%. The uncertainty in the η–η' mixing angle from the combined measurements, $\pi^\circ \to \gamma\gamma$, $\eta \to \gamma\gamma$,

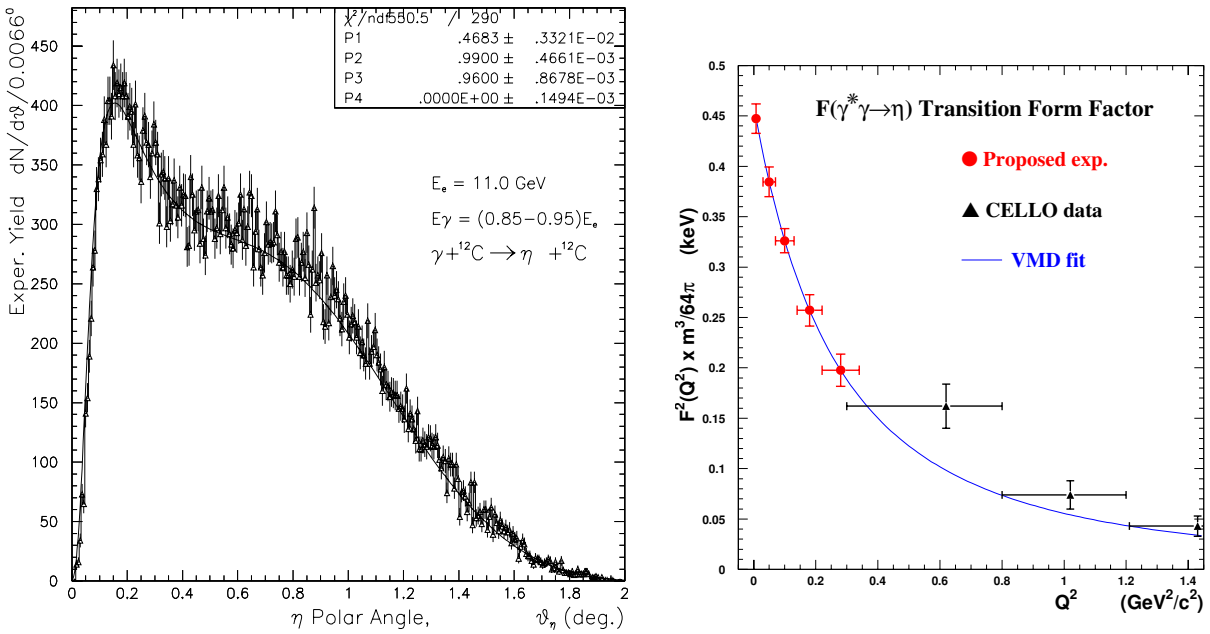

Figure 41: Left: Monte Carlo simulation of experimentally measured angular distribution of $\eta\gamma\gamma$ events on ^{12}C. Right: Projected uncertainties for a measurement of the η transition form factor.

and $\eta' \to \gamma\gamma$, would amount to $\sim 2\%$, to be compared with the present knowledge of this mixing angle of $\sim 8\%$.

In addition, using Primakoff electroproduction it is possible to gain access to the transition form factors $F_{\gamma\gamma^* P}$ for one off-shell photon. So far, the transition form factors have been determined in collider experiments [Be91], where $Q^2 \geq 0.6$ (GeV/c)^2, except for the recent form factor for the η' measured by the L3 collaboration [Ac98a] where Q^2 is as low as 0.05 (GeV/c)^2 but with a large error on Q^2. Measurements of the π°, η, and η' transition form factors at very low Q^2 [$\sim$ 0.001–0.5 (GeV/c)^2] will also enable the extraction of the slope of the transition form factor, and determine the size of the meson's electromagnetic interaction radius model-independently.

An example of an 11 GeV measurement of the η transition form factor is given in Fig. 41 (right). Such a determination of the slope of the π° and η form factors would allow one to uniquely fix an $\mathcal{O}(p^6)$ low-energy constant in the effective chiral Lagrangian [Bi88, Mo95]. With a measurement of the η' form factor slope, one could also have a clear test of how well the U(3) flavor symmetry implied by the large N_c limit holds. In this limit, the same $\mathcal{O}(p^6)$ low-energy constant should determine all slopes.

2.B.4 Low-Energy Quark-Hadron Duality

Understanding the structure and interaction of hadrons in terms of the quark and gluon degrees of freedom of QCD is one of the greatest unsolved problems of the standard model. While at present we can only rarely describe the physics of hadrons directly from QCD, we know that in principle it should just be a matter of convenience in choosing to describe a process in terms of quark-gluon or hadronic degrees of freedom. This fact is referred to as *quark-hadron duality*, and means that one can use either set of complete basis states to describe physical phenomena. At high energies, where the interactions between quarks and gluons become weak and quarks can be considered asymptotically free, an efficient description of phenomena is possible in terms of quarks; at low energies, where the effects of confinement make strongly coupled QCD highly nonperturbative, it is more efficient to work in terms of collective degrees of freedom, the physical mesons and baryons.

The duality between the quark and hadron descriptions reflects the relationship between confinement and asymptotic freedom, and is intimately related to the nature of the transition from nonperturbative to perturbative QCD. Achieving a better understanding of this transition was one of the main motivations for building Jefferson Lab.

Although the duality between quark and hadron descriptions is, in principle, formally exact, how this reveals itself specifically in different physical processes and under different kinematic conditions is the key to understanding the consequences of QCD for hadronic structure. The phenomenon of duality is quite general in nature and can be studied in a variety of processes, such as $e^+e^- \to$ hadrons, or semi-leptonic decays of heavy quarks [Vo88]. For the latter, one does not even need to invoke an averaging process – the results in terms of quark and hadronic variables are identical in the limit of infinitely heavy quarks [Is91]. One of the more intriguing examples, observed some 30 years ago, is in inclusive deep inelastic electron-nucleon scattering.

In studying deep inelastic scattering in the resonance region and the onset of scaling behavior, Bloom and Gilman [Bl70] found that the inclusive F_2 structure function at low W generally follows a global scaling curve that describes high-W data; the resonance structure function averages to this curve. Furthermore, the equivalence of the averaged resonance and scaling structure functions appears to hold for each resonance, over restricted regions in W, so that the resonance-scaling duality also holds locally. More recently, high-precision data on the F_2 structure function from Jefferson Lab [Ni00] have confirmed the earlier observations, demonstrating that duality works remarkably well for each of the low-lying resonances, including the ground state, to rather low values of Q^2 [~ 0.5 (GeV/c)^2]. This one-to-one correspondence is unlikely to generalize [Je00].

Bloom-Gilman duality can be thought of as a "truncated" version of duality, in the sense that one can apparently describe the physical process with a limited set of quark states, as in perturbative QCD calculations, or in terms of a few resonances which average to the quark result. Understanding duality therefore gives insight into the relationship between inclusive (deep inelastic scattering) and exclusive (resonance production) processes.

Bloom-Gilman duality can be formulated in the operator product expansion (OPE) language of QCD moments of structure functions, in which contributions are organized according to powers of $1/Q^2$ [Ru75]. The leading terms are associated with free quark scattering, and are responsible for the scaling of the structure function. The $1/Q^2$ terms involve interactions between quarks and gluons and hence reflect elements of confinement dynamics. The weak Q^2-dependence of the low moments of F_2 can be interpreted within the OPE as indicating that the non-leading, $1/Q^2$-suppressed, interaction terms do not play a major role even at low Q^2 [≈ 1 (GeV/c)^2].

On the other hand, while the OPE formalism allows us to organize hadronic observables in terms of an asymptotic expansion, it does not tell us *a priori* why certain matrix elements are small or cancel. This can only be addressed via numerical solutions of QCD or experiment. Since the details of quark–hadron duality are expected to be process-dependent [Je00], there is no reason to expect the accuracy to which it holds and the kinematic regime where it applies to be similar for different observables. In fact, there could be qualitative differences between the workings of duality in spin-dependent structure functions and spin-averaged ones, or for different hadrons – protons compared with neutrons, for instance. Data available relevant to these issues are inadequate: there are some data on the F_2 structure functions of the proton and deuteron [Ni00, Ni00a]; the data on the g_1 and g_2 structure functions (which correspond to cross-section differences) are either of poor quality or in kinematics not relevant to duality considerations; and there are essentially no data on the longitudinal-to-transverse structure function ratio, R. It is vital for our understanding of duality and its practical exploitation that the spin and flavor dependence of duality be established empirically.

An important consequence of duality is that the strict distinction between the resonance and deep inelastic regions is quite artificial – both regions are intimately related, and properly averaged resonance data can help us understand the deep inelastic region. For example, at $Q^2 = 1$ (GeV/c)^2 about 70% of the total cross section comes from the resonance region, $W < W_{\rm res} = 2$ GeV. However, because of duality the resonances and the deep inelastic continuum conspire to produce only about a 10% correction to the lowest moment of the scaling F_2 structure function at the same Q^2 [Ji95a]. The resonances should therefore be viewed as an integral part of the deep inelastic scaling structure functions.

It is standard procedure in global analyses [Ma98, La95] of deep inelastic scattering to omit from the database the entire resonance region below $W = 2$ GeV. Including the vast quantity of data that has been excluded would not only improve the statistics significantly, but also decrease the uncertainties that arise from extrapolations into the regions excluded by the W cuts. This is especially pertinent for structure functions at large x_{Bj}, where for finite Q^2 one is always limited by the kinematics to $x_{Bj} < x_{Bj,\rm res} = Q^2/(W^2_{\rm res} - M^2_N + Q^2)$. In extending data to very large x_{Bj} at a finite Q^2 one always encounters the resonance region. A revolutionary application of duality, if one understands the workings of the resonance–deep inelastic interplay, would allow access to the region of very high x_{Bj}, which has not been possible in any other experiment.

The region of $x_{Bj} \approx 1$ is an important testing ground for mechanisms of spin-flavor symmetry breaking in valence quark distributions of the nucleon [Cl79, Me96, Is99]. With nuclear targets it would permit a measurement of the nuclear medium modification of the nucleon structure function (nuclear EMC effect) [Ge95] at large x_{Bj}, where the deviation from unity of the ratio of nuclear to nucleon structure functions is largest and the sensitivity to different nuclear structure models greatest.

Another largely unexplored domain with potentially broad applications is the production of mesons (M) in semi-inclusive electron scattering, $eN \to e'MX$. At high energy the scattering and production mechanisms factorize: the cross section at leading order in QCD becomes a simple product of the structure function, which gives the probability of finding a quark in the nucleon, and a quark $\to$ meson fragmentation function, or the probability that the quark hadronizes into the meson M. The usefulness of semi-inclusive production lies in its ability to identify individual quark species in the nucleon by tagging specific mesons in the final state, so that both the flavor and spin of quarks and antiquarks can be uniquely determined.

The extent to which factorization applies at lower energy is an open question, and the signatures of duality in the resonance region of semi-inclusive scattering need to be investigated. It is imperative therefore that both of these questions be answered experimentally. It is worth stressing that confirmation of factorization and truncated duality would open the way to an enormously rich semi-inclusive program, allowing unprecedented spin and flavor decomposition of quark distributions. Such a program is discussed briefly below.

CEBAF at 12 GeV would provide a unique opportunity to shed light on all the issues associated with Bloom-Gilman duality. Several examples are discussed in greater detail in the following.

Recent results

Substantial progress has been made over the past twenty years both theoretically in understanding QCD and experimentally in determining the scaling behavior of the F_2 structure function. By combining these data with new, precision, resonance data from Jefferson Lab [Ni00], it has been possible to revisit quark-hadron duality more quantitatively, addressing the recent theoretical interest in the topic (see, for example, [Ji95a, Be95, We96, Ri98, Co98, Ca95a, An96a]). Parameterizations of deep inelastic data were found to equal (within 10%) an average of the resonance region F_2 spectra at disparate kinematics (see Fig. 42). This echoes the original Bloom and Gilman observation of duality. The above results – namely that duality seems to be holding and the resonances average to the perturbative scaling curve – indicate that higher twist contributions to the lower F_2 moments are small or cancelling on average, even in the low-Q^2 regime where they should be largest due to their $1/Q^2$ behavior. Higher twists can be viewed in this light as deviations from duality.

Although the dynamical origin of local duality is not understood, it seems intricately intertwined with the behavior between the $Q^2 \to 0$ limit, where only elastic scattering contributes to the moments, and $Q^2 > 5$ (GeV/c)^2, where deep inelastic scattering already dominates the lower moments [Ar00]. In the region $0.2 < Q^2 < 5$ (GeV/c)^2 the nucleon resonances contribute to a substantial part of the moments, and, on average, seem to be indistinguishable from deep inelastic scattering at $Q^2 > 1$ (GeV/c)^2. This is consistent with the findings of Bloom and Gilman, as shown quantitatively in Ref. [Ni00] for the second moment. In the $Q^2 < 1$ (GeV/c)^2 transition region, the contribution of the coherent elastic peak to the second moment dies out, whereas the nucleon resonances already show the onset of their duality behavior, in that they tend to oscillate [already at $Q^2 \approx 0.2$ (GeV/c)^2] around a single smooth curve, resembling neutrino/antineutrino xF_3 data or a valence-like sensitivity only [Ni00a]. Furthermore, the nucleon resonances shuffle their strength around such that, at $Q^2 \approx 1$ (GeV/c)^2, they have, if properly averaged, reached the same behavior as a function of x_{Bj} and Q^2 as one would expect from deep inelastic data.

Thus, the world's data on F_2 are reasonably well described down to $Q^2 \sim 1$ (GeV/c)^2 by models obtained by fits to deep inelastic scattering. This includes the nucleon resonance data, which average to a similar scaling curve due to local duality. Local duality seems to describe the transition from the elastic contribution only, at $Q^2 = 0$, through the excitations of the nucleon resonances, into the scaling region.

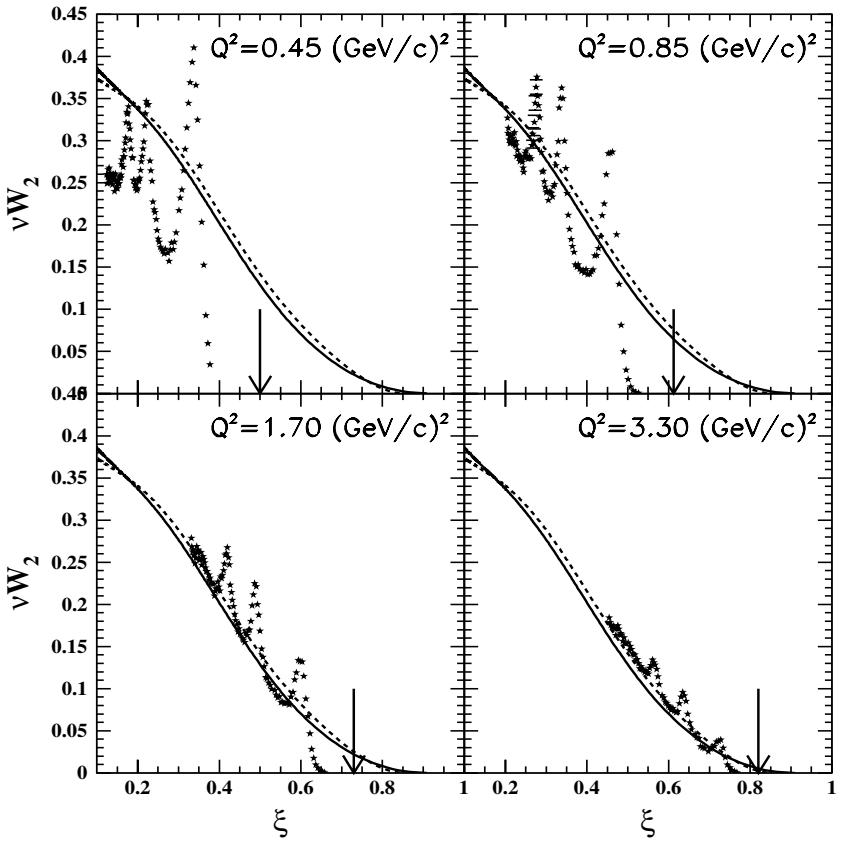

Figure 42: Sample hydrogen νW_2 structure function spectra obtained at $Q^2 = 0.45, 0.85, 1.70$, and 3.30 $(\mathrm{GeV}/c)^2$ and plotted as a function of the Nachtmann scaling variable ξ. Arrows indicate elastic kinematics. The solid [dashed] line represents the NMC fit of deep inelastic structure function data at $Q^2 = 10$ $(\mathrm{GeV}/c)^2$ [$Q^2 = 5$ $(\mathrm{GeV}/c)^2$].

Duality in unpolarized structure functions

While duality has been studied extensively for the F_2 structure function at Jefferson Lab, and approved proposals exist to continue this work at lower Q^2 values, duality remains essentially untested for the F_L (or F_1) structure functions. The reason for this is that no relevant data exist; no separated measurements exist at x_{Bj} values $\gtrsim 0.5$ below $Q^2 \approx 10$ (GeV/c)^2.

There are predictions [Ca95a] and some scant experimental evidence [En00] that the longitudinal structure function exhibits duality. In contradiction, there are data and models [Wh92, Ta96] that hint that higher twist effects may be quite large in the longitudinal structure function at low Q^2 values. Unfortunately, no measurements are available to sort out this controversy.

The necessary measurements require separation of the longitudinal and transverse components of the cross section, traditionally accomplished by linear fits to data at fixed (x_{Bj},Q^2) values but differing virtual-photon polarization ϵ, requiring a wide range in beam energies and spectrometer angles. An 11 GeV CEBAF is the perfect machine for carrying out these measurements. The longitudinal structure function can be measured precisely in the range $0.1 < Q^2 < 10$ (GeV/c)^2, fully covering both the large x_{Bj} regime and the nucleon resonance region.

Evolution of the parton distribution functions at large x_{Bj}

Parton distribution functions (PDFs) are determined experimentally from the cross sections for a number of hard processes by using a procedure referred to as *global fitting* [Ma98, La95, Gl98]. A fully quantitative description of the proton structure in terms of PDFs relies, however, on our ability to unravel the Q^2-dependence of the data in detail. In particular it is important to obtain more quantitative information on the boundary or "transition" regions of x_{Bj} and Q^2 where perturbative QCD (pQCD) evolution regulated by the Q^2-evolution [Gr75] equations can no longer be expected to describe the main mechanism responsible for the Q^2-dependence of the data, and nonperturbative contributions become important. In pQCD analyses performed to date, higher-twist terms have been extracted from DIS data by applying a cut in the kinematics at $W^2 \geq 10$ GeV^2 [Vi92, Al00]. In Refs. [Ni99, Li00] it was shown, however, that only a relatively small higher-twist contribution, consistent with the one obtained in Ref. [Vi92, Al00], is necessary in order to describe the entire set of F_2 structure function data, including the low-W^2 region which is dominated by nucleon resonances; this is consistent with the applicability of duality. Detailed analyses of large x_{Bj} evolution would be possible with an 11 GeV beam at JLab. Given a better constraint on the Q^2-dependence in this kinematic region, one could, as mentioned also in Section 2.B.1, derive parameterizations for the PDFs at large x_{Bj} directly from the data without necessarily resorting

to theoretical inputs [*e.g.*, $F_2 \approx (1 - x_{Bj})^a$ with $a \approx 3$].

Duality in spin-structure functions

Deep inelastic scattering experiments in a long series dating back to the late seventies [Al76, Ba83, As89, An93, Ab98b, Ad94a, Ab97, Ab99a, Du91, Ar97] have studied the spin structure functions. The proposed 11 GeV JLab beam energy opens up opportunities for additional studies of the spin structure in the region of the resonances, particularly in connection with the question of polarized parton-hadron duality.

What is required for new, detailed studies of duality, similar to those already performed for the F_2 structure function, are additional spin-structure function data in the resonance region. To obtain higher-order moments to utilize in an OPE analysis, data at large x_{Bj} are imperative. A large body of resonance region data is also required in order to determine whether the g_1, g_2 data oscillate around a global curve, and whether this curve corresponds at moderate Q^2 values to the curve obtained from deep inelastic scattering. The questions of whether the polarized structure functions will exhibit local duality and/or valence-like sensitivity are completely unresolved.

The main advantages of a high-energy beam are that it opens up a wide range of kinematic coverage at large x_{Bj} and the resonance region for duality studies and that it provides the ability to reach larger values of Q^2 at smaller scattering angles than at low energy, with the attendant larger cross sections. Studies of possible 11 GeV measurements of the spin asymmetry $A_1^{p,n}$, assuming duality to hold, indicate a dramatic increase in x_{Bj} range afforded by utilizing duality-averaging. The 11 GeV beam energy will provide a good cross check of the lower x_{Bj} region, and allow extension of these measurements up to $x_{Bj} \sim 0.9$, using either solid-state polarized hydrogen and deuterium targets or high-pressure gaseous ^{3}He targets in conjunction with either the spectrometers in Halls A and C or the upgraded CLAS in Hall B.

Duality and pions at high transverse momenta

While the phenomenon of duality in inclusive scattering is well established, duality in the related case of meson photo- and electro-production has not been tested experimentally. First we concentrate on reactions where the pion exits with transverse momentum large enough that it is directly produced at short range and exits the reaction in kinematic isolation from other reaction products [Br99]. Direct pion production is calculable within pQCD by virtue of the pion's large transverse momentum: the cross section for hard pion photoproduction can be written as

a kinematic factor times a scaling function [Af00], where the latter is a function that, in general, depends on several variables but in the limit of large t and large m_X depends only on the variable x_{Bj} (up to logarithmic corrections).

A goal here is to see what happens at smaller recoiling mass m_X, particularly in the resonance region. The scaling curve will become bumpy at low m_X, and one may ask whether the resonances, averaged over their own widths, reproduce the established scaling curve, and whether the resonance peak-to-background ratio remains constant for a given resonance as $|t|$ increases.

One needs, of course, to have a scaling region where m_X is large and direct pion production is dominant. One problem when the energy or transverse momentum is not high is a background coming from soft processes, which can be estimated assuming vector-meson dominance (VMD). One can reduce the VMD background by having the photon off shell. For a 12 GeV incoming beam, preliminary estimates based on earlier work [Af00a] indicate that with photons space-like by 1 $(\mathrm{GeV}/c)^2$ there is a significant scaling region with m_X between 2 and 3 $(\mathrm{GeV}/c)^2$ and with direct pion production dominating both the fragmentation and VMD processes. There is also a resonance region with m_X between 1 and 2 $(\mathrm{GeV}/c)^2$. Thus, an 11 GeV beam at CEBAF would clearly allow this category of semi-inclusive duality experiments to be performed.

Fragmentation duality

Related to the above case is semi-inclusive deep inelastic scattering in parallel kinematics. Here a parton exits the initial reaction, and then, at some distance later, fragments into a jet of hadrons, one of which is the observed pion. This is in contrast to the process described above, where, at large transverse momentum, short-range direct production dominates. Here again duality would manifest itself with an observed scaling in the meson plus resonance final state.

Assuming one is in a kinematic region that mimics single-quark scattering, the question here (in analogy with the inclusive scattering case) is whether the remaining part of the process can be described in terms of a process where the struck quark hadronizes into the detected meson. As mentioned above, such a factorization approach is strictly valid at asymptotic energies only, as at low energies there may not be clear separation of the target and current fragmentation regions [Sl88, Fr94a]. However, similar to the inclusive case (where the nucleon resonances average at low energies to the scaling curve), the nucleon resonances remaining in the final state after the production of a fast meson may average to the fragmentation function. Where the usual Bloom-Gilman duality involves comparison of a structure function over some range in Bjorken x_{Bj} at low W^2 (and hence low Q^2) with that structure function over the same range in x_{Bj} but at high W^2

(and Q^2), we may find a similar behavior in terms of the fragmentation functions $D_i^h(z, Q^2)$ in the case of semi-inclusive meson electroproduction. The variable $z = E_h/\nu$, where ν is the electron energy loss. (For orientation, in the limit of $z \to 1$, one approaches the exclusive limit.) Given the (x_{Bj}, Q^2)-dependent part, we can look for a truncated duality behavior in the (z, Q^2)-dependent part.

In practice, we will extract the meson yield dN^m/dz over a range of z at several values of x_{Bj} and Q^2. This allows the comparison of dN^m/dz in the resonance region to that in the deep inelastic regime, which we obtain from the quark model or from parameterizations of data. Sparse information from both older Cornell data and recent JLab data strongly suggests that 6–11 GeV will provide the right kinematic region to study the onset of the duality phenomenon in meson electroproduction [Be75, En00a].

Here the combination of two high-momentum spectrometers reaching the smallest angles possible (the HMS-SHMS combination) is of prime importance. This will enable us to verify meson duality, and, if also quantified, access fragmentation functions and parton distributions (through a flavor decomposition) in hitherto inaccessible regions.

2.B.5 Low-Energy Fragmentation Functions

The production of mesons (M) in semi-inclusive electron scattering, $eN \to e'MX$, yields insights into the quark structure of the nucleon that are unavailable in inclusive measurements. As mentioned in Section 2.B.4, at asymptotic energy the scattering and production mechanisms factorize into a parton distribution function and a quark $\to$ meson fragmentation function. The extent to which factorization applies at lower energy is an open question. Nonetheless, confirmation of factorization (or truncated duality) at lower energies would open the way to an enormously rich semi-inclusive program, allowing unprecedented spin and flavor decomposition of quark distributions. By measuring deep inelastic π^+ and π^- yields from hydrogen and deuterium targets, the HERMES experiment demonstrated sensitivity to the light-quark-sea flavor asymmetry comparable to the Fermilab E866 Drell-Yan measurement at much higher Q^2 and ν. There is, additionally, some preliminary experimental indication that factorization seems to hold at lower than asymptotic energies, provided one makes an additional cut in z [Ac98, En00a]. With the high luminosity available at Jefferson Lab, a high-precision separation of the x_{Bj} and z-dependence of meson production cross sections becomes possible, allowing tests of factorization at low (Q^2, ν). Figure 43 shows the quality of the data we might obtain at two fixed values of z, as a function of x_{Bj}, to probe the assumption of factorization. Additionally, one can carry out more complete tests of independent

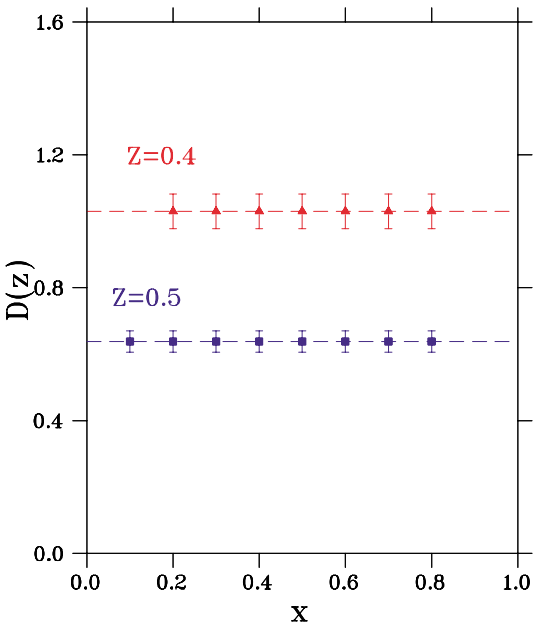

Figure 43: The projected mean fragmentation function as a function of x_{Bj} for two bins in z. The uncertainties represent statistics only for a two-day measurement for each bin of z.

fragmentation [Ch99] in which the asymmetry of the total charged-pion yield is compared to the proton-neutron difference ratio of polarized and unpolarized deep inelastic structure functions.

To exhibit the importance of understanding the onset of factorization, we highlight two examples in Fig. 44: (i) a measurement of semi-inclusive pion asymmetries using polarized proton and deuterium targets in CLAS, to extract the ratio of the polarized to unpolarized valence down-parton distribution function, adding complementary information to the measurement of A_1^n described before; and (ii) a projected extraction of the flavor asymmetry of the light-quark sea from semi-inclusive deep inelastic scattering, assuming factorization (or, less strictly, fragmentation duality) works for $Q^2 > 2$ $(\mathrm{GeV}/c)^2$ and $z > 0.3$. The latter measurement could be carried out either in Hall A or Hall C in less than one month of beam time. Please note that only statistical uncertainties are shown. Systematic uncertainties due to nuclear corrections are expected to be a substantial contribution to the flavor asymmetry for $x_{Bj} \geq 0.3$. With an 11 GeV JLab beam energy one could easily extend these measurements to other mesons, such as charged kaons, and to other nuclei, to investigate the nuclear dependence of semi-inclusive meson production.

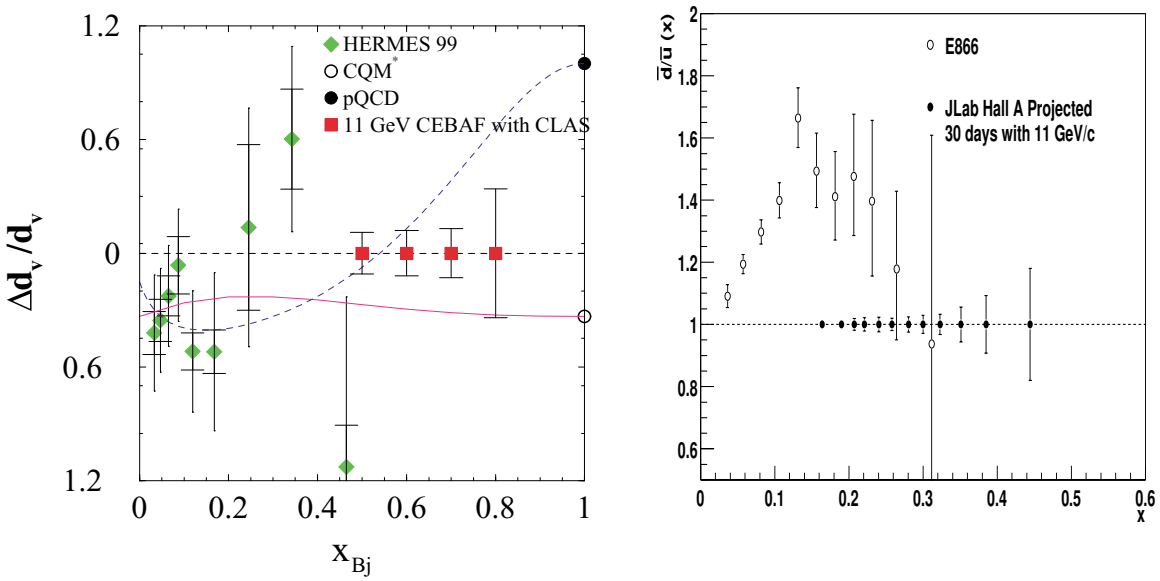

Figure 44: Examples of low-energy fragmentation. *Left*: The ratio of polarized to unpolarized valence down parton distribution functions. The solid squares represent the predicted accuracy (dominated by systematics for $x_{Bj} < 0.8$) for an 80 day measurement in Hall B. The solid curve uses wavefunctions from a constituent quark model. The dashed curve uses pQCD-constrained fits to the world data set. *Right*: The projected precision of $\bar{d}/\bar{u}$ extractions (right) assuming either fragmentation duality or factorization work with strict Q^2 and z cuts, and an 11 GeV JLab beam energy. The experiment would take one month of beam time, either in Hall A (shown here) or Hall C. The published measurements of E866 [Ha98] are shown for comparison. Only statistical uncertainties are shown.

2.C Campaign 3: Understanding the Origin of the NN Force

At large distances ($\gtrsim$1.5 fm), the origin of nuclear forces is well understood. Meson exchange and, in particular, pion exchange provide us with a coherent and powerful framework that has been confirmed elegantly by the observation of meson-exchange currents: the electromagnetic probe couples to (and reveals) the charged mesons when they travel between two hadrons.

In contrast, the mechanism controlling the NN interaction for short distances could be very different, and remains to be identified. Some of the simplest possibilities include (see Fig. 45): that the three quarks in each proton interact only by gluon exchange, that one quark is exchanged between each nucleon, and that a quark "Z"-graph exchange occurs (this would include the known, long-range meson-exchange force between nucleons). In some of these cases the nucleons and the hadrons lose their identity, and direct interactions between their constituents become relevant. When two quarks in different hadrons come close enough (within the gluon correlation length), they exchange gluons which have no time to recombine into a pomeron. Alternately, the quarks may be interchanged between the two hadrons without having time to recombine into a meson. Experiments are needed to guide the development of models that describe this nonperturbative sector of QCD.

Experiments addressing the origin of the short-distance behavior of the nuclear force are already an important part of the CEBAF research program at 6 GeV. Examples include:

- The study of meson photoproduction and of photodisintegration of few nucleon systems at large angles is sensitive to quark-interchange mechanisms.
- The study of strangeness photo- and electro-production takes advantage of the creation and the propagation of the strange quark in nuclear matter. Since it is not a normal building block of matter, the strange quark acts as an impurity whose motion traces the nature of the flow of energy and momentum transfer between hadrons.
- The study of the creation and the propagation of color dipoles of small transverse size gives access to multi-gluon exchange mechanisms that may lead to van der Waals forces between overall color singlets. This issue is being addressed through ϕ meson photoproduction at large momentum transfer and through attempts to observe color transparency at moderate Q^2.

While these studies will continue to be pursued using 11 and 12 GeV beams from CEBAF, the increased energy and duty factor open two important new opportunities: the study of charm photoproduction near threshold, and the comprehensive study of color transparency.

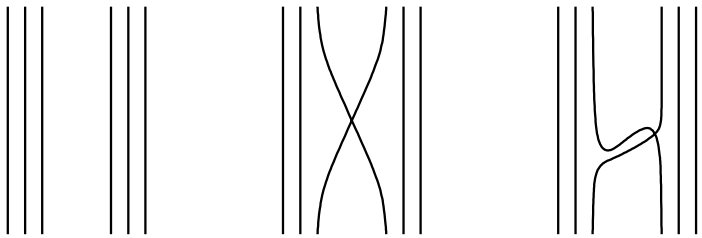

Figure 45: Three of the simplest interactions between two nucleons: pure gluon exchange, quark exchange, and meson exchange.

2.C.1 J/ψ Photoproduction near Threshold

The threshold production of charmonium and open charm production open up a new window into QCD dynamics; in particular, these reactions are sensitive to multiquark, gluonic, and so-called "hidden color" correlations in nucleons and nuclei[4]. In contrast to diffractive charm production at high energy, which tests the behavior of the gluon structure functions at small x, charm production near threshold tests the structure of the target near $x = 1$ and its short-range behavior.

This difference results from the kinematics of the reaction products. For J/ψ production off the nucleon, the threshold energy is $E_\gamma = 8.20$ GeV, and because of the large mass of the charmed quark [$m_c \approx 1.5$ (GeV/c)^2] the $c\bar{c}$ fluctuation of the photon travels over a short coherence length $l_c \cong 2E_\gamma/4m_c^2 = 0.36$ fm (see Fig. 46). The large mass of the charmed quark also imposes a small transverse size $r_\perp \sim 1/m_c = 0.13$ fm on this fluctuation. The minimum value allowed for the momentum transfer is large [$-t_{\min} \sim 1.7$ (GeV/c)^2 at threshold, and ~ 0.6 (GeV/c)^2 at $E_\gamma = 10$ GeV]. Thus charm production near threshold implies a small impact parameter ($b \sim 1/m_c \sim 0.2$ fm). All five valence quarks (the two heavy charm quarks in the probe and the three light quarks in the target) must be in the same small interaction volume. As a consequence, all the quarks must be involved in the reaction mechanism. For nucleon targets, this implies that three-gluon exchange may dominate two-gluon and one-gluon exchange, and open the way for the study of correlations between valence quarks.

Relying on the short-distance behavior of hadronic matter [Ho97, Br92], Brodsky *et al.* [Br01] showed that the charm production cross section can be cast in a simple form using general properties of perturbative QCD. For two-gluon exchange, the cross section of the $\gamma p \to J/\psi p$ reaction takes

[4]The "hidden color" language must be used with caution. With color treated as a quark label, a multiquark system can be expanded with fixed clusters in a color basis or in a basis where only color singlet clusters are used. These two bases are equivalent.

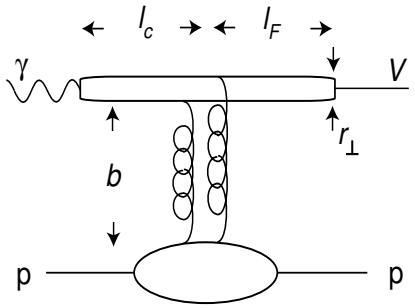

Figure 46: The characteristic time scales in J/ψ production on the proton.

the form:

$$\frac{d\sigma}{dt} = \mathcal{N}_{2g}\frac{1}{16\pi}\frac{(1-x)^2}{R^2\mathcal{M}^2}F_1^2\left(\frac{t}{4}\right) \tag{27}$$

while for three-gluon exchange it takes the form:

$$\frac{d\sigma}{dt} = \mathcal{N}_{3g}\frac{1}{16\pi}\frac{(1-x)^0}{R^4\mathcal{M}^4}F_1^2\left(\frac{t}{9}\right) \tag{28}$$

where $x \approx (2m\mathcal{M}+\mathcal{M}^2)/(s-m^2)$ and $\mathcal{M}$ is the mass of the $c\bar{c}$ pair. The relative weight of the two- and three-gluon exchange terms is controlled by the probability $1/R^2\mathcal{M}^2$ that two quarks in the proton (of radius $R \sim 1$ fm) are found within a transverse distance $1/\mathcal{M}$ (see [Br79]). $F_1(t)$ is the isoscalar proton form factor. This argument takes into account the fact that the momentum transfer is shared between two or three valence quarks in the proton. This implies that the t distribution for the three-gluon exchange cross section is flatter than the t distribution for the two-gluon exchange cross section. The upper limit of the normalization coefficient, $\mathcal{N}$, was estimated by assuming that each channel saturates the experimental cross section measured at Stanford [Ca75] and Cornell [Gi75] around $E_\gamma = 12$ GeV. As depicted in Fig. 47, this conjecture is consistent with the limited data that are available [Ca75, Gi75, An77]. Clearly 12 GeV beams from an upgraded CEBAF will allow a more comprehensive determination of the J/ψ photoproduction cross section between threshold and 12 GeV.

On few-body targets each exchanged gluon may couple to a colored quark cluster and reveal the hidden color part of the nuclear wavefunction, a domain of short-range nuclear physics where nucleons lose their identity. It is striking that in $\gamma d \to J/\psi pn$ the $|B_8\overline{B_8}\rangle$ hidden color state of the deuteron couples naturally by two gluons to the $J/\psi pn$ final state [La94] (see Fig. 48). Such a contribution may dominate subthreshold production, since the high momentum of the nucleon suppresses quasifree mechanisms. The threshold for J/ψ production on deuterium is ~ 5.65 GeV, while on heavy nuclei the threshold is simply the J/ψ mass, 3.1 GeV.

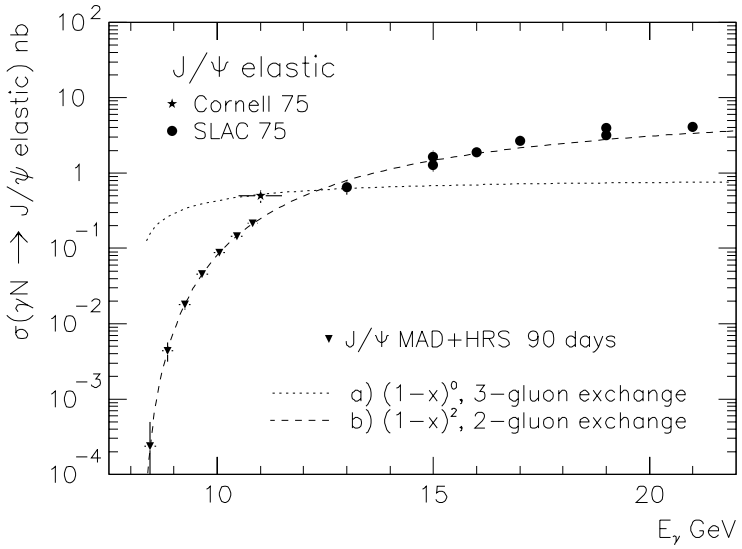

Figure 47: The variation of the cross sections of J/ψ photoproduction near threshold for two- and three-gluon exchange mechanisms. The inverted triangles show the expected accuracy at CEBAF with 11 GeV beam.

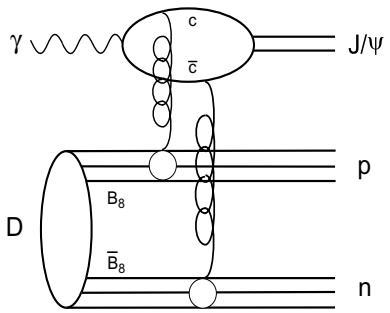

Figure 48: The simplest diagram to reveal hidden color state in deuterium [La94].

Table 3: The values of nuclear transparencies for ψ propagation, calculated in the model used by the SLAC measurement [An77b], for three values of $\sigma_{\psi N}$. The last column presents the expected statistical error, $\delta\sigma_{\psi N}$ for a $\sigma_{\psi N}$ measurement at CEBAF using 11 GeV beam, assuming a statistical error of 3% for the yields on every target.

	A						
	9	12	27	63	108	207	$\delta\sigma(\sigma_{\psi N})$, mb
T for $\sigma_{\psi N}$=1.0 mb	0.982	0.980	0.974	0.963	0.952	0.929	0.28
T for $\sigma_{\psi N}$=3.5 mb	0.938	0.931	0.908	0.870	0.833	0.751	0.24
T for $\sigma_{\psi N}$=7.0 mb	0.876	0.863	0.816	0.740	0.665	0.502	0.17

The formation length, l_F, over which the $c\bar{c}$ pair evolves into a J/ψ after its interaction with a nucleon, is given by:

$$l_F \cong \frac{2}{m_{\psi'} - m_{J/\psi}} \left[\frac{E_{J/\psi}}{2m_c}\right] \cong 0.22 E_\gamma \tag{29}$$

Near threshold l_F is about 1 fm, closer to the size of the nucleon than to the size of the nucleus. This is the ideal situation for determining the scattering cross section of a full-sized charmed meson on a nucleon, in contrast to the situation at higher energies where the cross section is sensitive to the interaction of a compact $c\bar{c}$ pair with the entire nucleus. The study of the A-dependence of the J/ψ photoproduction cross section at SLAC at 20 GeV [An77b] gave $\sigma_{J/\psi} = 3.5 \pm 0.8 \pm 0.5$ mb. Unfortunately, the need to subtract a large calculated background and the lack of information on the J/ψ kinematics makes it impossible to disentangle coherent and incoherent photoproduction in this experiment. The study [Ge92] of hadroproduction gave $\sigma_{J/\psi} \approx 7$ mb, but after correction [Hu98] for energy loss of the incoming hadron and coherence effects this value went down to ≈ 3.6 mb.

On the theoretical side, QCD calculations [Kr99] predict that $\sigma_{J/\psi} \approx 0.3$ mb at 20 GeV, and that it falls rapidly as the energy is reduced. In contrast, a calculation by Brodsky [Br97] based on the van der Waals potential yielded $\sigma_{J/\psi} \approx 7$ mb at low energies. Both the disagreement between these theoretical estimates and the poor quality of the available data call for a new measurement of J/ψ photoproduction on several nuclei in the range of energy $E_\gamma \approx 10$ GeV, with good process identification and determination of the J/ψ momentum. The systematic error of such a measurement will be smaller than in Ref. [An77b]. The statistical error was estimated using the same model for nuclear transparency as was used for the SLAC experiment [An77b]. This model, based on a semiclassical eikonal approximation for the rescattering [Go69, La72], predicts the values for nuclear transparency, $T = \sigma_{\gamma A}/(A \cdot \sigma_{\gamma N})$, given in Table 3.

Even though the $c\bar{c}$ pair is created with rather high momentum at threshold, it may be possible

Table 4: Experimental resolutions, σ, of important physics variables in the charm experiments possible at JLab

Setup	$\sigma(M)/M$	$\sigma(E_\Psi)/E_\Psi$	$\sigma(E_\gamma)/E_\gamma$	σt (GeV/c)^2
Hall D, tagged beam	0.010	0.004	0.001	0.03
HRS+MAD	0.002	0.001	0.002	0.014
ECAL	0.035	0.007	0.01	0.11

to observe reactions where the pair is captured by the target nucleus, forming "nuclear-bound quarkonium" [Br90]. This process should be enhanced in subthreshold reactions. There is no Pauli blocking for charmed quarks in nuclei, and it has been estimated that there is a large attractive van der Waals potential binding the pair to the nucleus [Lu92]. The discovery of such qualitatively new states of matter would be very significant.

Besides possible applications in connected domains (for instance, the knowledge of the J/ψ-N scattering in the search for the quark-gluon plasma), all these studies select gluonic exchange mechanisms between hadrons or quark clusters. The observation of a gluonic potential between color-neutral states is of utmost importance as it would open up the possibility to trace part of the short-range nucleon-nucleon interaction to such a color force. Only the high intensity and duty factor of the beams that will be available from an upgraded CEBAF make it possible to realize the new experiments that are essential for the exploration of this frontier of our knowledge.

The issue of experimental feasibility has been worked out in detail [Ch01]. Three options were evaluated for the detector: Hall D, HRS+MAD of Hall A, and a dedicated, calorimeter-based experiment called "ECAL" here for brevity. These three options provide the resolutions for the key physics variables as shown in Table 4. The expected particle rates and background estimates are presented in Table 5.

In the open charm sector both Hall D and HRS+MAD would be able to do the measurement, depending on the background levels. The 4π acceptance of the Hall D detector and the energy resolution of its tagged beam could help to reduce the background considerably. However, the HRS+MAD mass resolution would be better. It is not clear yet which option is more advantageous. For J/ψ studies, the best option is the dedicated experiment (ECAL). With ECAL the complete program can be accomplished, including the search for rare phenomena like hidden color. Nevertheless, a pilot measurement of the "elastic production" cross section might be done with Hall D, and the A-dependence can be measured with HRS+MAD.

Table 5: A comparison of the experimental options to study charm at JLab. The background-to-signal ratio was estimated for 11 GeV photons. The last column shows the number of days of data-taking needed to achieve an average relative statistical accuracy of 10% in the cross-section measurement for an energy interval of 0.4 GeV above the threshold. This estimate has not been made for open charm since the background is, at the moment, uncertain.

Process	Setup	Recoil	Background / signal	$d\sigma/dt \propto (1-x)^2$		$d\sigma/dt \propto (1-x)^0$	
				events/ 90 days	days needed	events/ 90 days	days needed
$\gamma p \to J/\psi p$							
$J/\psi \to e^+e^-$	ECAL	Yes	0.10	$0.6{\cdot}10^5$	10	$3.0{\cdot}10^5$	0.2
$J/\psi \to l^+l^-$	HRS+MAD	No	<0.02	$2.4{\cdot}10^3$	190	$2.8{\cdot}10^4$	45
$J/\psi \to l^+l^-$	D tag	Yes	0.07	$2.6{\cdot}10^2$	640	$2.1{\cdot}10^3$	40
$\gamma p \to \Lambda_c^+ \overline{D}^\circ$							
$\overline{D}^\circ \to K^+\pi^-$	HRS+MAD	No	0.05	$2.9{\cdot}10^3$	-	$2.9{\cdot}10^4$	-
$\overline{D}^\circ \to K^+\pi^-$	D tag	Yes	0.25	$5.4{\cdot}10^2$	-	$3.4{\cdot}10^3$	-

2.C.2 Color Transparency

One of the fundamental predictions of QCD is the existence of color transparency (CT), a novel QCD effect that is predicted to have its most unexpected manifestation in $(e, e'p)$ at very high energy. Under the right conditions, three quarks, each of which would have interacted very strongly with nuclear matter, pass right through it. This can happen because three quarks can have a small color dipole moment. The prediction of color transparency relies on three key elements: (i) the weakness of the interaction of small, color singlet objects at high energies, (ii) the presence of small-transverse-size, pointlike configurations (PLC) in mesons and baryons, and (iii) a large coherence length at high energies which leads to the possibility of considering the scattering states as frozen during the collision.

Experiments at HERA, which studied the production of vector mesons by longitudinally polarized photons, have convincingly confirmed [Ab99] pQCD predictions on the presence of PLC in vector mesons and the smallness of the interaction between a small-size $q\bar{q}$ dipole and a nucleon. Another confirmation of the dominance of PLC and the weakness of small-size $q\bar{q}$-N interaction came from the E971 experiment at FNAL on high-p_t di-jet production from nuclei in the $\pi + A \to 2$ jets $+A$ reaction at $E_\pi = 500$ GeV [As99]. In this reaction CT effects lead [Fr93a] to a platinum/carbon cross-section ratio seven times larger than expected if soft physics would dominate. Evidence for color transparency effects was also reported in the incoherent vector-meson production

in DIS scattering of muons [Ad95]. These observations have firmly established the general concepts of CT. However, there are two fundamental questions yet to be answered: at what energy does CT begin to play a role; and is CT also a characteristic of nonperturbative QCD. These questions are intimately related to the understanding of the mechanism of the transition from the constituent-quark regime to the current-quark regime and to the origin of hadronic (NN) interactions at short distances. The 12 GeV Upgrade will cover the wide range of intermediate energies necessary to pursue an unambiguous answer to these questions. The major directions for the study of CT at intermediate energies are:

- Observation of CT in the propagation of both $q\bar{q}$ and qqq color-neutral states (the last phenomenon is absent in QED).
- Study of the interaction cross sections of small objects.
- Study of the dynamics of the expansion of small sized $q\bar{q}$ and qqq configurations.

The simultaneous investigation of $(e, e'N)$, $(e, e'NN)$ and coherent vector-meson production reactions will significantly contribute to the understanding of those mechanisms.

Color transparency in $(e, e'N)$ and $(e, e'NN)$ reactions

To define the momentum transfers, Q^2, at which the PLC starts to dominate the wavefunction of nucleons, the study of quasiexclusive hard reactions $l(h) + A \to l(h) + p + (A-1)^*$ was suggested in Refs. [Br82, Mu82]. If the energy and momentum transfer are large enough, one expects that both the projectile and the ejected nucleon travel through the nucleus in pointlike configurations, resulting in a cross section proportional to A. To determine the transparency the ratio $T = \sigma^{\rm Exp}/\sigma^{\rm PWIA}$ is measured, where $\sigma^{\rm Exp}$ is the measured cross section, and $\sigma^{\rm PWIA}$ is the cross section calculated when no final-state interactions are taken into account. An onset of CT would imply an increase of T with the ejectile momentum. Indeed, initial [Ca88] and subsequent [BNL98, BNL00] measurements of T in $A(p, 2p)X$ reactions by the EVA collaboration at BNL support the increase of T for $p_{\rm inc}$ between 6 and 10 GeV/c (but also show a subsequent decrease in T for higher $p_{\rm inc}$). A set of $A(e, e'p)$ experiments aimed at looking for color transparency were performed at SLAC [Ne95] and JLab [JL99]. The maximum Q^2 in these experiments was ≈ 8 (GeV/c)^2. The data are consistent with calculations that do not include CT effects, but they are not sufficiently accurate or at high enough Q^2 to rule out color transparency at the level predicted by several realistic CT models.

The 12 GeV Upgrade of CEBAF will improve the situation by pushing the measurement of T to

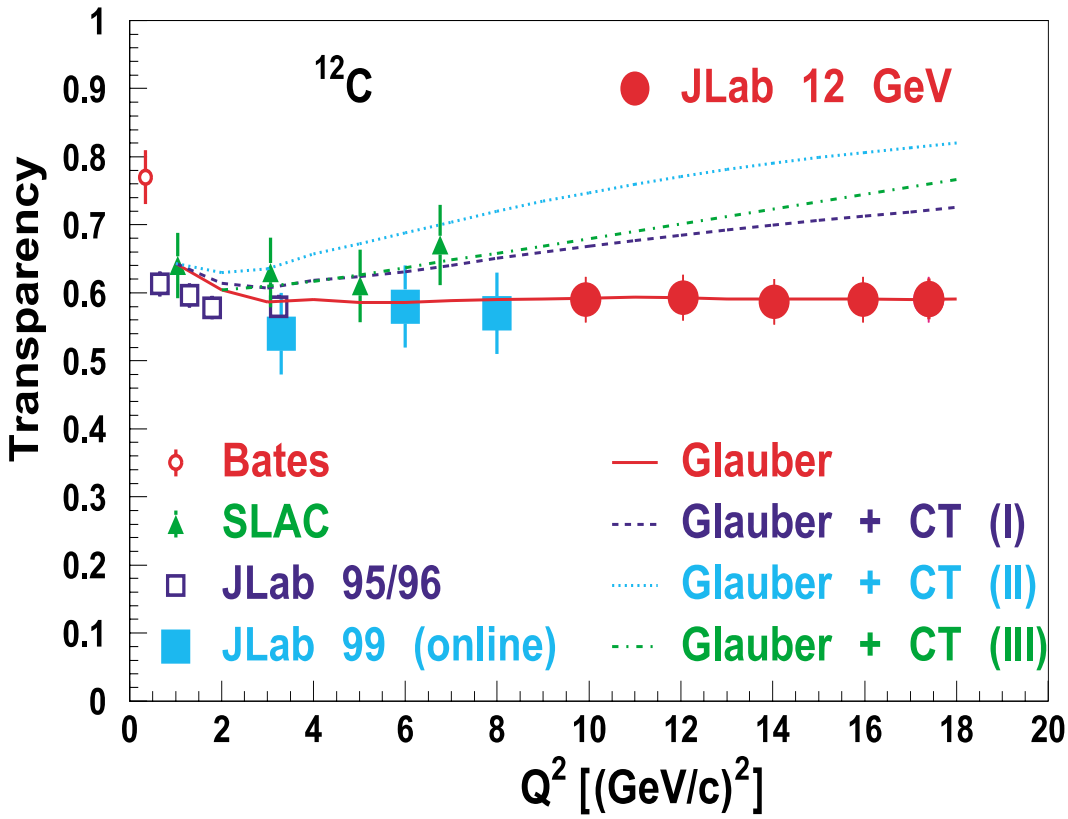

Figure 49: The Q^2 dependence of the nuclear transparency. The data are from Refs. [Ne95, Ab98, JL99]. The calculations are: "Glauber" – conventional Glauber calculation [Fr95]; Glauber+CT(I) and Glauber+CT(II) – minimal and maximal CT effects expected within quantum diffusion model [Fr95]; and Glauber+CT(III) – CT effects calculated in Ref. [Ni94]. A beam time of about one week is assumed.

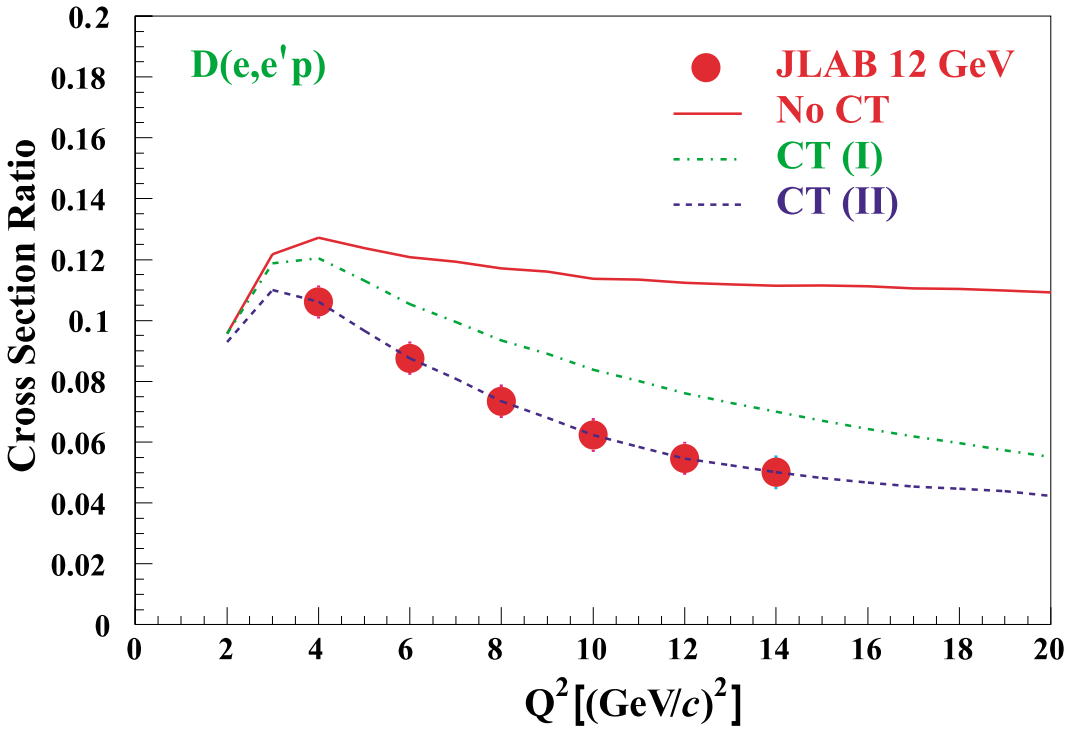

Figure 50: The Q^2-dependence of the ratio $R = \sigma(p = 400\ \mathrm{MeV}/c)/\sigma(p = 200\ \mathrm{MeV}/c)$ for the $(e, e'p)$ reaction on deuterium. The solid line: generalized Glauber approximation. Dashed and dash-dotted lines correspond to the minimal and maximal CT effects expected within the quantum diffusion model [Fr95b]. A beam time of about one month is assumed.

higher values of Q^2 where the CT predictions diverge appreciably from the prediction of conventional calculations, especially as the EVA data establish that, at least for nucleon momenta ≥ 7 GeV/c, the expansion effects are small enough not to mask an increase of T. Hence, measurements at $Q^2 \geq 12$ (GeV/c)^2 corresponding to comparable momenta of the ejected nucleon would unambiguously answer the question of whether one has entered the CT regime. These measurements would use the highest-momentum spectrometer available, the SHMS. Figure 49 displays both the present status and expected effects of CT in the measurement of T in $A(e, e'p)$ experiments, together with the typical accuracy expected from experiments feasible with 11 GeV beams from an upgraded CEBAF.

Although $A(e, e'p)X$ measurements will allow an unambiguous check of the existence of CT, a much wider range of reactions will be necessary to answer all three questions raised above. To obtain detailed knowledge of the nuclear interactions of PLCs one should also investigate processes where the ejectile, at low Q^2, interacted a second time during the passage of the nucleus [Eg94,

Fr95b, La98]. Here we emphasize the study of recoil nucleons with momenta $k > 300$ MeV/c. As a large fraction of the yield in this range originates from recoil nucleons with lower momenta rescattering, this yield should decrease substantially with the onset of CT, and give a measurable effect at lower Q^2 than in the example given above. An important advantage of this reaction is that the effect can be studied using the lightest nuclei (D, ^{3}He, ^{4}He) for which wavefunctions are much better known. In addition, there is a strong theoretical effort directed towards implementing Glauber theory and eikonal methods for $(e, e'p)$ reactions both on light and medium nuclei, which will aid in the interpretation of these measurements [Be96, Be00, Bi95, Bi96, Bi96a, De00, Gr94, It97, Je99, La91, La94a, Mo99].

The appropriate measure for color transparency in double-scattering reactions is the ratio of the cross section measured in the kinematics where the double scattering is dominant to the cross section measured in the kinematics where the effect of the Glauber screening is more important. Theoretical investigations of these reactions [Eg94, Fr95b] demonstrated that it is possible to separate these two kinematics by choosing two momentum intervals for the recoil nucleon: 300 to 500 MeV/c for double scattering and 0 to 200 MeV/c for Glauber screening. Thus the suggested experiment will measure the Q^2-dependence of the ratio $R = \sigma(p = 400\ \text{MeV}/c)/\sigma(p = 200\ \text{MeV}/c)$. Figure 50 demonstrates the feasibility of such an experiment in the case of the energy upgrade to 12 GeV using the HMS and SHMS spectrometers in Hall C. In addition to the $D(e, e'pn)$ process, one can consider excitation of baryon resonances in the spectator kinematics, such as $D(e, e'pN^*)$ and $D(e, e'N\Delta)$. The latter process is of special interest for looking for the so-called chiral transparency – the disappearance of the pion field of the ejectile.

Color transparency effects in coherent vector-meson production from the deuteron

It is widely expected that one should observe the onset of CT in the electroproduction of mesons earlier than in the case of nucleon knockout. The simple explanation is that it is easier to bring the $q\bar{q}$ pair of a meson close together to form a PLC, than the qqq state of the baryon. We plan to study vector-meson electroproduction from a deuterium target for a beam energy of 11 GeV in the kinematic range of $Q^2 > 1$ (GeV/c)^2 and $x_{Bj} < 0.4$. Measurements of the reaction $e + d \to e' + V + d'$ for transferred momenta $-t$ up to 1 (GeV/c)^2 will allow the investigation of single- and double-scattering mechanisms in the production of vector mesons. The main focus in these measurements will be the study of the rescattering part of the amplitude [Fr98] at different kinematics. CT will diminish the probability of such a rescattering, and the predicted CT effect should be visible already at $Q^2 \sim 2$ (GeV/c)^2.

The fact that such a rescattering channel can be isolated in coherent vector-meson production from deuterium is well known from the photoproduction experiment at SLAC [An71], which demonstrated unambiguously that the cross section is dominated by rescattering of the produced meson off the spectator nucleon at $-t \geq 0.6$ (GeV/c)^2.

The proposed measurements will study the relative change of the slopes in two regions (single and double scattering) as a function of Q^2. As is well known in lepto-production processes, the longitudinal interaction lengths play an important role and have a characteristic Q^2-dependence: $l_c = 2\nu/(Q^2 + m_V^2 - t_{\rm min})$. An important aspect of the measurements here is the separation of l_c effects from color transparency effects [Ac99]. This can be achieved by keeping l_c (or x_{Bj}) fixed in the Q^2 scan of the t-dependence. At 11 GeV beam energy the t-dependence of coherent production can be studied with CLAS up to Q^2 of 5 (GeV/c)^2 at l_c ~0.8 fm [Cl00a]. Figure 51 shows the expected ratio $R_c = [\sigma(0.8)/dt]/[d\sigma(0.4)/dt]$ of the cross sections for ρ electroproduction at transferred momenta $-t = 0.4$ (GeV/c)^2 (where the cross section is dominated by single scattering) and $-t = 0.8$ (GeV/c)^2 (where the cross section is dominated by double scattering) as a function of Q^2 for different model approximations. It would also be interesting to measure the cross section for ϕ electroproduction, which can give us the information about the interplay of the soft and hard pomeron in QCD.

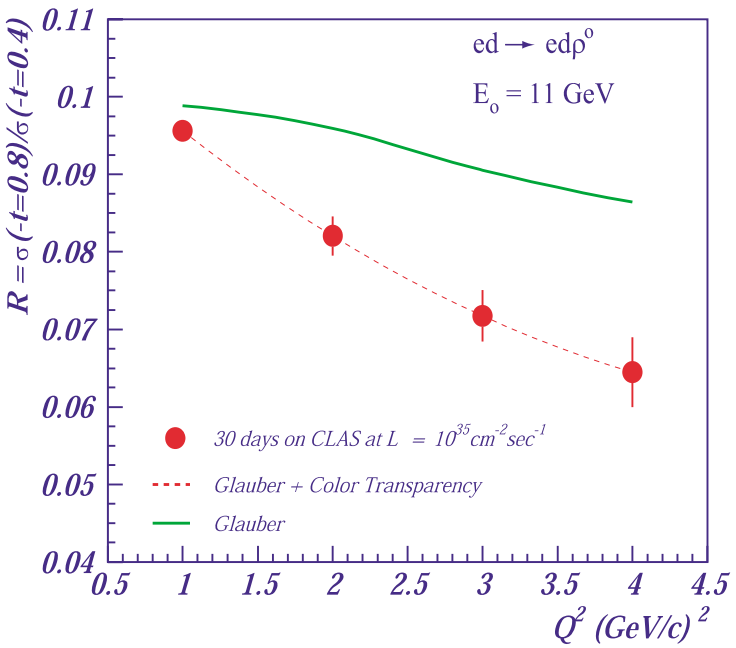

Figure 51: Expected errors on the ratio of cross sections for ρ production at $-t = 0.4$ and 0.8 $(\mathrm{GeV}/c)^2$ for 30 days of running on CLAS with an 11 GeV beam. Kinematics is fixed at around $l_c = 0.8$. The solid line is the calculation assuming no CT; the points and dashed line are with CT effects [Fr98].

2.D Campaigns 4 & 5: Testing the Limits of the Meson/Nucleon Description of Nuclei and Probing the Limits of the "Standard Model" of Nuclear Physics

One of the main motivations for building CEBAF was the investigation of the fundamental structure of nuclear matter. The aim was to probe in detail the nucleonic component of nuclear wavefunctions, and to look for manifestations of the underlying quark degrees of freedom. The results of the first investigations (in particular the measurement of the quadrupole deuteron form factor) confirm the presence of high-momentum nucleonic components in the deuteron at least up to momenta of ~ 600 MeV/c, as well as the presence of phenomena such as the large-angle photodisintegration of the deuteron, where one needs to go beyond the description based on hadronic degrees of freedom.

To date our knowledge of the structure of nuclei is limited to their behavior near equilibrium. We have been able to probe nuclei "gently" and to understand their low-energy excitation spectrum in terms of interactions and rearrangements of unperturbed nucleons. The bulk of their high-energy excitation is almost unknown. A natural question is, what happens when an energy of few GeV (comparable to the nucleon mass) is transferred to a nucleus and when nucleons are emitted at large angles? This must involve short-range mechanisms where nucleons overlap and where interactions between their constituents become relevant. This is the field of short-range correlations (SRC).

The pressing questions to be investigated include: the direct observation of SRC in nuclei, the determination of the shortest distance scale for which the notion of meson exchanges remains effective, and the identification of the distance scale at which direct constituent interactions like quark exchanges between nucleons, or "kneading" of the constituents of bound nucleons, becomes important. Average distances between nucleons in SRC are $\sim$ 1–1.2 fm, which is a factor $\sim 1\frac{1}{2}$ smaller than the average internucleon distances. Here the local densities of nuclear matter in SRC exceed the average nuclear densities by at least a factor of 4, so the investigation of the structure of SRC would have astrophysical implications important to our understanding of the dynamics of neutron star cores, which possess similar densities.

These and many related questions have been before us for decades. Why does CEBAF make a difference? The reason is the much better energy and momentum resolution of CEBAF, and its ability to perform correlation experiments for rare processes. Here our experience from nucleon structure studies can serve as a guide. It is well known that the crucial breakthrough in the study of nucleon structure occurred when it became possible at SLAC to study inclusive electron scattering processes at sufficiently high momentum transfer that quarks were knocked out of the nucleons with momenta much larger than those of the spectator quarks. This requires both large Q^2 and sufficiently large missing mass W. Further progress was made when correlation experiments were

done, where the leading hadrons were used to tag different flavors. As a result of these studies we now know the single-parton densities in nucleons quite well. In the case of nuclei these conditions correspond to the requirement that to probe the nucleonic structure of SRC it is necessary to reach momentum transfers $|\vec{q}| \gg 2k_N$, where k_N is the momentum of the nucleon in the correlation, and to have $q_0 \gg 1$ GeV/c to ensure that the ejected nucleon moves fast relative to the rest of the nucleus. This corresponds to $Q^2 \geq 1.5 - 2$ (GeV/c)^2 and the energies of the knocked-out nucleons ≥ 1 GeV. This kinematics first became reachable at CEBAF at 4–6 GeV.

To probe the limits of the nucleonic picture of SRC one must go beyond the energy presently accessible at JLab. Previous inclusive measurements of the parton structure of nuclei have demonstrated limits of the standard, many-nucleon model of nuclei. These include the EMC effect [Au83, Bo83], which unambiguously requires the presence of non-nucleonic degrees of freedom in nuclei, and the observation of a suppression of the antiquark distribution in nuclei [Al90], which contradicted predictions of an enhancement based on the mesonic picture of the short-range nuclear forces. To investigate these effects further and to reach an understanding of the parton structure of nuclei, energies higher than 6 GeV are necessary. CEBAF at 11 GeV opens unique opportunities for measuring quark distributions over a broad range of x, exploring the parton structure of superdense nuclear matter, and investigating the parton structure of bound nucleons, which cannot be probed at the available energies (≤ 6 GeV). In this respect, studies at CEBAF will nicely complement the study of the high-temperature, high-density region of the phase diagram of nuclear matter (planned at RHIC and LHC via relativistic heavy-ion collisions) with the exploration of the low-temperature, high-density phase (see Fig. 52).

2.D.1 Probing the Limits of the Standard Model of Nuclear Physics: Few-Body Form Factors

Measurements of the elastic form factors of the deuteron and the helium isotopes are of crucial importance in understanding their electromagnetic structure and testing the "standard model" of light nuclei that is based on the meson-nucleon framework, the impulse approximation (IA), and meson-exchange currents (MEC) [Ca98]. Such measurements offer unique opportunities for studying the short-range nucleon-nucleon interaction, few-body wavefunctions, isobar and three-body force contributions, and effects from possible quark-cluster admixtures. Large-momentum-transfer measurements can also test "nuclear chromodynamics" predictions based on quark dimensional scaling (QDS) and perturbative QCD (pQCD) [Ca97].

The starting point of the conventional theoretical approach of elastic scattering from few-body

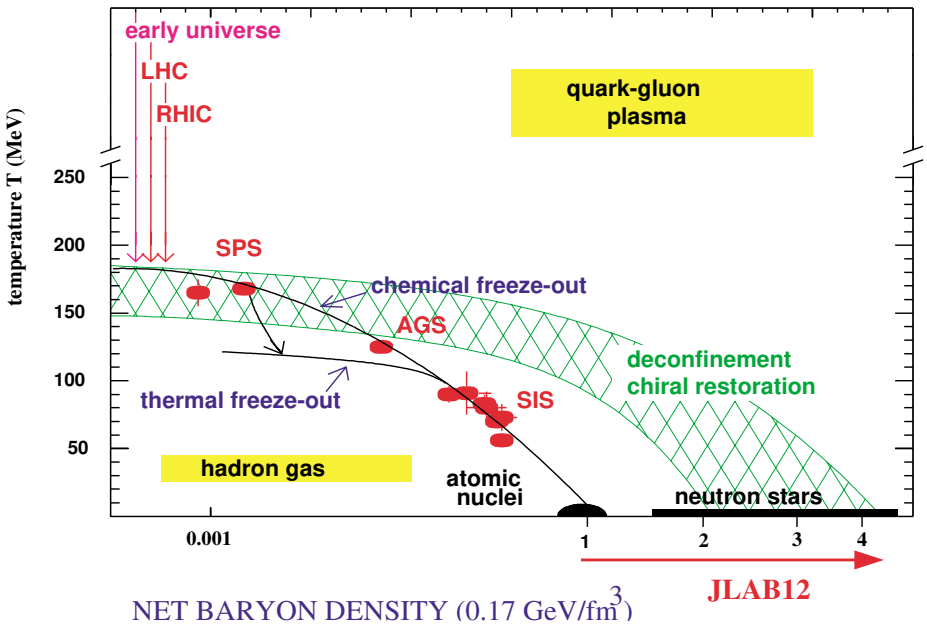

Figure 52: Phase diagram for nuclear matter.

systems is the impulse approximation, where the incident electron interacts with one of the nucleon constituents of deuterium or helium. The form factors of light nuclei are then convolutions of the nuclear wavefunction with the form factors of the constituent nucleons. At large momentum transfers the effects of relativity cannot be ignored, and either corrections must be made to the IA or fully relativistic approaches developed (as has been done in the case of the deuteron [Hu90]. It has long been understood and overwhelmingly supported by the available data that the few-body form factors are sensitive to the presence of meson-exchange currents and isobar configurations that augment the IA picture [Ca98].

At distances much less than the nucleon size, the underlying quark substructure of the nucleons cannot be ignored. This has led to the formulation of so-called hybrid quark models [Di89] that treat few-body nuclei as quark clusters when the internucleon separation becomes smaller than ∼1 fm. At sufficiently "large" momentum transfers, the few-body form factors are expected to be calculable in terms of only quarks and gluons within the framework of pQCD. The first attempt at a quark-gluon description of the few-body elastic form factors was based on the dimensional-scaling quark model (DSQM) [Br73], where the underlying dynamical mechanism during elastic scattering is the hard rescattering of the constituent quarks via exchange of hard gluons. The Q^2-dependence of this process is then predicted by simply counting the number n of gluon propagators ($n = 5$ for

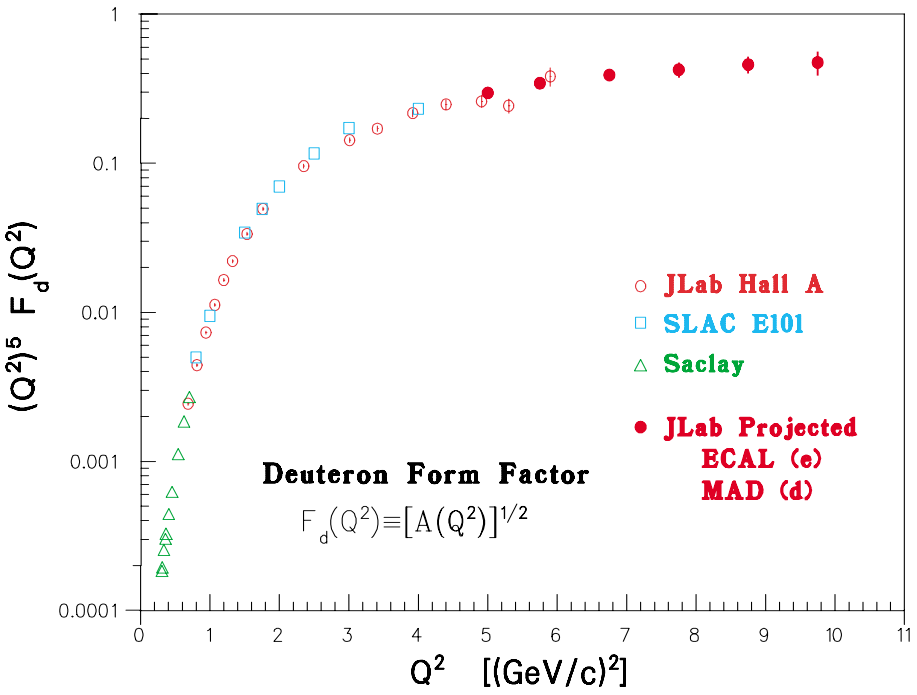

Figure 53: Projected data for the deuteron form factor $F_d(Q^2)$ with an 11 GeV JLab beam. Also shown are existing JLab, SLAC, and Saclay data.

deuterium, 8 for ^{3}He, and 11 for ^{4}He), which implies that the elastic structure functions $A(Q^2)$ of the few-body systems should follow the power law: $\sqrt{A(Q^2)} \sim (Q^2)^{-n}$. This prediction was later substantiated, for the deuteron case, in the pQCD framework, where it was shown [Br83] that to leading order:

$$\sqrt{A(Q^2)} = \left[\alpha_s\left(Q^2\right)/Q^2\right]^5 \sum_{m,n} d_{mn} \left[\ln\left(\frac{Q^2}{\Lambda^2}\right)\right]^{-\gamma_n-\gamma_m},$$

where $\alpha_s(Q^2)$ and Λ are the QCD strong coupling constant and scale parameter, and $\gamma_{m,n}$ and d_{mn} are QCD anomalous dimensions and constants.

The 12 GeV energy upgrade of the JLab electron beam and the proposed spectrometer facility upgrades will be ideal for improving and extending the existing elastic structure function measurements of light nuclei to higher momentum transfers. These measurements will test the limits of the standard model of few-body nuclei, and may uncover a possible transition to a quark-gluon description of the few-body form factors, as predicted by quark dimensional scaling and perturbative QCD.

Figure 53 shows the recent JLab Hall A and older SLAC and Saclay data [Al99] on the deuteron form factor, $F_d(Q^2) \equiv \sqrt{A(Q^2)}$, multiplied by $(Q^2)^5$. It is evident that the data show an approach to a scaling behavior consistent with the power law of DSQM and pQCD. Although several authors have questioned the validity of QDS and pQCD at the momentum transfers of this experiment [Is84], similar scaling behavior has been reported in deuteron photodisintegration at moderate photon energies [Bo98]. It is extremely important to test this apparent scaling behavior by extending the deuteron $A(Q^2)$ measurements to higher momentum transfers. Higher JLab beam energies in the range of 9–11 GeV are essential for such measurements. To separate elastic from inelastic scattering and to suppress backgrounds, recoil deuterons should be detected in coincidence with scattered electrons. A possible scenario would be to use the proposed Medium-Acceptance Device (MAD) to detect recoiling deuterons and a segmented electromagnetic calorimeter (ECAL) to detect scattered electrons. Assuming a 20-cm-long liquid-deuterium target and beam current of 70 μA, $A(Q^2)$ can be measured up to ~ 10 $(\mathrm{GeV}/c)^2$ in one month of beam time, as shown in Fig. 53. Such an experiment will double the Q^2 range of the existing data, which have been acquired over a period of 40 years. The observation of a diffractive structure (which cannot be ruled out from the existing data) would settle in the negative the question of the applicability of the QDS ideas at moderate momentum transfers once and for all. On the other hand, if the predictions are successful, the applicability of these ideas will not be proved: there are alternatives that give essentially the same predictions, and so many failures of the pQCD helicity selection rules at these energies that additional tests of the underlying dynamics will be required.

The existing data [Am94] on the ^{3}He form factor, $F(Q^2) \equiv \sqrt{A(Q^2)}$ (shown in Fig. 54), are in good agreement with the standard model (IA+MEC) calculations [Sc91] at low Q^2 but are fairly inconclusive at the largest momentum transfers. They are consistent with a change in slope at ~ 55 fm^{-2}, indicative of an onset of quark scaling [Ch78], but, at the same time, cannot exclude the presence of a second diffraction minimum as predicted by conventional meson-nucleon theory. As in the case of the deuteron, more measurements at higher Q^2 would be crucial in testing the quark-scaling prediction and a possible breakdown of the meson-nucleon framework. The energy upgrade of JLab will also allow new ^{3}He measurements that could double the Q^2 range of the existing data (taken also over a period of 40 years) in a single experiment with a tenfold better sensitivity. As in the case of the deuteron, recoiling nuclei will be measured with the MAD spectrometer and scattered electrons with a calorimeter. Assuming a 20-cm-long ^{3}He gas cryogenic target and an electron beam of 11 GeV with current of 70 μA, the ^{3}He $F(Q^2)$ can be measured up to ~ 150 fm^{-2} in one month of beam time, as shown in Fig. 54. It is evident that this experiment will be able to show whether the apparent change in slope of the SLAC data can be attributed to a classical diffraction minimum, or a quark-scaling approach as argued in Ref. [Ch78].

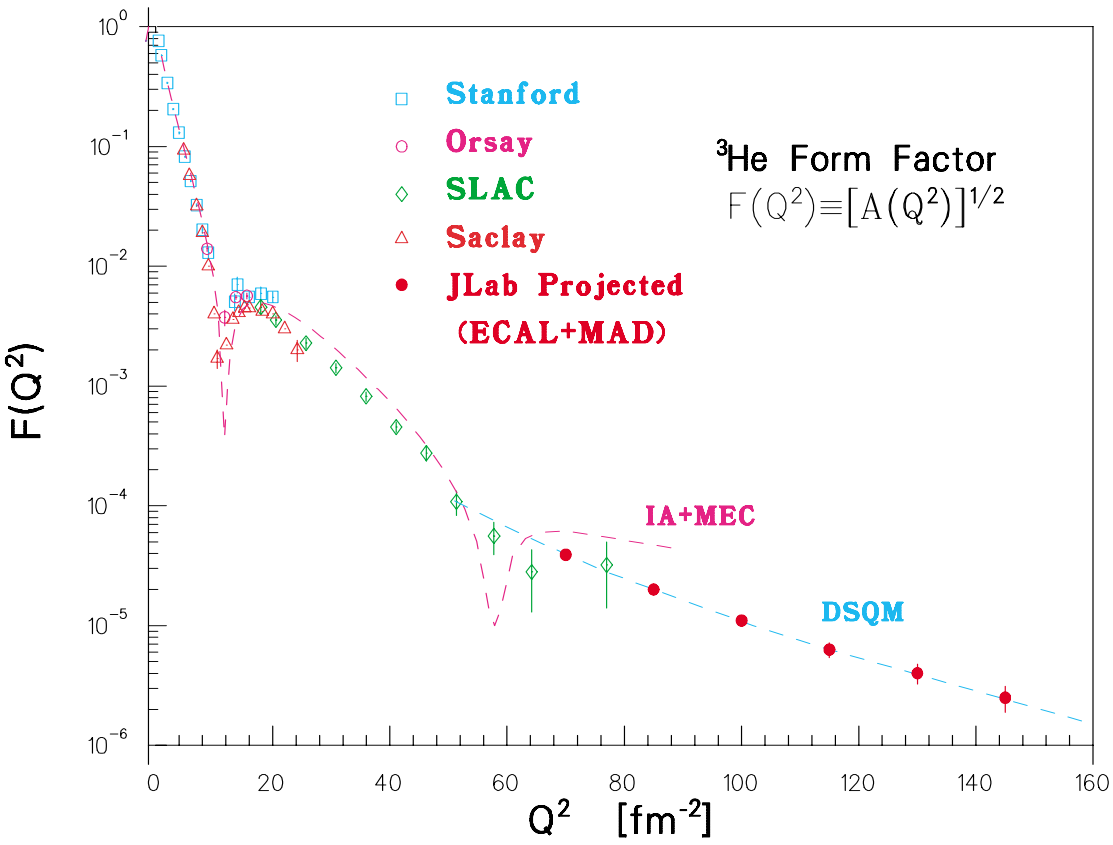

Figure 54: Projected data for the ^{3}He elastic form factor $F(Q^2)$ with an 11 GeV beam. Also shown are existing data and predictions of the standard model (IA+MEC) [Sc91] and the dimensional-scaling quark model (DSQM) [Ch78].

In summary, JLab with an 11 GeV electron beam would the ideal place to perform large-momentum-transfer measurements of the form factors of light nuclei. These measurements will test the limits of the nuclear standard model based on the impulse approximation and meson-exchange currents and are likely to establish the expected transition from the conventional meson-nucleon to the quark-gluon description of the few-body nuclear systems.

2.D.2 Probing the Limits of the Standard Model of Nuclear Physics: Short-Range Correlations in Nuclei

Observing short-range correlations (SRC) in nuclei has been an important goal of experimental nuclear physics for decades [Be99, Be67]. Not that these correlations are small – calculations of nuclear wavefunctions with realistic NN potentials consistently indicate that in heavy enough nuclei about 25% of the nucleons have momenta above the Fermi surface [Pa97]. This corresponds to about 50% of the kinetic energy being due to SRC. The experimental problem has been the unavailability of the high-momentum-transfer kinematics that could discriminate decisively between the effects of SRC in the initial- and final-state interactions. Though the final-state interactions in nucleon knockout do not disappear at large Q^2, two important simplifications occur which make extraction of the information about the short-range nuclear structure possible. First, in high-energy kinematics a "hidden" conservation law exists – the light-cone momentum fractions of slow nucleons do not change if the ejected nucleon elastically scatters off slow nucleons [Fr97]. Second, the rescatterings of a high-energy nucleon can be described by the generalized Glauber approximation, which takes into account a difference in the space-time picture of proton-nucleus scattering (a proton coming from $-\infty$) and the $A(e,e'p)$ process (a proton is produced inside the nucleus) and also accounts for the nonzero Fermi momenta of rescattered nucleons [Fr97].

There is a general consensus that Glauber theory is the appropriate tool for describing final state interactions for $E_p \gtrsim 1$ GeV, which corresponds to $Q^2 \geq 1.5$ (GeV/c)^2. On the other hand, pushing to Q^2 values that are too high is not optimal for the study of the nucleon degrees of freedom in nuclei. Indeed, it was suggested that at $Q^2 \geq 4$ (GeV/c)^2 one may encounter new phenomena related to the EMC effect [Fr88, Fr96]. Hence the optimal range for probing the nucleonic degrees of freedom is $1.5 \leq Q^2 \leq 4$ (GeV/c)^2. CEBAF at 6 GeV reaches the lower end of this range and can provide limited access to its upper part, but at the cost of low counting rates. At 11 GeV this whole range will be easily accessible for the upgraded CLAS while Halls A and C will be able to explore even higher Q^2. Studies of the $(e,e'N)$ and $(e,e'NN)$ reactions in this Q^2 range will allow us to measure directly nucleon momentum distributions up to momenta 500–700 MeV/c, as well as to measure how these momenta are balanced in nuclei: two- and three-nucleon short-range

correlation contributions versus those of the mean field.

The starting point for these studies is the simplest reaction $e + {}^2\mathrm{H} \to e\ p\ n$. It will provide a test of the basic principles of our current understanding of the dynamics of the electro-disintegration processes, especially after the CEBAF measurements of the deuteron form factors over a wide range of Q^2, since the wavefunction of the deuteron will be reasonably well known for a wide range of nucleon momenta for both S- and D-states. The progress in constructing tensor-polarized deuteron targets will make it feasible to study the same reaction using polarized targets at sufficiently large Q^2. In this case a direct separation of S- and D-wave contributions is possible. Since the D-wave is expected to play a key role over a wide range of nucleon momenta both in ${}^2\mathrm{H}$ and in heavier nuclei [Fr81, Fo96], this process will provide an ultimate test of our understanding of the short-distance NN interactions. In particular, it will allow making a clean discrimination between predictions of the Bethe-Salpeter and light-cone approaches to the description of the deuteron as a two-nucleon relativistic system [Fr88].

The $(e, e'N)$ reaction with the ejected nucleon along $\vec{q}$ for $A \geq 3$ is the next natural step in these studies. This process measures at large Q the light-cone density matrix of the nucleus, $\rho_A^N(\alpha, p_t)$, as well as the excitation energy of the residual system. That energy is expected to increase with increasing initial momentum of the knocked-out nucleon. (In the nonrelativistic approximation the average excitation energy is $\langle E_{\mathrm{rec}} \rangle \approx k^2/2m_N$, where $\vec{k}$ is the initial momentum of the knocked-out nucleon.) The availability of a large Q^2 and W range will allow us to perform a stringent test of the many-nucleon approximation in which the cross section should factorize into a product of the elementary eN elastic cross section (which drops in this Q-range by a factor of ~ 10) and the Q^2-independent spectral function. Note that the studies of the $A(e, e')$ processes for many A at $x \geq 1$ and $1 \leq Q^2 \leq 4\ (\mathrm{GeV}/c)^2$ at SLAC and CEBAF have confirmed an expected similarity in the shape of the wavefunction of the short-range correlations. Hence it will be sufficient to restrict the studies of SRC in $(e, e'N)$ and $(e, e'NN)$ processes to the lightest nuclei with $A = 3, 4$ to minimize the effects of the final-state interactions. Polarized ${}^3\mathrm{He}$ targets will play a special role for probing the SRC due to the relative simplicity of the wavefunction of the $A = 3$ system, and present a unique possibility to probe the spin structure of the pp and pn correlations. In particular, there exists kinematics where a minimum in the S-wave pp wavefunction can be probed, and the P-wave can be measured (some of these measurements will be performed already with an unpolarized target, while the polarized target will allow a number of cross checks and bring additional information). These measurements will provide stringent tests of the structure of the $A = 3$ system, and will test the current interpretations of the measurements of ${}^3\mathrm{He}$ form factors at large Q^2.

The $A(e, e'N_f N_b)$ reactions with N_f the forward- and N_b the backward-going nucleons will

allow one to investigate how the excitation energy is shared between nucleons. It is expected that the dominant contribution will originate from two-nucleon correlations. In this case N_b should carry most of the excitation energy. A comparison of the yields of (pp), (pn), and (nn) processes will provide a detailed check of the reaction mechanism and provide a quantitative comparison between the wavefunctions of two-nucleon SRC in the isospin zero and one channels. (The former is expected to dominate by a factor ≥ 4 over a large range of momenta.)

Although two-nucleon correlations are expected to produce a dominant part of SRC, the triple and higher SRC (where more than two nucleons come close together) are significant as well; they are likely to constitute $\sim 20\%$ of all SRC. They should manifest themselves in the low-excitation tail of the spectral function for large momenta of the knocked-out nucleon and can be best observed through the $A(e, e'N_f N_b)$ reaction and in processes with two backward-ejected nucleons [Fr88]. The latter reaction is especially interesting since it allows one to study the parton structure of three-nucleon correlations at very high densities. (See the discussion in the next section.)

Overall, this series of experiments at CEBAF can provide a detailed knowledge of the nucleonic component of the spectral function, including the SRC domain, that will constitute a major step forward in our understanding of the physics of the nucleus.

2.D.3 Testing the Limits of Nuclear Many-Body Physics: Probing Non-Nucleonic Degrees of Freedom in Nuclei

With the nucleon size being ~ 0.8 fm it is clear that nucleons start to overlap strongly already when the distance between them becomes ~ 1.2 fm. Hence dense nuclear matter may look very different from a system of densely packed nucleons. The properties of dense nuclear matter are closely related to many outstanding issues in QCD, such as chiral symmetry restoration, deconfinement, the onset of quark-gluon degrees of freedom, and the structure of the phase transition from the hadronic to the quark-gluon state of matter. In QCD, transitions to new phases of matter are possible in different density/temperature regimes. In particular, it has recently been suggested [Al98, Ra98] that nuclear matter could exist in a color superconductivity phase with the condensation of di-quarks. Recent estimates suggest that the average nuclear density could be right in between the dilute nucleon phase and superconducting phase [Ca00a]. If so, it is natural to ask whether one can observe precursors of such a phase transition by studying the quark-gluon properties of superdense droplets of nuclear matter, that is, configurations when two, three, or more nucleons come close together.

Since the internucleon distances in these correlations are at least a factor of 1.5 smaller than internucleon distances at average nuclear densities, one can probe droplets of nuclear matter at densities 3–5 times larger than in nuclear matter (see Fig. 52). From this viewpoint it is encouraging that the "EMC effect" data indicate that deviations from the expectations of the nucleon model of nuclei grow approximately linearly with the nuclear density, suggesting that the properties of the quark-gluon droplets could indeed deviate very strongly from those of a collection of nucleons.

These general arguments are in line with measurements of the parton densities in nuclei (the EMC effect, $\bar{q}_A/\bar{q}_N$, etc.), which unambiguously demonstrated that on the parton level a nucleus cannot be viewed as merely a collection of nucleons. Practically all the mechanisms suggested to explain the EMC effect address the question of the quark-gluon structure of SRC and/or the origin of the nuclear forces. These include:

a. Various patterns of mixing quarks (gluons) from different nucleons ranging from the deformation of the bound nucleon wavefunctions to "kneaded" (multiquark) states [Cl83, Ca83, Na84, Ja84, Fr85, Fr96].

b. A loss of momentum by nucleons to some fields that bind *undeformed* nucleons together [Er83, Fr83, Be84, Ak85, Ku89, Du85, Ju88, Ci89, Ka90, Me93, Bi89, Me94, Ku94].

c. The presence of Δ-isobars, N^*'s in nuclei, especially in the SRC [Fr83].

However, inclusive experiments at $x \leq 0.8$ have not allowed us to discriminate between such models. The broad (x, Q^2) range available at 11 GeV and the feasibility of correlation experiments suggest a strategy that will work.

The first step will be to use deep inelastic scattering off nuclei at $x \geq 1$ in the scaling limit to establish in a model-independent way (*i.e.*, not sensitive to the final-state interactions) the presence of superfast quark components in nuclei – quarks that carry a larger momentum fraction than a whole nucleon.

Theoretical estimates indicate that for $x \leq 1.5$ this will require $Q^2 \leq 20$ $(\mathrm{GeV}/c)^2$, so experiments will be feasible with $E_e = 11$ GeV. Several features of CEBAF and its experimental facilities (the good acceptance and high resolution of the CEBAF spectrometers, and the high intensity and small energy spread of the electron beam) are crucial for performing these measurements. Through a study of the Q^2-dependence of the cross section at fixed x it will be possible to observe for the first time the onset of scaling at $x \geq 1$ (Fig. 55), which will be the definitive signature for the existence of superfast quarks in nuclei.

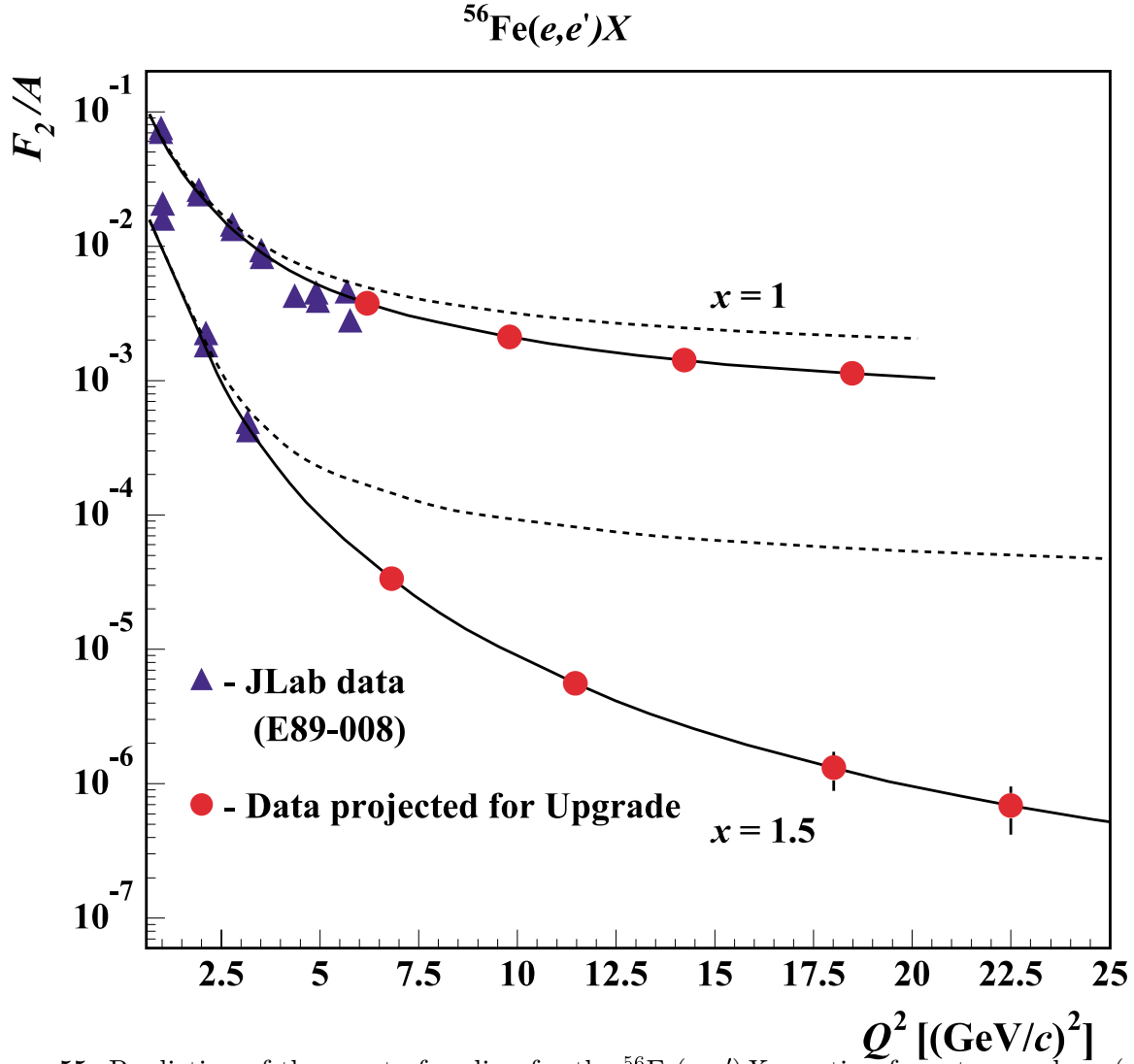

Figure 55: Prediction of the onset of scaling for the $^{56}\mathrm{Fe}(e,e')X$ reaction for a two-nucleon (solid line) and multi-nucleon (dashed line) short-range correlation model. The data shown are from Ref. [Ar99]. With the 12 GeV Upgrade data, measurements can be made to $Q^2 = 20$ (GeV/c)^2, where the solid and dashed lines will have separated by more than an order of magnitude for $x = 1.5$.

Comparing the cross sections for $A = 2$, 3, and 4 and for heavy nuclei will allow the model-independent separation of contributions of two-, three-, or more-nucleon SRC. The two-nucleon correlations are expected to dominate for $1.3 \geq x \geq 1$, leading to quark structure functions for $A \geq 12$ nuclei a factor of 5–6 larger than in the deuteron [Fr81, Fr88]. This ratio should be similar to the cross-section ratio for quasielastic scattering:

$$R_{A/D}(x, Q^2) \equiv \frac{2}{A} \frac{\sigma_{eA}(x, Q^2)}{\sigma_{e^2H}(x, Q^2)}$$

observed at $x \sim 1.5$, $4 \geq Q^2 \geq 1$ $(\mathrm{GeV}/c)^2$ at SLAC [Fr93]. Local nuclear densities probed in this case are three to four times larger than the average value, $\rho_0 \sim 0.17$ fm^{-3}. For larger $x \sim$1.5 higher correlations are expected to dominate, leading to an increase of $R_{A/D}(x \sim 1.5, Q^2 \sim 50$ $(\mathrm{GeV}/c)^2)$ [Fr81]. At the same time the local nature of generating $x \geq 1$ quarks will manifest itself experimentally through the same shape and probability per nucleon of the $x \geq 1$ component in ^{4}He and heavy nuclei. In this kinematics we expect to observe densities at least five times larger than ρ_0. Detailed studies of the A-dependence of $q_A(x, Q^2)$ at $1.5 \geq x \geq 1$ will provide important information about fluctuations of the local nuclear density as a function of average nuclear density as well as of the isospin of the correlations.

Measurement of the quark distribution at $x \geq 1$, in combination with the measurements of the light-cone nucleon density matrix (ρ_A^N) described in the previous campaign, will allow a check of whether $F_{2A}(x, Q^2) > 1$ can be described as a convolution of ρ_A^N and the *free* nucleon structure function. At the same time these measurements will establish in a model-independent way the relative importance of two- and three-nucleon SRC by comparing $F_{2A}(x, Q^2)$ for light and heavy nuclei and show the dependence of SRC on nuclear density.

The second step will be to study the tagged structure functions [Fr81, Fr88, Ci93] in order to compare directly the parton structure of the bound and free nucleon. This will start with the $e + ^2$H $\rightarrow e$ + backward nucleon + X reaction in the kinematics, where the momentum fraction carried by the struck quark in the moving nucleon ($\tilde{x}$) is sensitive to the EMC effect [$0.3 \leq \tilde{x} \leq 0.7$ (CEBAF at 11 GeV covers all of this region; see Fig. 56)] and continue to a similar reaction with ^{3}He and the tagging of two backward nucleons to consider deformations in the three-nucleon correlations. In contrast to the case of the inclusive EMC effect, different models predict [Fr88, Ca91, Ca95, Me97] a qualitatively different dependence of the experimental results on the modifications of the bound nucleon wavefunction, which range from a complete absence of modification to an effect comparable to the EMC effect for heavy nuclei in the color screening model, for tagged nucleon momenta $p_N \geq 300$ MeV/c. If the EMC effect for the bound nucleon is observed, one would be able to check whether the theoretical account of such deformations together with a realistic light-cone nucleon

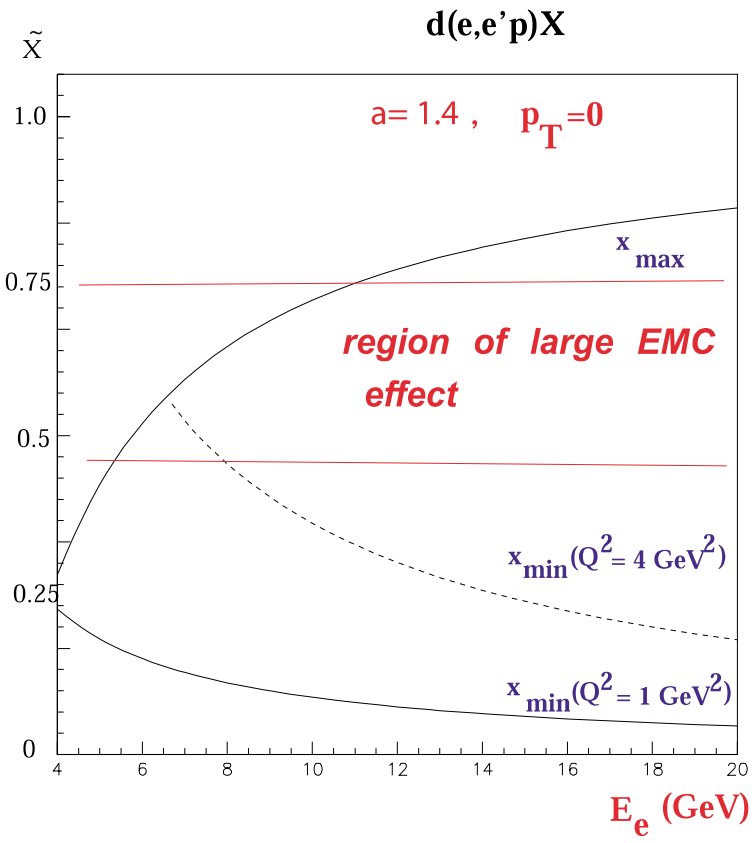

Figure 56: The scaling window for $\alpha = 1.4$, where α is the light-cone fraction of the knocked-out nucleon. The upper curve is defined by the requirement that the mass of the produced final hadronic state $W \geq 2$ GeV.

density (measured in the $A(e, e'p)$ processes) would reproduce $F_{2A}(x, Q^2) > 1$ in the scaling region.

The two-step strategy described above requires related studies that are important to cross-check all aspects of these studies:

- *Investigation of the reaction dynamics at* $Q^2 \geq 4(\mathrm{GeV}/c)^2$ The reaction dynamics of $(e, e'p)$ at GeV energy and momentum transfers has not been explored experimentally so far. It will be quite different from low energy, due to the diffractive nature of the high-energy NN interaction and the role of relativity. With the energy upgrade, one can study, for example, the reaction $e +^2 H \rightarrow e + p + n$ in parallel kinematics for recoil nucleon momenta $p_N = 400 - 500 MeV/c$ up to $Q^2 \approx 8(GeV/c)^2$. A study of this type is essential for our understanding of the baseline color transparency calculations and of short-range structures in the nucleus.

- *A test of the binding models of the EMC effect*, by measuring the position of the quasielastic peak at large Q^2. In these models, a shift of the nucleon spectral function to $\alpha < 1$ is expected, leading to a significant asymmetry in the cross section of the $(e, e'p)$ process in parallel kinematics near the quasielastic peak [Fr92].

- *Studies of special modes of deuteron breakup at high Q^2 using the upgraded CLAS* would be sensitive to meson-exchange currents, *e.g.*, $e + {}^2\mathrm{H} \rightarrow$ two forward protons + leading π^-, and processes such as production of backward Δ's off the deuteron and ^{3}He that are especially sensitive to the presence of Δ-isobar-like color-singlet clusters and six-quark clusters.

- *Probing quark degrees of freedom in large-angle electrodisintegration of the deuteron* will be a natural extension of the CEBAF photodisintegration experiment [Bo98]. This was the first case of a high-energy nuclear physics reaction for which descriptions based on the quark degrees of freedom and on the assumption that *the short-range NN forces are due to quark exchange* quantitatively agree with the data, while all theoretical descriptions invoking hadronic degrees of freedom qualitatively disagree with the data [Fr00]. Study of deuteron electrodisintegration at $E = 11$ GeV will allow a significant extension of the range of the observed energy scaling. A crucial prediction of the quark-exchange picture is that for a wide range of photon virtualities the cross section should depend on the photon virtuality as the pointlike Mott cross section.

In summary, the increase of electron energy to 11 GeV will significantly expand the possibilities for systematic studies of high-momentum-transfer processes with nuclei. The ultimate result of Campaigns 4 and 5 will be a detailed understanding of the hadronic and quark degrees of freedom in nuclear matter at high densities up to 4–5 times the average nuclear density.